AN ABSTRACT OF THE THESIS OF

DUK HWANG KIM (Name) for the Ph. D. (Degree) in Chemical Engineering (Major)

Date thesis is presented April 2, 1965

Title MOMENTUM TRANSFER IN CLIMBING-FILM FLOW IN AN ANNULAR DUCT

Abstract approved (Major professor)

Momentum transfer in an annular duct with upward gas-liquid flow was studied under the condition that the liquid flowed as a film only on the inner core of the annulus, the outer wall remaining dry.

Previous workers have studied climbing and falling liquid films in tubes or on vertical planes. With this type of apparatus it is very difficult to study pressure losses, gas velocity profiles, and the structure of the climbing film. The difficulty has been overcome by forming a liquid film on the inner core and maintaining a dry outer wall of an annular duct.

The column consists of a three-inch I. D. outer tube with a concentric one-inch O. D. inner core. The inner tube was supported laterally by sets of streamlined centering screws. The total length of the column was about 35 feet and the test section was 20 feet long. All measurements were made at two stations, the first was 76

inches from the liquid injector, the second 154 inches from the liquid injector. The liquid injector is a porous stainless steel cylinder with one inch O. D. and two inch length.

The air flow rates varied from 170 cfm to 410 cfm at 1 atmosphere pressure and 68° F temperature. The water flow rates used were 0.47 lbm/min and 0.79 lbm/min.

The study has two major divisions.

First division is the study of the mechanics of the air flow in the annulus as it is affected by the presence of the climbing film of liquid. This portion of the study involves an investigation of velocity profiles, the point of maximum velocity, friction losses, and the role of capillary waves in the annular flow.

It was found that:

1) the pressure loss for climbing film flow in an annulus can be predicted by the Lockhart and Martinelli correlation for two-phase flow in tubes,

2) the capillary waves of the climbing film affect only the location of the point of maximum air velocity and the air velocity profile at the inner portion of the annulus,

3) the location of the point of maximum air velocity shifts to the outer wall as water film is introduced,

4) the air velocity profiles in the inner portion of the annulus with the film present, plotted as u^+ versus y^+, are shifted downward,

relative to those for annular flow without the film, although they have same slope.

The second part is the study of the mechanics of flow of a climbing water film which has a solid wall as one boundary and highly turbulent air stream as the other.

The mean film thickness, wave length, and amplitude of the climbing film were measured by a photographic method. This method gave good results in the measurement of mean film thickness at the lower and moderate air velocities. However, the wave length and amplitude determined by this method have only a qualitative significance, because of the irregularity of wave shapes. With increasing air flow rates, the film thickness, wave length, and amplitude decreased. Generally the ratio of wave length to amplitude varied between 20 to 30.

As a first approximation, Kapitza's theory of wave formation in the vertical plane with downward flow, based on laminar conditions, was extended to the climbing film in an annular duct in order to obtain an expression for the mean film thickness, the velocity profile of liquid film, and the wave length. Comparison between the prediction and the experiment was found to be reasonably good.

The mean film thickness data for climbing film flow in an annulus was correlated with the Lockhart and Martinelli parameters, R_L and X, and was compared with the correlation for climbing film

flow in a tube. If a unique correlation for climbing film flow in both tubes and annuli exists (this is the original proposal of Lockhart and Martinelli), it would appear that the region in the vicinity of $x = 0.01$ is a transition region. More data at high water flow rates are necessary to reach a general conclusion concerning the correlation.

MOMENTUM TRANSFER IN CLIMBING-FILM FLOW IN AN ANNULAR DUCT

by

DUK HWANG KIM

A THESIS

submitted to

OREGON STATE UNIVERSITY

in partial fulfillment of
the requirements for the
degree of

DOCTOR OF PHILOSOPHY

June 1965

APPROVED:

Redacted for Privacy

Professor of Chemical Engineering

In Charge of Major

Redacted for Privacy

Head of Department of Chemical Engineering

Redacted for Privacy

Dean of Graduate School

Date thesis is presented April 2, 1965

Typed by Opal Grossnicklaus

ACKNOWLEDGMENTS

I would like to express my grateful appreciation to the following:

To Dr. James G. Knudsen, professor of Chemical Engineering, for suggesting the problem and for being very generous with his time and assistance during the course of the project.

To the National Science Foundation for its financial assistance.

To the Department of Chemical Engineering, Jesse S. Walton, Head, for the use of its facilities.

To Mr. Robert C. Mang and Mr. Antony Sutey for their aid in construction of the equipment.

To Mr. James Divine for his preliminary review of this thesis.

To my mother for her encouragement.

And finally to my wife, Chung, who typed several times the rough draft of this thesis.

TABLE OF CONTENTS

TABLE OF CONTENTS (Continued)

LIST OF FIGURES

LIST OF FIGURES

LIST OF TABLES

MOMENTUM TRANSFER IN CLIMBING-FILM FLOW IN AN ANNULAR DUCT

INTRODUCTION

Two-phase, gas-liquid flow occurs frequently in a variety of process equipment such as water tube boilers, wetted wall columns, and coolant channels of nuclear reactors. There are several regimes of gas-liquid flow which are determined by gas and liquid flow rates. One commonly encountered regime is that in which the liquid moves as a film on the surface of the duct and the gas flows as a core adjacent to the liquid film. This type flow is commonly called climbing film or falling film flow depending upon direction of bulk flow. Previous workers in two-phase film flow have observed a significant increase in heat and mass transfer rates at the surface (11, 15, 45). However much of the information on high heat and mass transfer in film flow is empirical and gives little information about the basic phenomena. A study of the transfer mechanism is therefore essential in order to predict and understand the phenomena which occur.

Most previous investigators have used smooth pipes, vertical planes, and inclined planes. In the present study a long annular duct in which the outer wall was maintained dry and the film formed on the inner wall was used. The use of an annular duct with one dry wall has certain advantages over the use of a circular tube. Static

pressures, air velocity profiles, and the film structure are more easily determined when the outer wall is dry. The column used was constructed of two concentric tubes. The liquid (water) was injected at the base of the inner core and climbed upward outside it. The gas and liquid flow rates were controlled to bring about an annular two-phase flow (climbing film flow). This simultaneous upward flow of gas and liquid in a vertical annular tube results in the phenomenon of "climbing film" flow; that is the gas flows rapidly upward adjacent to a thin layer of liquid which rises relatively slowly next to the outer wall of the inner core. The drag of the gas on the liquid overcomes the force of gravity, so that the liquid is lifted up and gains potential energy at the expense of the pressure energy of the gas.

This dissertation is concerned only with momentum transfer in climbing film flow. The study divides itself into two major divisions. First is the study of the mechanics of the air flow in the annulus as it is affected by the presence of the climbing film of liquid. This portion of the study involves an investigation of velocity profiles, points of maximum velocity, friction losses, and the role of capillary waves in the annular flow.

The second part is the study of the mechanics of flow of the climbing liquid film which has a solid boundary at one side and highly turbulent air stream boundary at the other. The difficulty

of this study occurs at the gas-liquid interface where waves are generated by the turbulent air stream. It is necessary to know the exact nature of the climbing film wave, the nature of the turbulence of the air, and exact way in which the one influences the other. Kapitza's theory of wave formation in the vertical plane was extended to the climbing film flow in an annular duct, and the velocity profile, mean film thickness, and wave length of the thin water film were predicted. In conjunction with this mean film thickness, wave length, and amplitude of the climbing-film wave were measured.

Lockhart and Martinelli's correlation which is best among reported correlations was applied to friction loss and film thickness data.

This study is an initial investigation of climbing-film flow in annular ducts. Much information must be obtained before the exact mechanism which occurs in the climbing film flow can be elucidated. However this study presents important measurements and indicates the direction toward a more fundamental approach to the subject.

PREVIOUS WORK AND THEORETICAL CONSIDERATIONS

Single Phase Annular Flow

A brief review of single phase annular flow will be mentioned.

Rothfus (43) reviewed critically the literature concerned with experimental investigations on turbulent annular flow up to 1948. Since that time Rothfus, Monrad and Senecal (44), Knudsen and Katz (25) Walker, Whan and Rothfus (47), Fredrickson and Bird (12) have presented measurements of pressure gradients and velocity profiles for turbulent annular flow.

Recently Meter and Bird (35) derived an expression relating friction factor and Reynolds numbers in annuli, using the Prandtl's mixing length theory. Their resultant equation is similar to an empirical expression in smooth annuli which has been recommended by Rothfus and coworkers (41).

$$\sqrt{\frac{1}{f_2}} = 4.0 \log_{10}(Re_2\sqrt{f_2}) - 0.4$$

The results of most workers have indicated that the position of maximum velocity for turbulent flow is the same as that theoretically predicted (and substantiated) for laminar flow in annuli. Brighton and Jones, however, with very precise methods of measurement, determined that the location of the point of maximum velocity was nearer to the inner pipe wall than for laminar flow and

was a function of the dimensions of the two concentric tubes. These workers also mentioned that the friction factors for flow in annuli with smooth walls are slightly higher (1 to 10 percent) than those for pipe flow when compared on the basis of equivalent diameter.

Laminar Flow in Plain Annuli (26)

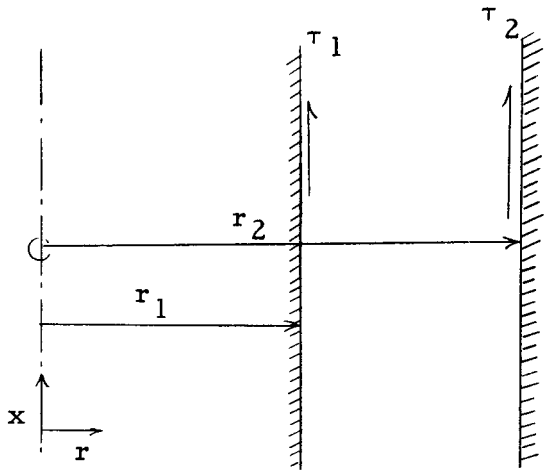

The differential equation and boundary conditions for incompressible, constant viscosity laminar flow in vertical annuli are

$$\frac{g_c}{\rho}\frac{\partial P}{\partial x} + g = \frac{\nu}{r}\frac{\partial}{\partial r}\left(r\frac{\partial u}{\partial r}\right)$$

$$\text{at} \quad r = r_1, \quad u = 0 \qquad (1)$$

$$r = r_2, \quad u = 0$$

$$r = r_m, \quad u = u_m \quad \text{or} \quad \frac{\partial u}{\partial r} = 0$$

The solution of the above boundary value problem is

$$u = \frac{g_c}{2\mu}\left(\frac{\partial p}{\partial x} + \rho\frac{g}{g_c}\right)\left(\frac{r^2}{2} - \frac{r_2^2}{2} + r_m^2 \ln\frac{r_2}{r}\right) \qquad (2)$$

If U is the average velocity, then

$$u = 2U\frac{r_2^2 - r^2 - 2r_m^2 \ln(\frac{r_2}{r})}{r_2^2 + r_1^2 - 2r_m^2} \tag{3}$$

where r_m is the theoretical position of the maximum velocity for laminar flow in an annuli,

$$r_m = \sqrt{\frac{r_2^2 - r_1^2}{2\ln\frac{r_2}{r_1}}} \tag{4}$$

a result that is a consequence of the solution of Equation (1).

The shear stress at any radius r is given by

$$\tau = \frac{4\mu U (r_m^2 - r^2)}{g_c r (r_2^2 + r_1^2 - 2r_m^2)} \quad \text{for } r < r_m, \tag{5}$$

$$\tau = \frac{4\mu U(r^2 - r_m^2)}{g_c r(r_2^2 + r_1^2 - 2r_m^2)} \quad \text{for } r > r_m. \tag{6}$$

Letting $r = r_1$ and r_2 in Equations (5) and (6) respectively, τ_1 and τ_2 may be obtained. The ratio of these two shear stresses is

$$\frac{\tau_1}{\tau_2} = \frac{r_2(r_m^2 - r_1^2)}{r_1(r_2^2 - r_m^2)} \tag{7}$$

By considering appropriate portions of the annular fluid, it may be shown that

$$\tau_1 = \left(-\frac{dp_f}{dx}\right)\frac{r_m^2 - r_1^2}{2r_1} \tag{8}$$

$$\tau_2 = \left(-\frac{dp_f}{dx}\right)\frac{r_2^2 - r_m^2}{2r_2} \tag{9}$$

Since Equations (7), (8) and (9) are derived from a force balance, they are also valid for turbulent flow in annuli and are the basic equations used to calculate shear stress from experimental data such as pressure gradient and the point of maximum velocity.

Turbulent Flow in Plain Annuli

Determination of both pressure losses and velocity distributions for turbulent flow in annuli relies on experimental data rather than theoretical analysis. Most experimental results on friction factors have used equivalent diameter as the characteristic length in defining both friction factor and Reynolds number. For smooth annuli with diameter ratios $\left(\frac{d_1}{d_2}\right)$ in the range 0.1 to 0.8 the friction factor-Reynolds number relation is the same as for smooth tubes. Various workers (7) have included the effect of diameter ratio in the friction factor-Reynolds number correlation. Prengle and Rothfus (41) defined a Reynolds number based upon the equivalent hydraulic diameter of the portion of the annulus outside the point of maximum velocity

$$Re_2 = \frac{4r_H U\rho}{\mu} \tag{10}$$

where

$$4r_H = \frac{2(r_2^2 - r_m^2)}{r_2} \tag{11}$$

They then defined a friction factor in terms of the shear stress at the outer wall

$$f_2 = \frac{2\tau_2 g_c}{\rho U^2} \tag{12}$$

By substituting Equation (9) into Equation (12),

$$f_2 = \frac{(r_2^2 - r_m^2) g_c}{r_2 \rho U^2} \left(-\frac{dP_f}{dx}\right) \tag{13}$$

Rothfus and coworker (41) found that for $10,000 < Re_2 < 45,000$ and for long annuli

$$\frac{1}{\sqrt{f_2}} = 4.0 \log_{10}(Re_2 \sqrt{f_2}) - 0.4 \tag{14}$$

which is the same form as the Nikuradse (37) friction factor Reynolds number relation for smooth tubes.

Equation (14) is based upon the position of maximum velocity being the same as that for laminar flow. Many workers have reported this to be the case. However, recent accurate measurements by Brighton and Jones (3) indicate that the position of maximum velocity for turbulent flow in smooth annuli is nearer to the inner tube than for laminar flow. The use of Equation (14) and the definitions in Equations (10) and (13) require a knowledge of the position of maximum velocity which for turbulent flow can only be

determined experimentally. In addition, the effect of roughness on one of the walls or the presence of a film of liquid on one of the walls on the velocity profiles is not known.

Recently, however, Hewitt (19) has proposed an approximate method to treat data of annular flow, where the inner wall is rough and the outer wall is smooth, without relying on the measurement of the velocity profile. Hewitt defined Reynolds numbers and friction factors as follows:

$$Re_1 = \frac{U_1 d_{e_1} \rho}{\mu} \tag{15}$$

$$Re_2 = \frac{U_2 d_{e_2} \rho}{\mu} \tag{16}$$

$$d_{e_1} = \frac{2\left(r_m^2 - r_1^2\right)}{r_1} \tag{17}$$

$$d_{e_2} = \frac{2\left(r_2^2 - r_m^2\right)}{r_2} \tag{18}$$

$$f_1^1 = \frac{\left(\frac{-dP_f}{dx}\right)\frac{d_{e_1}}{4}}{\rho U_1^2} \tag{19}$$

$$f_2^1 = \frac{\left(\frac{-dP_f}{dx}\right)\frac{d_{e_2}}{4}}{\rho U_2^2} \tag{20}$$

$$U_1\left(r_m^2 - r_1^2\right) + U_2\left(r_2^2 - r_m^2\right) = U\left(r_2^2 - r_1^2\right) \tag{21}$$

where

$$f_1^1 = \frac{\tau_1}{\rho U_1^2} \tag{22}$$

$$f_2^1 = \frac{\tau_2}{\rho U_2^2} \tag{23}$$

A velocity profile in addition to the pressure drop and U is required to evaluate all parameters from the above seven equations, (15-21), and the friction factor equations for smooth walls.* Hewitt used a universal empirical law

$$\frac{u_m - u}{u^*} = \frac{1}{k} \ln \frac{y_m}{y}$$

as another relationship among the parameters, so that one could avoid measurement of the velocity profile. By integration, he derived following equation,

$$\frac{U_1}{U_2} = \frac{\frac{\sqrt{f_2^1}}{k}\left(\frac{r_m + 3r_2}{2r_m + 2r_2}\right) + 1}{\frac{\sqrt{f_1^1}}{k}\left(\frac{r_m + 3r_1}{2r_m + 2r_1}\right) + 1} \tag{24}$$

In all, there are nine equations including the friction factor equation* which can be solved for the nine unknown parameters, Re_1, Re_2, f_1^1, f_2^1, U_1, U_2, de_1, de_2, and r_m.

---

*Hewitt used

$$f_1^1 = 0.00070 + 0.0625(Re_1)^{-0.32}$$

or $$f_2^1 = 0.00070 + 0.0625(Re_2)^{-0.32}$$

Vertical Cocurrent Two-phase Gas-liquid Flow

The possible regimes of vertical two-phase flow are illustrated in Figure (1). They can be observed sequentially as the gas flow rate increases at constant liquid flow rate (4). When only a small flow rate of air is introduced, the air flows upward as small bubbles. With increasing air flow rates, the mode of air flow changes consecutively from bubble to piston, churn, and annular (climbing film). At very high air flow rates, the water is evenly dispersed in droplets in the air stream. The same flow patterns can also be observed in a single tube at whose wall a constant heat flux is transferred into the water to generate steam. At the inlet, water flows as a single phase. Farther along the tube the flow pattern changes, since steam is being generated, from single phase water to bubble, piston, churn, and finally annular flow. Further along, the tube contains only high quality steam.

The annular (climbing) film regime has been the subject of many previous investigations. The regime of vertical cocurrent annular film flow is, thus, defined as that in which the liquid flows as a uniform annular film on the tube wall while the gas flows as a central core inside the liquid annulus.

In the present study, the annular climbing film was formed on the outer surface of the inner core of an annular duct with the other

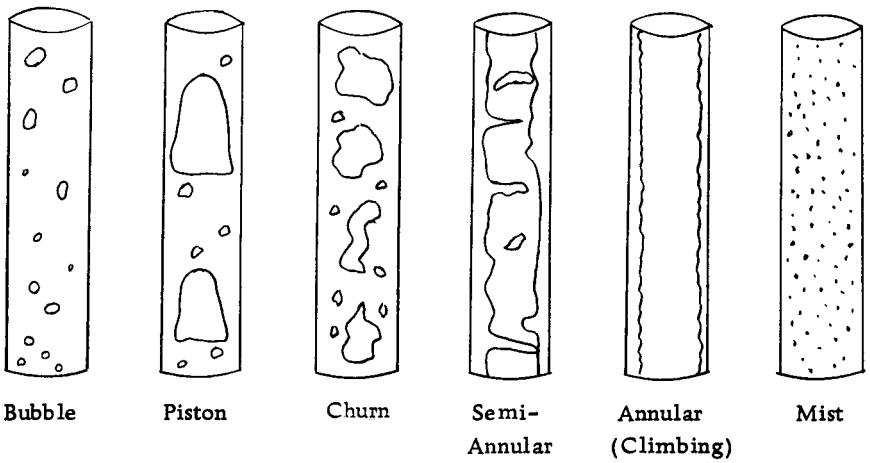

Figure (1) Regimes of Two-Phase Flow.

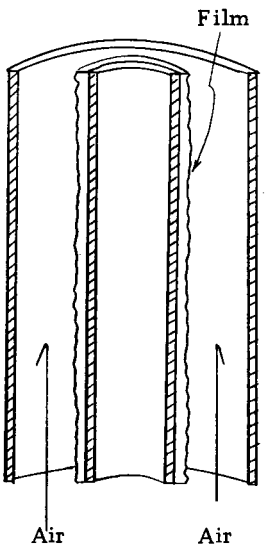

Figure (2) Climbing film flow in an annular duct.

wall remaining dry (Figure 2).

As can be seen in Figure (2), the measurement of air velocity profiles, pressure gradients, and the determination of the film structure are easier with the climbing film in an annulus than with a film in a tube.

Two-phase Climbing Film Flow

Simplified Models for Climbing Film Flow

Two-phase gas-liquid climbing film flow has been studied extensively and several mathematical models proposed to relate bulk flow rates, liquid film thickness and pressure drops.

Lockhart and Martinelli (32) related the pressure gradient for two-phase flow to that of the gas and liquid flowing separately at the same mass rate. They defined two dimensionless parameters X and Φ, where X is a function of the pressure gradients for the separate phases and Φ relates the pressure gradient for the single phases to that for two phase flow. They postulated, subject to experimental verification, that a unique relation existed between the two dimensionless parameters, X and Φ. They also proposed that the film thickness was a function only of the dimensionless variable X. The functions, for climbing film flow in tubes, depended on the flow conditions of the gas and liquid, (i. e., laminar or turbulent),

and were given in graphical form by Lockhart and Martinelli. The difficulty in this correlation is, consequently, to determine when the transition occurs from laminar to turbulent flow.

In 1952 Dukler and Bergelin (9) examined theoretically the hydrodynamic relationships in a system comprised of a turbulently flowing core of gas exerting a shear stress on a liquid film on the wall of a tube. Using the von Karman universal velocity profile in the liquid film, a simplified relation between film thickness and pressure drop was developed by them for the downward flow of a turbulent film with interfacial shear (between gas and liquid) acting in the direction of the liquid flow. They were the first to consider theoretically the interfacial shear stress in two-phase flow.

Laird (28) derived a relationship between pressure gradients, liquid hold-up, flow rates, and tube dimensions, assuming laminar flow in both the gas and liquid phases. The usefulness of the relationship is, however, limited since it is not possible to predict either the pressure gradient or the liquid hold-up from a knowledge of the flow rates and tube dimensions alone. Laird also studied gas flow behavior in a channel with flexible walls which were given mechanical wave motion. He observed from the rubber tube model studied that pressure losses increased rapidly with increase of wave length, wave amplitude and wave frequency in the Reynolds number range from 300 to 4000.

In 1955 Calvert and Williams (4) developed a method of predicting liquid hold-up and pressure drop for flowing systems in which the liquid, lifted up by the gas flowing as a central core, moved upward as a continuous climbing film along the smooth pipe wall. A mathematical description of the flow of the liquid film was derived through an analytical procedure, similar to that of Dukler and Bergelin, based on the Prandtl and von Karman theories of turbulent flow. They presented an equation for shear stress in the liquid film. (See equation 4 in Calvert and Williams (4)).

In 1960 Anderson and Mantzouranis (1) extended and modified the method of Dukler and Bergelin, using the von Karman universal velocity profile in the liquid film, and compared their theory with their own experimental results for air-water mixtures in a 1/2-inch glass tube. Their predictions of the liquid film thickness agreed to ± 15 percent with experimental results. In their model they made the assumption that the shear stress within the film was constant and equal to the shear stress at the wall. This is the same as Prandtl's original assumption for pipe flow. Data of Collier and Hewitt (5) showed that the assumption of constant shear stress in the liquid film introduced large errors at large film thicknesses, although the predictions based on this assumption were good at moderate and low film thicknesses.

Later, Dukler (8) divided the downward flowing film into two

regions and applied the Deissler and the von Karman eddy viscosity equations to the proper regions in the film to generate a velocity profile of the liquid film, assuming the shear distribution in the film was linear. His solutions were obtained for downward flow only.

Hewitt (18) applied the downward flow analysis of Duler to upward flow and introduced refinements to give the correct shear stress distribution in the liquid film. He used the same shear stress distribution as Calvert and Williams derived. The resultant theory has correlated fairly well (±30 percent) both his original film thickness data (20) and more recent measurements by Gill and Hewitt (13). Hewitt concluded, however, that the theory used might still prove inadequate as it did not take into account energy transport in the spray and the effect of surface waves on the film.

Recent works such as Hewitt, King and Lovegrove (20), Gill and Hewitt (13), Gill, Hewitt and Lacey (14) have supported the validity of Lockhart and Martinelli's correlation in annular flow in smooth tubes. In 1964 Dukler, Wicks and Cleveland (10) compared critically the prediction of certain correlations for pressure drop and hold-up in horizontal flow with selected experimental data. They also concluded that the Lockhart-Martinelli's correlation, oldest of the five tested, showed the best agreement with a set of carefully culled experimental data on pressure drop and that Hughmark's correlation for hold-up gave the best agreement with experimental

hold-up data.

From a review of previous work it is concluded that the correlation of Lockhart-Martinelli can be applied to the climbing film flow data taken during the present study, since there is accumulated evidence in favor of this correlation and also the correlation should be applicable to any two-phase flow system. However the comparison of present available correlations with experimental data reported showed the available basic theory was incorrect (27). This may be due to the fact that simple models mentioned above did not consider wave and entrainment phenomenon on the film surface.

Wave Motion in the Liquid Film

The theory and the measurements made to date have helped principally to point up the complexity of the problem and to provide badly needed data for design. They have contributed little to understanding of the basic phenomena, such as high pressure drop and high heat and mass transport phenomena at the air-water interface. Lacey, Hewitt and Collier (27) attributed the lack of understanding to the wave motion and the entrainment phenomena. In theoretical studies the main difficulty is postulating a suitable mathematical model and in obtaining a solution to the non-linear momentum equation. Experimental work is hampered by difficulties in measuring the velocity profile in the liquid film. This is one of the most important

quantities which remain to be determined.

Many investigators, however, have attempted to explain theoretically the mechanism of wave generation by wind on the ocean and the phenomenon of energy transfer from the wind to the water. There is accumulated evidence in favor of Miles' mathematical theory. A linearized momentum equation is commonly used and water is considered nearly inviscid. The most successful models concerning ocean waves are described below.

The model proposed by Phillips (39) assumed as its essential mechanism the direct action of turbulent fluctuations in aerodynamic pressure on the surface of the water, but neglected all interaction between air flow and the surface waves. The initiation and early development of waves may be a consequence of fluctuations in the normal pressure upon the water surface and waves develop rapidly by means of a resonance mechanism which occurs when a component of the surface pressure distribution moves at the same speed as the free surface wave with the same wave numbers.

In 1957 Miles (36) showed that an exponential build-up of water waves of velocity c could occur if the mean air-flow velocity U in the direction of wave propagation varied with height y above the water surface in such a way that the second derivative of the mean air velocity U with respect to y was negative. The turbulence of the air was neglected. In other words, his postulated mechanism of

generation of waves is the interaction between mean air flow and surface waves.

The mean rate at which energy is transferred from a parallel shear flow U(y) to a surface wave of wave length $\frac{2\pi}{k}$ and wave speed c is given by

$$\overline{\dot{E}} = -\rho g \cdot c \frac{\pi}{k} \left(\frac{U_c''}{U_c'} \right) \overline{v_c^2} \qquad (1)^*$$

where the subscript c implies values at the critical layer defined by

$$U(y_c) = c$$

or anticipating the extension to obliquely moving waves,

$$U(y_c) \cos\theta = c$$

The Phillips' model can be regarded as providing the initial wavy disturbance of the water surface, which should then grow exponentially by Miles' shear flow mechanism of energy transfer, rather than linearly by Phillips' forced-vibration mechanism.

In thin wavy film flow on vertical or inclined planes, the theory of wave generation is not as advanced as for ocean waves. The waves are quite different in nature. Whereas ocean waves are gravity waves, the waves of the thin film are capillary waves. However, a few works in this area are worthy of mention.

---

*This equation was also derived by Lin (31).

Jeffrey (23) proposed the sheltering model to explain wave generation. The wind passing over any waves already existing on the surface induces a variable pressure distribution and a component which is in phase with the wave slope supplies further energy to the wave, resulting in its continued development. This periodic component of wind stress is described by a "sheltering coefficient". Inertial effects and tangential stresses due to wind are neglected. For a wave in which the energy gained from the wind just balances the viscous dissipation, the sheltering coefficient is required to have a value of approximately 0. 27.

Kapitza (24) theoretically analysed the problem of flow of thin layers of a viscous liquid under the influence of a constant bulk force, taking surface tension into account. This theory led to a good approximation of the phase velocity and of the amplitude of the waves. Tailby and Portalski (46) have concluded from their experimental results that Kapitza's theory is capable of prediction of the onset of wave formation in film flow down a vertical plate.

In 1957 Benjamin (2) studied wave formation in laminar flow down an inclined plane, being bounded on one side by a free surface influenced by surface tension. He used a series solution to solve the Orr-Sommerfeld equation and predicted the length and velocity of the waves and the value of Reynolds number at which observable waves should first develop.

In 1957, Hanratty and Engen (16) studied the interaction between a turbulent air stream and a moving water surface in a parallel channel. Their measurements of the pressure drop and of the velocity profile in the gas reflected the effect of changes of the liquid surface upon the flow in the gas phase.

In 1961 Hanratty and Hershman (17) applied the theory proposed by Jeffreys, explaining roll wave transition on a liquid surface, to the cocurrent flow of a gas and liquid. They reported good agreement between experiment and theory.

In 1964 Portalski (40) discussed high rates of transport phenomena for falling film flow. In his discussion these high rates of transfer were explained by the high bulk mixing due to the wave. He applied Kapitza's theory of wave formation to explain how eddies were generated in a falling liquid film and concluded that the formation of eddies promoted vigorous bulk mixing and surface renewal in the film so that it gave, as a result, a high rate of transfer.

A search of the literature has not revealed a theoretical solution of capillary wave motion in the climbing film flow in tubes or in annular ducts.

Extension of Kapitza's Solution to the Climbing Film Flow

From a review of previous results it appeared that an extension of Kapitza's solution to include energy transfer at the interface

in climbing film was possible. The energy transfer at the interface is based upon that developed for ocean waves.

For the present investigation, where the film flows upward on the inner core of an annulus, the film is considered so thin compared to inner core that the curvature may be neglected. By considering the axial symmetry of the system, the motion of the liquid in the film is seen to be quasi-two dimensional. Hence by orienting the x-axis along the direction of the motion and the y-axis perpendicular to the film surface, the governing differential equations of flow in the film are:

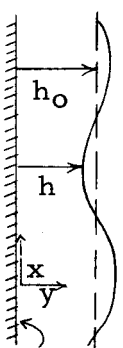

$$\frac{\partial u}{\partial t} + u\frac{\partial u}{\partial x} + v\frac{\partial u}{\partial y} = -\frac{1}{\rho}\frac{\partial P}{\partial x} + \nu\frac{\partial^2 u}{\partial y^2} - g \qquad (1)$$

$$0 = \frac{\partial P}{\partial y} \qquad (2)$$

$$\frac{\partial u}{\partial x} + \frac{\partial v}{\partial y} = 0 \qquad (3)$$

Equations (1) and (2) may be derived from the Navier-Stokes equations and the assumption that the velocity u in the x-direction does not change significantly with respect to x. Equation (3) is the continuity equation in two-dimensions for an incompressible fluid. Four boundary conditions are necessary to solve the differential equations,

$$\text{at } y = 0, \qquad u = v = 0 \qquad (4)$$

$$\text{at } y = h(x, t), \quad \frac{\partial u}{\partial y} = \frac{F(x, t)}{\mu} \qquad (5)$$

$$P = P_\sigma(x, t) + P_G(x) \qquad (6)$$

As seen above there is no velocity component along the x-axis nor along the y-axis at the interface between the wall and the fluid film. The conditions at the interface between the liquid and air are unknown. However, the momentum which is transferred from the air into the film at the interface cause the liquid to climb upward along the inner tube. This momentum transfer described by F(x, t), is a function of both x and t. The pressure of the liquid film at the interface must be equal to the summation of the air pressure, P_G, and the surface pressure, P_σ. The surface pressure is due to the surface tension. With small deformations of the surface in one direction the surface pressure may be expressed as

$$P_\sigma = -\sigma \frac{\partial^2 h}{\partial x^2} \tag{7}$$

where σ is the surface tension (29).

Since the pressure is not a function of y as shown by Equation (2), the pressure in Equation (1) can be replaced with the boundary condition,

$$P = P_\sigma + P_G \quad \text{at } y = h(x, t)$$

Equation (1) becomes

$$\frac{\partial u}{\partial t} + u\frac{\partial u}{\partial x} + v\frac{\partial u}{\partial y} = -\frac{1}{\rho}\left[\frac{\partial P_G}{\partial x} + \frac{\partial P_\sigma}{\partial x}\right] + \nu\frac{\partial^2 u}{\partial y^2} - g \tag{8}$$

$$= \frac{\sigma \partial^3 h}{\rho \partial x^3} - \frac{1}{\rho}\frac{\partial P_G}{\partial x} + \nu\frac{\partial^2 u}{\partial y^2} - g \tag{9}$$

From the continuity equation,

$$v = -\int_o^y \frac{\partial u}{\partial x} dy = \frac{\partial h}{\partial t}$$

Hence, the final equations and the boundary conditions for the climbing film in laminar motion are

$$\frac{\partial u}{\partial t} + u\frac{\partial u}{\partial x} - \left(\int_o^y \frac{\partial u}{\partial x} dy\right)\frac{\partial u}{\partial y} = -\frac{\sigma \partial^3 h}{\rho \partial x^3} - \frac{1}{\rho}\frac{\partial P_G}{\partial x} + \nu\frac{\partial^2 u}{\partial y^2} - g \qquad (11)$$

$$\frac{\partial h}{\partial t} = -\frac{\partial}{\partial x}\int_o^y u dy \qquad (10)$$

at $y = 0$, $u = 0 = v$ (4)

at $y = h(x, t)$, $\frac{\partial u}{\partial y} = \frac{F(x, t)}{\mu}$ (5)

There is no general method for solving the non-linear differential equation. The technique to be used is to propose a simplified model which can be solved to give an approximate velocity profile. The velocity profile thus obtained is used in the above differential equation but still using the simplified boundary conditions associated with simplified model.

The assumptions made are as follows:

1) Convective terms are negligible compared to other terms.

2) At the air-water interface, $\frac{\partial u}{\partial y} = \frac{F}{\mu}$ and $P = P_G(x)$

where the force acting on liquid surface, F, is constant.

The assumption (1) is good when the motion is laminar. In slow motion the viscous forces are considerably greater than the inertia

forces because the latter are of the order of the velocity squared, whereas the former are linear with velocity. In case of laminar wave motion Brooke-Benjamin (2) points out that although the film flow is always unstable, that is, a class of undamped waves exist for all finite values of Reynolds number, the rates of amplification of unstable waves may be shown to become very small when Reynolds number is small, and their wave lengths to become very large. The assumption (2) says that the film has a constant thickness.

Thus the modified differential equation and boundary conditions are

$$\nu\frac{\partial^2 u}{\partial y^2} - g - \frac{1}{\rho}\frac{\partial P_G}{\partial x} = 0 \tag{13}$$

$$\text{at } y = 0, \quad u = 0 \tag{14}$$

$$\text{at } y = h, \quad \frac{\partial u}{\partial y} = \frac{F}{\mu} \tag{15}$$

where $\frac{\partial P_G}{\partial x}$ is a known constant and can be measured experimentally.

Integrating Equation (13) yields

$$\frac{\partial u}{\partial y} = (\frac{1}{\mu}\frac{\partial P_G}{\partial x} + \frac{g}{\nu})y + C_1$$

and finally gives

$$u = (\frac{1}{\mu}\frac{\partial P_G}{\partial x} + \frac{g}{\nu})\frac{y^2}{2} + C_1 y + C_2$$

Applying the boundary conditions,

$$C_2 = 0$$

$$C_1 = \frac{F}{\mu} - (\frac{1}{\mu}\frac{\partial P_G}{\partial x} + \frac{g}{\nu})h$$

and letting $(\frac{1}{\mu}\frac{\partial P_G}{\partial x} + \frac{g}{\nu}) = A_1$

the resultant velocity profile is,

$$u = A_1\frac{y^2}{2} + (\frac{F}{\mu} - A_1 h)\cdot y \tag{16}$$

Next u is averaged with respect to the film thickness,

$$\begin{aligned}\bar{u} &= \frac{1}{h}\int_o^h u\,dy \\ &= \frac{1}{h}\int_o^h (\frac{A_1}{2}y^2 + c_1 y)dy \\ &= \frac{A_1 h^2}{6} + \frac{c_1 h}{2}\end{aligned} \tag{17}$$

Solving for A_1, it is found

$$A_1 = \frac{3}{h^2}(\frac{h}{2}\frac{F}{\mu} - \bar{u})$$

Thus, the first approximation of the velocity profile is,

$$u = \frac{3}{2h^2}(\frac{h}{2}\frac{F}{\mu} - \bar{u})\cdot y^2 + [\frac{F}{\mu} - \frac{3}{h^2}(\frac{h}{2}\frac{F}{\mu} - \bar{u})h]\,y$$

$$= \frac{3}{h^2}\cdot[\frac{h}{2}\frac{F}{\mu} - \bar{u}][\frac{y^2}{2} - hy] + \frac{F}{\mu}y \tag{18}$$

Substituting Equation (18) into (11),

$$\begin{aligned}&-\frac{3}{h^2}(\frac{y^2}{2} - hy)\frac{\partial \bar{u}}{\partial t} - \{\frac{3}{h^2}(\frac{h}{2}\frac{F}{\mu} - \bar{u})(\frac{y^2}{2} - hy) + \frac{F}{\mu}y\}\cdot\{\frac{3}{h^2}(\frac{y^2}{2} - hy)\frac{\partial \bar{u}}{\partial x}\} \\ &\quad + \{\frac{3}{h^2}\frac{\partial u}{\partial x}(\frac{y^3}{6} - \frac{hy^2}{2})\}\cdot\{\frac{3}{h^2}\cdot(\frac{h}{2}\frac{F}{\mu} - \bar{u})(y-h) + \frac{F}{\mu}\} \\ &\quad = \frac{\sigma}{\rho}\frac{\partial^3 h}{\partial x^3} + \frac{3\nu}{h^2}(\frac{h}{2}\frac{F}{\mu} - \bar{u}) - \frac{1}{\rho}\frac{\partial P_G}{\partial x} - g\end{aligned} \tag{19}$$

where $\bar{u}$ is a function of t and x, since h is function of t and x.

Upon rearrangement,

$$-\frac{3}{h^2}\left(\frac{y^2}{2} - hy\right)\frac{\partial \bar{u}}{\partial t} - \frac{\partial \bar{u}}{\partial x}\left\{\frac{9}{h^3}\frac{1}{2}\frac{F}{\mu}\left(\frac{y^2}{2} - hy\right)^2\right.$$

$$-\frac{9}{h^4}\left(\frac{y^2}{2} - hy\right)^2\bar{u} + \frac{3}{h^2}\frac{F}{\mu}\left(\frac{y^3}{2} - hy^2\right)$$

$$-\frac{9}{h^3}\frac{1}{2}\frac{F}{\mu}\left(\frac{y^3}{6} - \frac{hy^2}{2}\right)(y - h) + \frac{9}{h^4}\left(\frac{y^3}{6} - \frac{hy^2}{2}\right)(y - h)\bar{u}$$

$$\left.-\frac{3}{h^2}\frac{F}{\mu}\left(\frac{y^3}{6} - \frac{hy^2}{2}\right)\right\} = \frac{\sigma}{\rho}\frac{\partial^3 h}{\partial x^3} + \frac{3\nu}{h^2}\left(\frac{h}{2}\frac{F}{\mu} - \bar{u}\right) - \frac{1}{\rho}\frac{\partial P_G}{\partial x} - g \qquad (20)$$

Equation (20) is integrated with respect to y and then divided by the film thickness h to obtain

$$\frac{\partial \bar{u}}{\partial t} + \frac{\partial \bar{u}}{\partial x}\left\{\frac{9}{10}\bar{u} - \frac{1}{5}\frac{Fh}{\mu}\right\}$$

$$= \frac{\sigma}{\rho}\frac{\partial^3 h}{\partial x^3} + \frac{3\nu}{h^2}\left(\frac{h}{2}\frac{F}{\mu} - \bar{u}\right) - \frac{1}{\rho}\frac{\partial P_G}{\partial x} - g. \qquad (21)$$

On substitution of Equation (18) into (10), resultant equation is

$$\frac{\partial h}{\partial t} = -\frac{\partial}{\partial x}\int_o^h u\,dy$$

$$= -\frac{\partial}{\partial x}\left\{\frac{F}{\mu}\frac{h^2}{2} - h\left(\frac{h}{2}\frac{F}{\mu} - \bar{u}\right)\right\}$$

$$= -\frac{\partial}{\partial x}(h\bar{u}) \qquad (22)$$

Following Kapitza's procedure, let the film thickness be written as

$$h = h_o(1 + \phi) \qquad (23)$$

where $h_o\phi$ is the deviation of the surface from average thickness. The film thickness, h, and velocity, $\bar{u}$, are functions of the argument (x - ct), where c is the phase velocity.

Therefore,

$$\frac{\partial \bar{u}}{\partial t} = -c\frac{\partial \bar{u}}{\partial x} \tag{24}$$

$$\frac{\partial h}{\partial t} = -h_o c\frac{\partial \phi}{\partial x} \tag{25}$$

Now substitute Equations (23), (24) and (25) into Equation (22)

$$-h_o c\frac{\partial \phi}{\partial x} + \frac{\partial}{\partial x}\{h_o(1 + \phi)\bar{u}\} = 0$$

$$\frac{\partial}{\partial x}\{(c - \bar{u})h_o(1 + \phi)\} = 0 \tag{26}$$

Integrating Equation (26) it follows

$$h_o(1 + \phi)(c - \bar{u}) = \text{constant}$$

$$= h_o(c - u_o)$$

where u_o is the velocity at the average stream cross section h_o.

Thus, solving for $\bar{u}$,

$$\bar{u} = c - \frac{c - u_o}{1 + \phi} \tag{27}$$

and expanding $(1 + \phi)^{-1}$ in binomial series,

$$\bar{u} = u_o + (c - u_o)\phi - \frac{(c - u_o)}{2}\phi^2 + \ldots \tag{28}$$

$$\frac{\partial \bar{u}}{\partial x} = (c - u_o)(1 - \phi)\frac{d\phi}{dx} + \ldots \tag{29}$$

Now substitute Equations (22), (24), (25), (28) and (29) into (21),

$$-c(c - u_o)(1 - \phi)\frac{d\phi}{dx} + \{(c - u_o)(1 - \phi)\frac{d\phi}{dx}\}$$

$$:\{-\frac{1}{5}\frac{F}{\mu}h_o(1 + \phi) + \frac{9}{10}[u_o + (c - u_o)\phi - \frac{(c - u_o)}{2}\phi^2]\}$$

$$= \frac{\sigma h_o}{\rho}\frac{d^3\phi}{dx^3} + \frac{3\nu}{2}\frac{F}{\mu}\frac{1}{h_o(1 + \phi)}$$

$$- \frac{3\nu}{h_o^2(1 + \phi)^2}[u_o + (c - u_o)\phi - \frac{(c - u_o)}{2}\phi^2]$$

$$- \frac{1}{\rho}\frac{\partial P_G}{\partial x} - g \qquad (30)$$

Rearrangement of Equation (30) yields

$$\frac{\sigma h_o}{\rho}\frac{d^3\phi}{dx^3} + (c - u_o)(c + \frac{1}{5}\frac{F}{\mu}h_o - \frac{9}{16}u_o)\frac{d\phi}{dx}$$

$$+ \frac{3\nu}{2}\frac{F}{\mu}\frac{1}{h_o} - \frac{3\nu}{h_o^2}u_o - \frac{3\nu}{h_o^2}(c - 3u_o + \frac{h_o F}{2\mu})\phi$$

$$- \frac{1}{\rho}\frac{\partial P_G}{\partial x} - g = 0 \qquad (31)$$

where ϕ^2, ϕ^3 terms are neglected.

In order to have an undamped periodic solution, it is necessary that

$$\frac{3\nu}{2}\frac{F}{\mu}\frac{1}{h_o} - \frac{3\nu}{h_o^2}u_o - \frac{1}{\rho}\frac{\partial P_G}{\partial x} - g = 0 \qquad (32)$$

$$\frac{3\nu}{h_o^2}(c - 3u_o + \frac{hF}{2\mu}) = 0 \tag{33}$$

From Equation (32)

$$(\frac{1}{\rho}\frac{\partial P_G}{\partial x} + g)h_o^2 - \frac{3F}{2\rho}h_o + 3\nu u_o = 0$$

and the mean film thickness is

$$h_o = \frac{\frac{3F}{2\rho} \pm \sqrt{\frac{9F^2}{4\rho^2} - 12\nu u_o(\frac{1}{\rho}\frac{\partial P_G}{\partial x} + g)}}{2(\frac{\partial P_G}{\partial x}\frac{1}{\rho} + g)} \tag{34}$$

From Equation (33),

$$c = 3u_o - \frac{h_o F}{2\mu} \tag{35}$$

Introducing Equation (35) into (31) gives

$$\frac{\sigma h_o}{\rho}\frac{d^3\phi}{dx^3} + (c - u_o)(c + \frac{1}{5}\frac{F}{\mu}h_o - \frac{9}{10}u_o)\frac{d\phi}{dx} = 0 \tag{36}$$

Therefore the solution of equation (36) is*

$$\phi = a \sin k(x - ct) \tag{37}$$

where

$$k = \sqrt{\frac{\rho(c - u_o)}{\sigma h_o}(c + \frac{1}{5}\frac{F}{\mu}h_o - \frac{9}{10}u_o)} \tag{38}$$

---

*The ergodic principle- the mean value of the function with respect to x at a constant t is equal to the mean value of the function with respect to time at a constant x- is used in solving Equation (36).

and the cosine term is discarded to satisfy the zero initial condition. Substituting Equation (35), which is a first approximation, into Equation (38) gives

$$k = \sqrt{\frac{\rho(2u_o - \frac{h_o F}{2\mu})}{\sigma h_o}} \left(\frac{21}{10}u_o - \frac{3}{10}\frac{F}{\mu}h_o\right) \qquad (38)'$$

Consequently, the velocity profile of the liquid film and the film thickness are respectively (first approximation)

$$u = \frac{3}{h^2}\left[\frac{h}{2}\frac{F}{\mu} - u_o - (c - u_o)\phi \ldots\right]\left[\frac{y^2}{2} - hy\right] + \frac{F}{\mu}y \qquad (39)$$

and

$$h = h_o(1 + \phi) \qquad (23)$$

Now the amplitude, $h_o\phi$ which is equal to $h_o a$, as a first order approximation, will be estimated by an energy balance on the film.

The energy transferred from the air stream is balanced by the energy dissipation in the film and the potential energy gained by the film.

The energy transferred from the air stream is the combination of energy due to normal and tangential force, and is expressed by

$$\frac{\Delta P}{\Delta x} u_o h + F \cdot c$$

The energy dissipation is expressed as

$$E_d = \frac{\mu}{g_c} \int_o^h \left(\frac{\partial u}{\partial y}\right)^2 dy$$

$$= \frac{\mu}{g_c}\left[\frac{3}{h}\right]\left[\frac{hF}{2\mu} - u_o - (c - u_o)\alpha \sin k(x - ct)\right]^2 + \frac{F^2 h}{g_c \mu}$$

$$- \frac{3F}{g_c}\left[\frac{hF}{2\mu} - u_o - (c - u_o)\alpha \sin k(x - ct)\right]$$

The potential energy gained by the liquid film is

$$\frac{\rho g Q}{2\pi r_1 g_c h}.$$

Thus, the constant α, which is related to the amplitudes of the capillary waves in the climbing film, can be estimated from the following energy balance,

$$\frac{\Delta P}{\Delta x} u_o h + F \cdot c = \overline{E_d}(h, \alpha, F) + \frac{\rho g Q}{2\pi r_1 g_c h}, \tag{24}$$

where $\overline{E_d}$ is a rate of an averaged energy dissipation with respect to t and x.

The remaining task is to estimate a momentum transfer at the air-water interface, F.

Estimation of the Momentum Transfer at Air-water Interface

The equation of motion for the climbing-film flow system is

$$\rho u \frac{\partial u}{\partial x} = -\frac{\partial P}{\partial x} + \frac{1}{r}\frac{\partial}{\partial r}(r\tau) - \rho g \tag{1}$$

where $\frac{\partial P}{\partial x}$ is assumed constant.

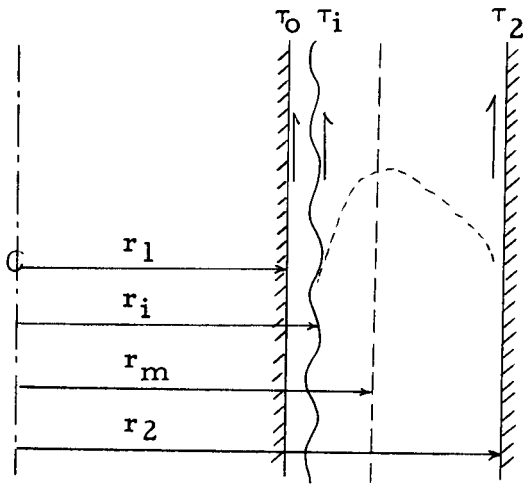

By rearrangement Equation (1) and integration of the resultant equation, one may obtain following equations

$$\frac{dP}{dx} + \rho g + \rho u \frac{\partial u}{\partial x} = \frac{1}{r}\frac{d}{dr}(r\tau)$$

$$\frac{dP}{dx}\int_1^2 r dr + \rho g \int_1^2 r dr + \rho \int_1^2 u \frac{du}{dx} r\, dr = [\, r\tau]_1^2$$

$$\frac{dP}{dx} + \rho g + \frac{\rho}{(r_2^2 - r_1^2)} \frac{d}{dx}\int_1^2 u^2 r\, dr = \frac{2[\, r\tau]_1^2}{r_2^2 - r_1^2} \qquad (2)^*$$

Equation (2) is a general momentum equation in annuli. If one assumes no mass transfer at air-water interface and no entrainment, the Equation (2) can be used at any region in the annuli with the climbing-film. If Equation (2) is applied to proper region, one may get the following momentum equations at each region.

---

*When 2 refers to the region beyond r_m, sign of τ should be changed.

1) For the liquid film.

$$\frac{dP}{dx} + \rho_L g + \frac{\rho_L}{r_i^2 - r_1^2} \frac{d}{dx} \int_{r_1}^{r_i} u^2 r\, dr = \frac{2(r_i \tau_i - r_1 \tau_1)}{r_i^2 - r_1^2}$$

Let $R_L = \dfrac{r_i^2 - r_1^2}{r_2^2 - r_1^2}$. Then the above equation becomes

$$\frac{dP}{dx} + \rho_L g + \frac{\rho_L}{R_L(r_2^2 - r_1^2)} \frac{d}{dx} \int_{r_1}^{r_i} u^2 r\, dr$$

$$= \frac{2(r_i \tau_i - r_1 \tau_1)}{R_L(r_2^2 - r_1^2)} \qquad (3)$$

2) For the gas stream between r_i and r_m.

Let $R_1 = \dfrac{r_m^2 - r_i^2}{r_2^2 - r_1^2}$. Then momentum equation becomes

$$\frac{dP}{dx} + \rho_g \cdot g + \frac{\rho_g}{R_1(r_2^2 - r_1^2)} \frac{d}{dx} \int_{r_i}^{r_m} u^2\, r\, dr$$

$$= - \frac{2 r_i \tau_i}{R_1(r_2^2 - r_1^2)} \qquad (4)$$

3) For the gas stream between r_m and r_2.

Let $R_2 = \dfrac{r_2^2 - r_m^2}{r_2^2 - r_1^2}$. Then momentum equation becomes

$$\frac{dP}{dx} + \rho_g \cdot g + \frac{\rho_g}{R_2(r_2^2 - r_1^2)} \frac{d}{dx} \int_{r_m}^{r_2} u^2 r\, dr$$

$$= - \frac{2 r_2 \tau_2}{R_2(r_2^2 - r_1^2)} \qquad (5)$$

4) For all the gas stream

Let $R_G = \dfrac{r_2^2 - r_i^2}{r_2^2 - r_1^2}$. Then momentum equation becomes

$$\frac{dP}{dx} + \rho_g \cdot g + \frac{\rho_g}{R_G(r_2^2 - r_1^2)} \frac{d}{dx} \int_{r_i}^{r_2} u^2 r\, dr$$

$$= - \frac{2(r_2 \tau_2 + r_i \tau_i)}{R_G(r_2^2 - r_1^2)} \qquad (6)$$

5) For both streams

$$\frac{1}{2}\frac{dP}{dx}(r_2^2 - r_1^2) + \frac{\rho_L g}{2}(r_i^2 - r_1^2) + \frac{\rho_g g}{2}(r_2^2 - r_i^2)$$

$$+ \frac{\rho_L}{2} \frac{d}{dx} \int_{r_1}^{r_i} u^2 r\, dr + \frac{\rho_g}{2} \frac{d}{dx} \int_{r_i}^{r_2} u^2 r\, dr$$

$$= - 2(r_2 \tau_2 + r_1 \tau_1)$$

By using notation of R_L and R_G, the above equation becomes

$$\frac{dP}{dx} + (\rho_L R_L + \rho_g R_G) g + \frac{\rho_L}{r_2^2 - r_1^2} \frac{d}{dx} \int_{r_1}^{r_i} u^2 r\, dr$$

$$\frac{\rho_g}{r_2^2 - r_1^2} \frac{d}{dx} \int_{r_i}^{r_2} u^2 r\, dr = -2 \frac{(r_2 \tau_2 + r_1 \tau_1)}{r_2^2 - r_1^2} \qquad (7)$$

From the fact that the kinetic term is negligible compared with other terms, one may neglect the kinetic term. By dividing Equation (4) by Equation (5), one may obtain

$$\frac{\tau_i}{\tau_2} = \frac{r_2}{r_i}\frac{R_1}{R_2} \tag{8}$$

Finally, from the above equations and assumptions made, the shear stress at inner wall, interface and outer wall are

$$\tau_1 = \frac{1}{r_1}\{r_i\tau_i - (\frac{dP}{dx} + \rho_L \frac{g}{g_c})\frac{(r_i^2 - r_1^2)}{2}\} \tag{9}$$

$$\tau_i = \tau_2 \frac{r_2}{r_i}\frac{R_1}{R_2} \tag{10}$$

$$\tau_2 = -\frac{(r_2^2 - r_m^2)}{2r_2}(\frac{dP}{dx} + \rho_g \frac{g}{g_c}) \tag{11}$$

Another method to estimate the momentum transfer at the air-water interface is to utilize the energy transfer mechanism of ocean waves which was derived by Miles. Assuming the energy transfer mechanism in the climbing film flow is the same as in ocean waves, Miles' momentum transfer at the interface,

$$F = -\rho_g \overline{uv} = -\rho_g c \frac{\pi}{k}(\frac{U_c''}{U_c'})\overline{v_c}^2$$

can be used, where u and v are velocity component in air stream.

EXPERIMENTAL PROGRAM

The main objectives of this experiment were to investigate the mechanism of both the air flow and the liquid film flow in the annular duct.

Most previous investigations have been conducted using smooth pipe and the climbing water film formed on the inner wall of the pipe as mentioned in the previous section. This type of flow has been called two-phase annular flow. It was proposed at the outset of the present investigation that the film would be formed on the outer surface of the inner core of an annulus, with the outer wall remaining dry, the upward climbing film of water being carried by a cocurrent air stream flowing in the 35-foot long annular duct.

In order to accomplish the above-mentioned objectives, the following experimental program was undertaken.

1) An investigation on small scale apparatus to determine minimum air flow rate and pressure to maintain stable climbing film flow. Data obtained were used to design a large test section.

2) A study of the pressure gradients with and without the climbing film in two different regions, A and B, which are shown in Figure (4). Flow conditions used in the experimental work are shown in Table (I).

Table (I) Range of variable studied.

Air Flow Rate*	Water Flow Rate
From 170 cfm	0.47 lb_m per minute
To 400 cfm	0.79 lb_m per minute

* At 1 atm. and 68° F

3) Measurement of mean air velocity profile to determine effect of the presence of the climbing water film. The mean velocity profiles were measured at two locations at various air mean velocities between 85 ft/sec and 150 ft/sec and at 0.47 lbm/min and 0.79 lbm/min water flow rate.

4) Direct measurements of shear stress on the wall of the inner core (wetted) and of the outer wall (dry) to compare with pressure gradient results.

5) Measurement of the average film thickness, wave length, and wave amplitude in order to determine the characteristics of the liquid flow.

DESCRIPTION OF APPARATUS

General Description of the Column

The column consisted of a three-inch inside diameter outer tube and a one-inch outside diameter inner core. The outer tube and flanges were all plexiglas (Acrylic plastic) while aluminum tube was used as the inner core. This inner tube was supported laterally by sets of streamlined centering screws. The total length of the column was about 35 feet including a 20-foot long test section. The first measurement location was 76 inches above the liquid injector and the second was 78 inches above the first. These dimensions were determined after consideration of the entrance and end effects. A sketch of the column is shown in Figure (3).

The column had four major parts as follows:

(1) The air source, including the heat exchanger and calming section,

(2) The liquid injection section,

(3) The test section,

(4) The air-water separator.

With the exception of the test section (Figure 4), the parts are described in detail on the following pages.

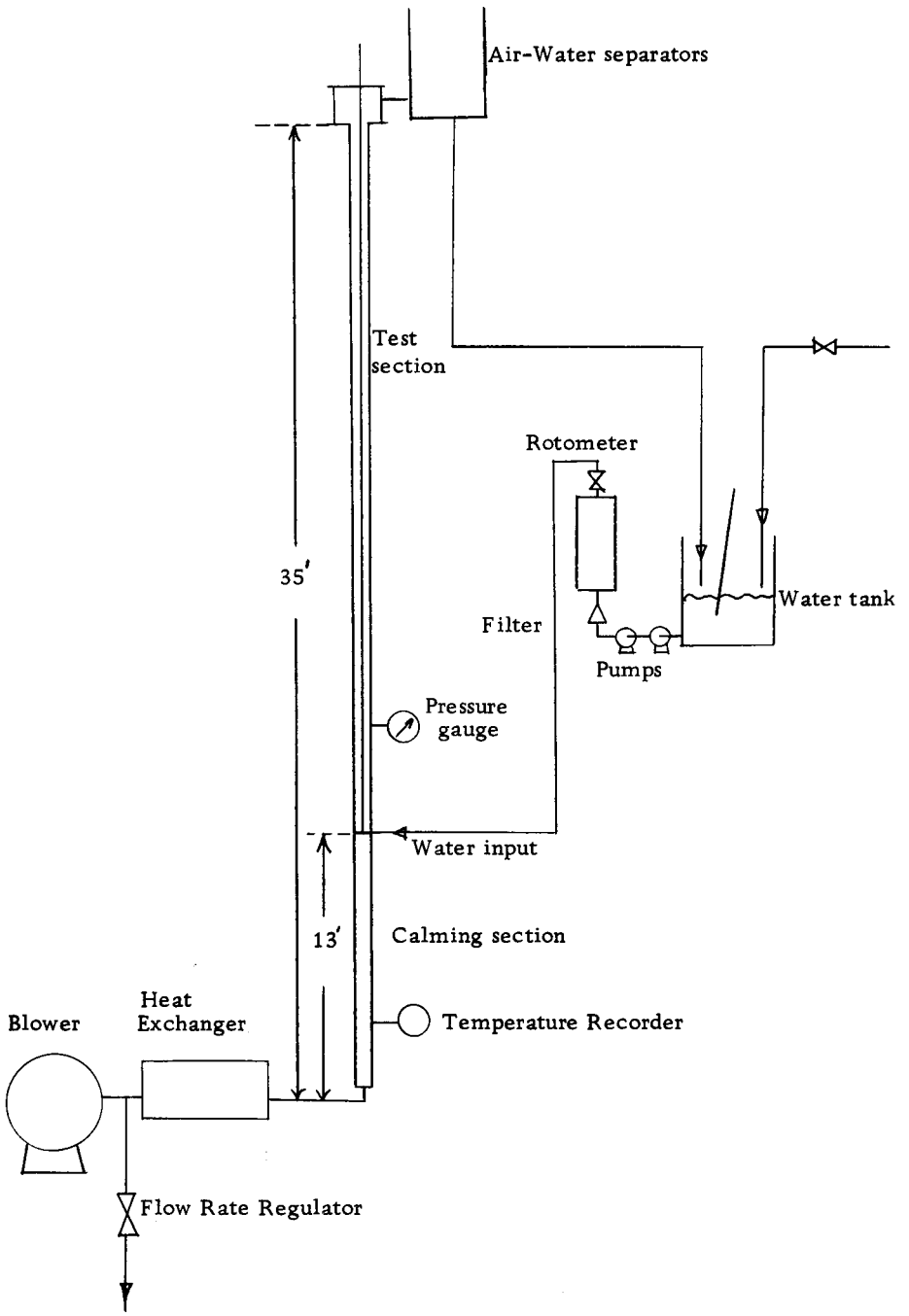

Figure (3) Schematic Flow Diagram.

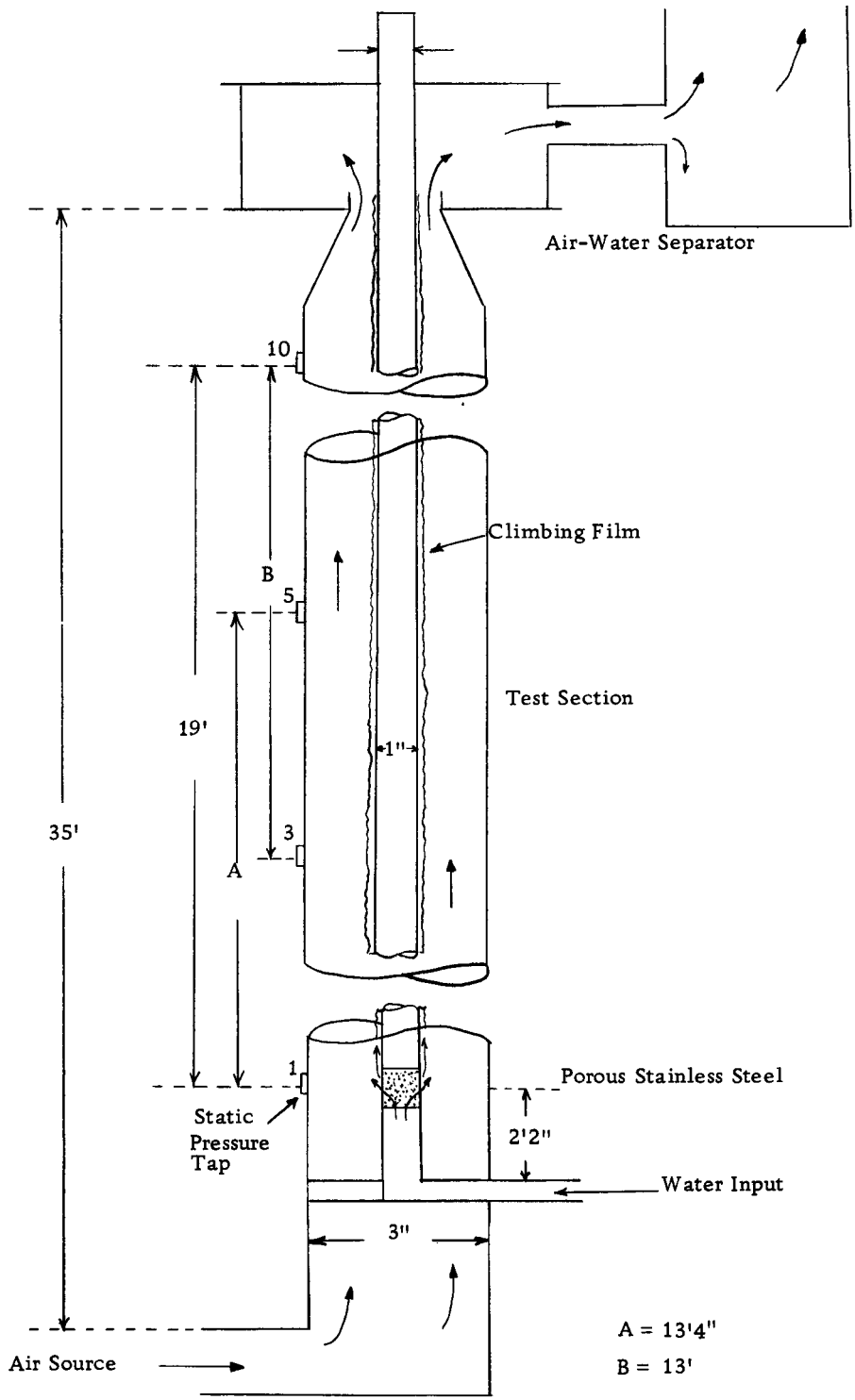

Figure (4) Test Section.

Air Source

The air was supplied by a Sutorbilt 8HB blower, which was driven by 30 HP, 1760 RPM General Electric A-C induction motor. The blower was rated at 550 cfm (1 atm., 68 F) at 9 psi outlet pressure. The size of blower was determined by the preliminary experiments which indicated the minimum flow rate and pressure of air to maintain a stable film was about 200 cfm and 1.5 psi respectively.

The air from the blower passed through a water cooled finned tube heat exchanger. Outlet air temperature was recorded continuously. The cooled air passed through a calming section which consisted of seven, 15 inch long and 7/8 inch diameter copper tubes.

In order to eliminate the vibration from the blower, two flexible tubes, 10 inch long, were installed between the blower and the heat exchanger, and between the heat exchanger and test section.

Liquid Injection

The water was pumped from a water tank into the inner core (Figure 5) and then passed through a porous stainless steel section into the annulus (Figure 6). The porous section, one inch outside diameter and 3/64 inch thick, was a two inch long hollow cylinder.

Air-water Separator

At the top of the column two air-water separators were used to recover the water for re-use. Near the top, the outside tube converged from a 3-inch to a 2-inch diameter tube over a length of $5\frac{1}{2}$ inches so that the air completely carried out all the water. The tube then diverged rapidly to 10 inches at the top of the column. After the first expansion, the air-water mixture passed to an 8.5 cubic foot drum which was completely open at one end and the inlet of which was a 3-inch pipe inserted tangentially to the surface of drum so that the air-water mixture would flow, as in a cyclone separator.

The reducing section, Figure (7), was made from laminated plexiglas and had a conical hole, which varied from 3 inches at one end to 2 inches at the other end drilled through it. The first expansion section, Figure (7), was a short brass cylinder 10 inches in diameter.

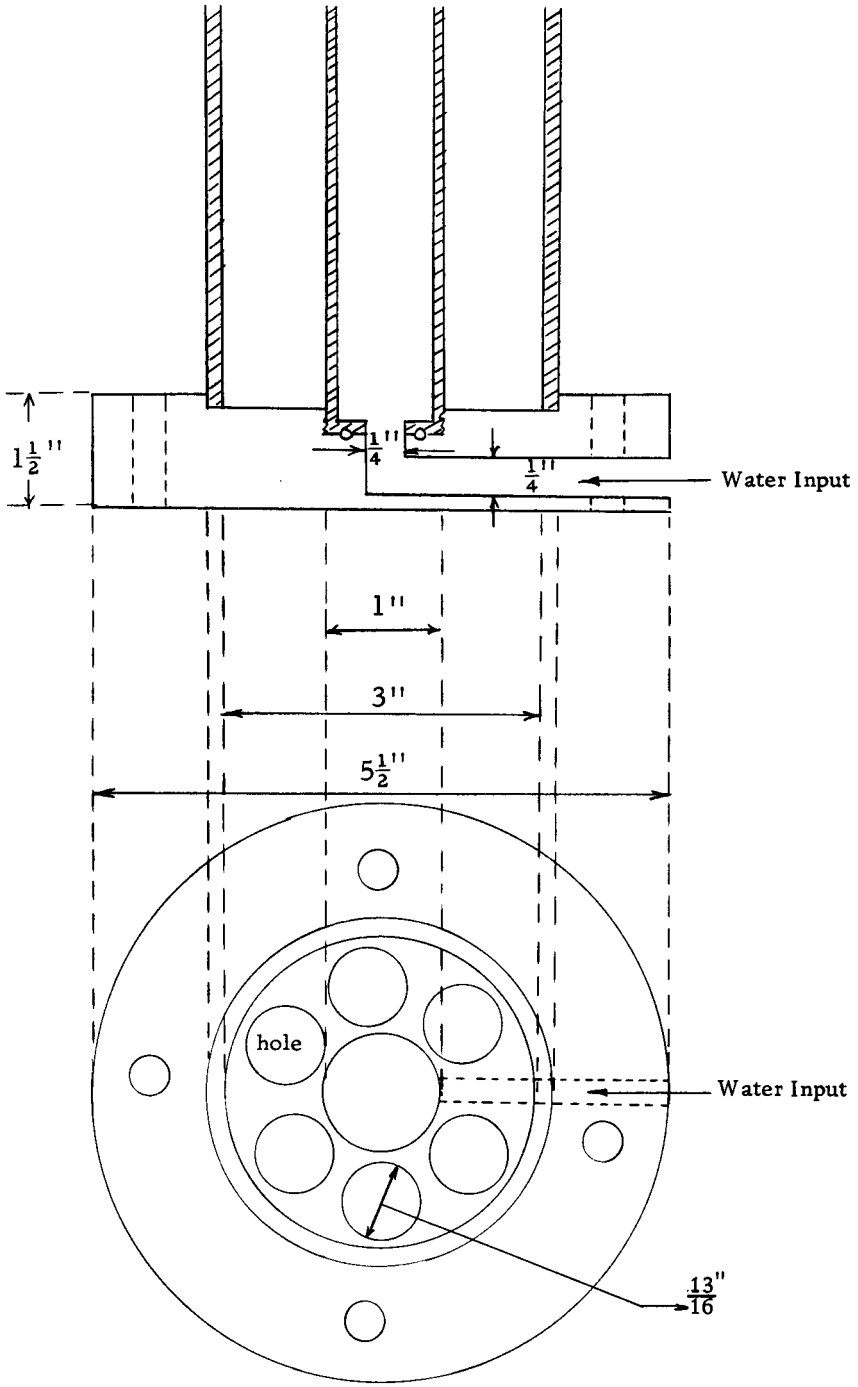

Figure (5) Liquid injection system.

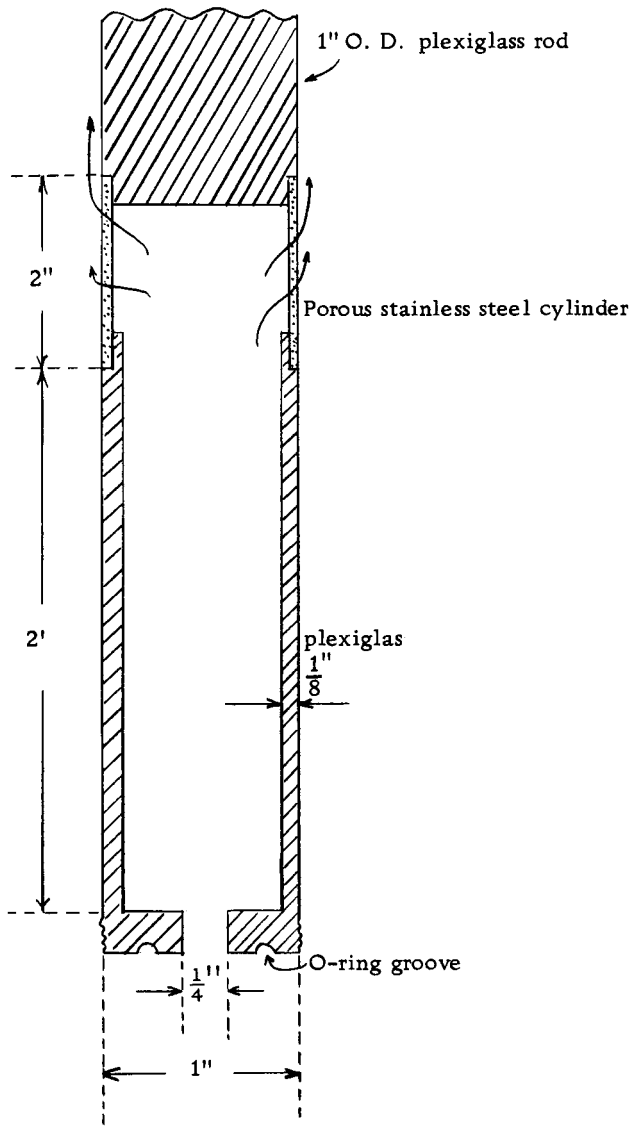

Figure (6) Liquid injector.

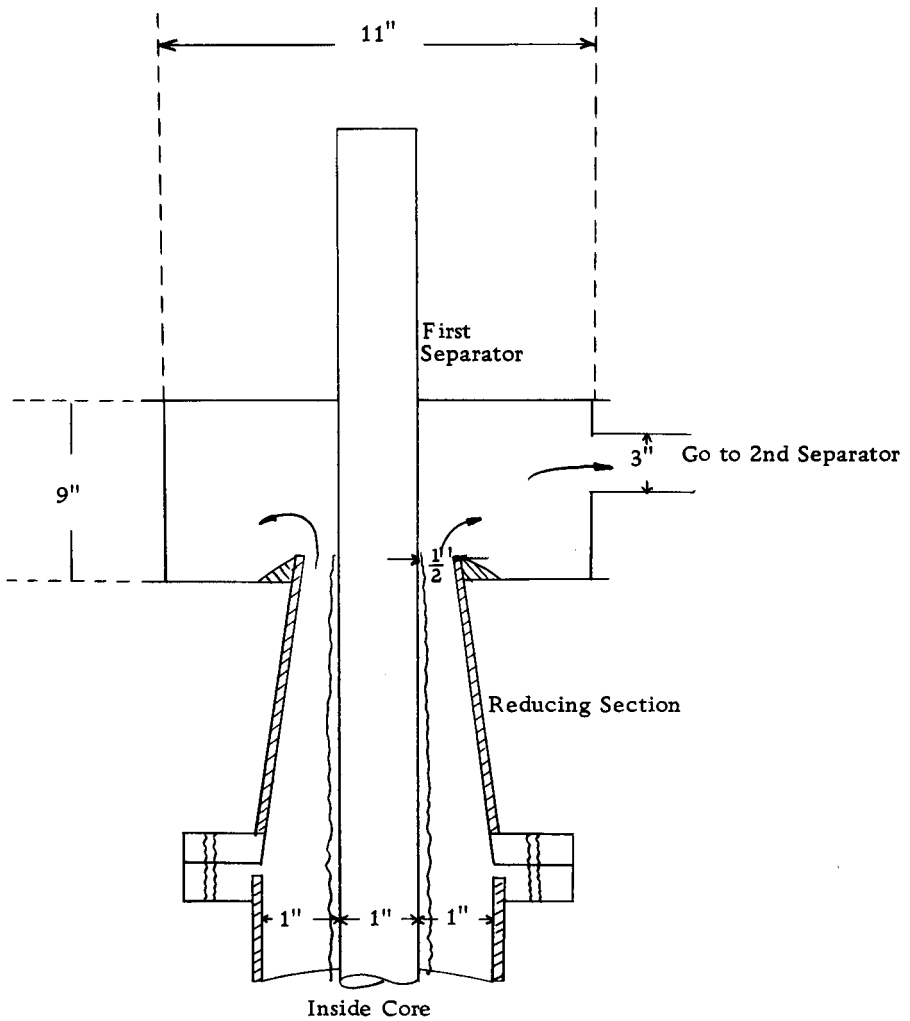

Figure (7) Reducing Section and First Air-Water Separator.

EXPERIMENTAL EQUIPMENT

Measurement of Shear Stress

Shear Stress on the Dry Wall

A Preston tube was used to measure the shear stress on the dry wall. Ludwieg and Tillman (34) established, within the limits of experimental accuracy, that there is a region near the wall in which equation $\frac{U}{U^*} = f(\frac{yU^*}{\nu})$, is satisfied, where $U^* = \sqrt{\frac{\tau_w}{\rho}}$ and f is a certain function. This means that the velocity in this region is a function only of the variables ρ, μ, τ_w and some suitable length. However, the velocity is related to the difference of kinetic pressure and static pressure. Consequently, if one is able to define the certain function F which gives relationship between the difference of kinetic and static pressure and the friction on the wall similar to following equation

$$\frac{(P_k - P)d^2}{\rho\nu^2} = F\left(\frac{\tau_w d^2}{\rho\nu^2}\right)$$

where P_k is kinetic pressure, P static pressure and d outside diameter of circular pitot tube, then τ_w, the shear stress at the wall, can be determined from the measurement of difference of kinetic and static pressure near the wall by using a pitot tube which is in

contact with the wall. Theoretically, the function F can be derived from equation

$$\frac{U}{U^*} = f\left(\frac{yU^*}{\nu}\right).$$

Preston applied the above theory for measuring the shear stress and experimentally found the relationship (42),

$$\log\frac{\tau_w d^2}{4\rho\nu^2} = 2.604 + \frac{7}{8}\log\frac{(P_k - P)d^2}{4\rho\nu^2} \qquad (1)$$

Two Preston tubes were made out of 0.0544-inch stainless steel hypodermic tubing, and 1/8 inch brass tubes shown in Figure (8). The calibration to find the function F was carried out in the annulus used, but with only air flowing. Description of calibration and calibration curve is shown in Appendix (I).

Shear Stress on the Wetted Wall

Since it is inconvenient to use a Preston tube to measure shear stresses on the wetted wall of the column, a heating element was developed for this purpose. The theory of shear stress measurement by means of the heating element is shown in Appendix (II).

As shown in Figure (9), the heating element consisted of the heating wire and the heated surface (called the heating element) from which heat is transferred into the annulus. One junction of the Copper-Constantan, 30 BWG thermocouple was inserted in the heating element, the other in the water tank, to measure the

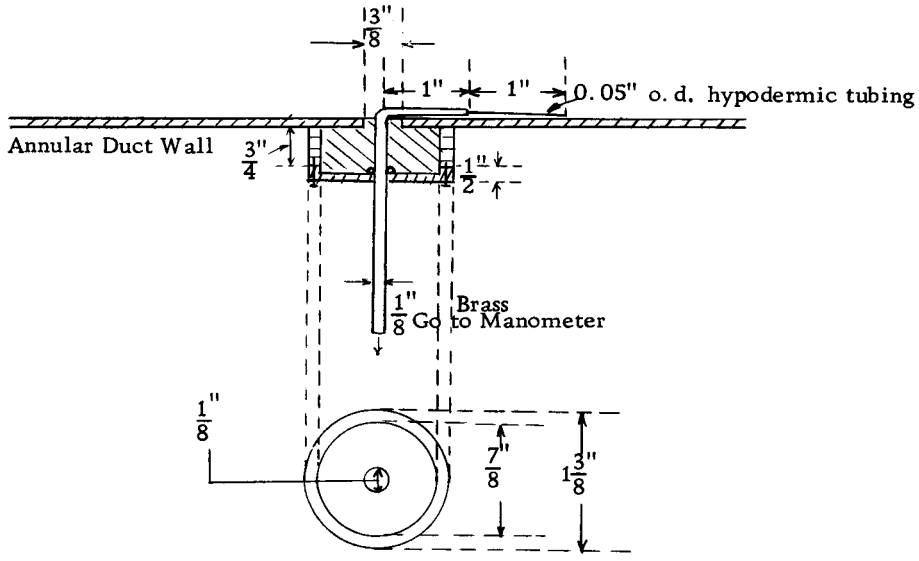

Figure (8) Preston Tube.

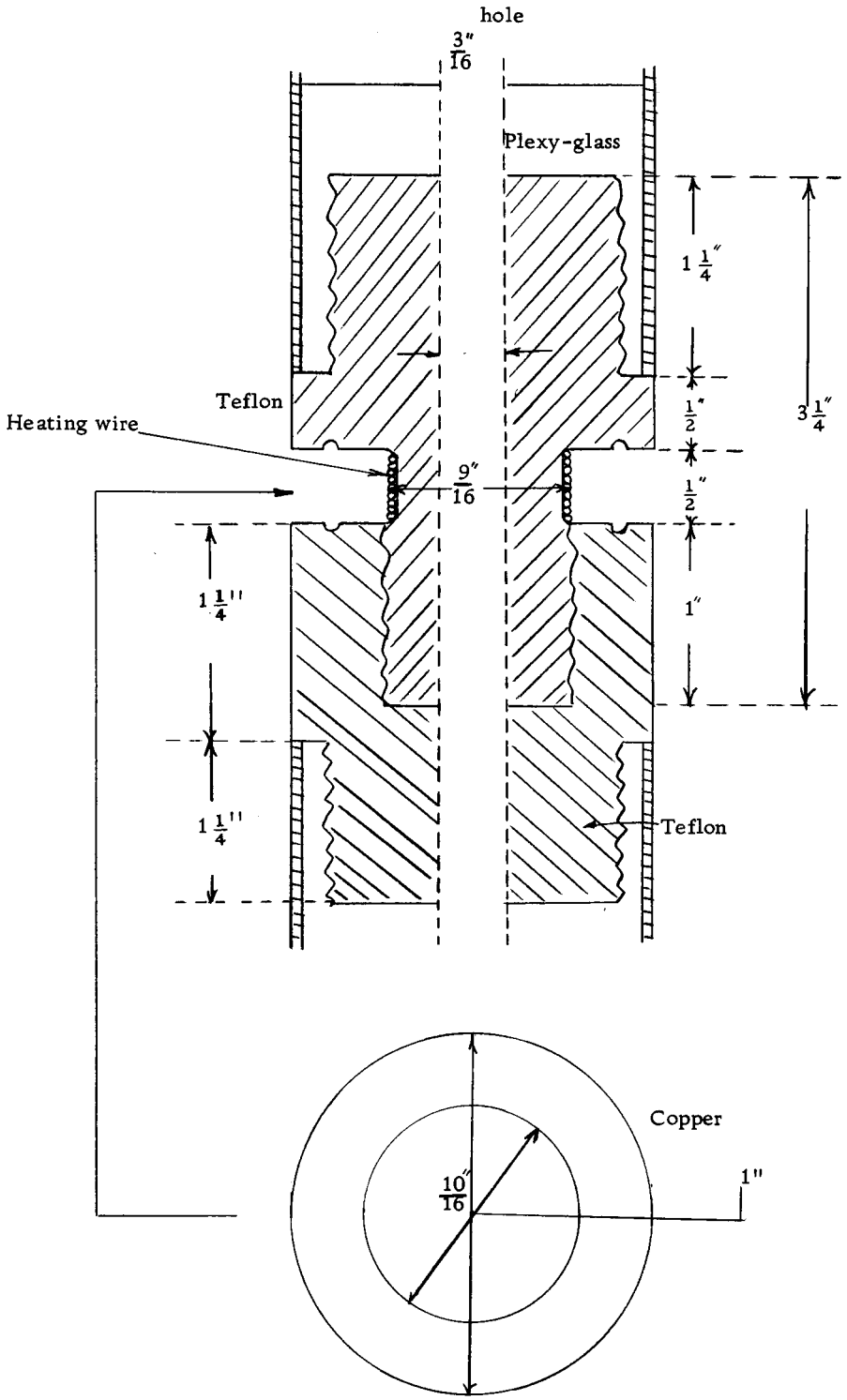

Figure (9) Heating Element.

temperature differences between the element and the fluid.

In order to have good heat and electrical insulation, teflon was used as the main body of the element. The resistance wire was a 28 BWG enameled wire and with resistance of 2.61 ohms per foot. The outer portion of the heating element was copper.

The heating element was calibrated in a 10-foot long annular column filled with water. The outside tube was 2 inches in diameter, the inner core was 1 inch in diameter. The calibration curve is also shown in Appendix (II).

Measurement of the Air Velocity Profile

A pitot tube, 0.02 inch O.D., was used to measure the air velocity profile in the annulus. The tube was mounted on a traversing mechanism and the position determined by means of a Tumico dial indicator which has 1 inch range and 0.0005 inch scale. Static and kinetic pressure taps were connected to a 50-inch inclined (14.27° from the horizontal) differential manometer which was filled with a fluid with a specific gravity of 0.83.

Measurement of the Film Characteristics: Film Thickness, Wave Length and Amplitude

Numerous methods to measure the thickness of thin films have been proposed. They are, for example, the conductance,

light absorption, photographic and fluorescence spectrometer methods. Since both wave length and amplitude as well as film thickness were to be determined, a photographic method was used. The discussion of this technique is presented by Collier and Hewitt (6).

The photographs were taken with one-foot long magnifier box and a Hasselblad camera, model 1000 F, with an 80mm standard lens which is a coated Carl Zeiss Tessar f/2. 8 lens with preselector for the Hasselblad. It can focus down 20 inches from the film plane. The above extension box had a magnification of 7X to 10X.

An electronic stroboscope was used in order to obtain the short flash duration necessary to stop the motion of the climbing film. This was a model 1531-A Strobotac manufactured by the General Radio Company. The medium intensity single flash of 2. 2 million beam candlepower with a 1. 2 microsecond duration (measured at one-third peak intensity) gave satisfactory results.

The photographs were taken on Kodak Tri-X Panchromatic film which has an ASA rating of 400.

The method employed was to focus in the plane normal both to the inner core and to the two hypodermic (0. 05 inch) needles which were inserted as a reference scale. The light from the strobotac was arranged to come from behind the inner core. The resultant image, therefore, gave a sharp outline of the air-water interface or the inner tube wall-air interface.

Measurement of Flow Rates

Air Flow Measurement

A two-inch, sharp-edged orifice plate was made from 1/16 inch brass sheet, seven inches in diameter to measure the air flow rates. Radius taps were installed. The orifice was calibrated with a critical flow prover, Meteric Orifice Flow Prover Type CR, size 2 made by the American Meter Company. The calibration was also checked by integration of the velocity profiles.

The calibration curve and the description of the technique used are shown in Appendix (III).

The pressure taps on each side of the orifice plate were connected to a 36-inch differential manometer which was filled with a fluid of specific gravity 2.962.

A pressure gage and open mercury filled manometer were installed to measure absolute pressure at the entrance of test section.

Water Flow Measurement

A 1/3-hp and a 1/15-hp Eastern pump were connected in series between the water tank and the porous injection section. A pressure gage and filter, the General Filter, model 1A-25A, made by

General Filters, Inc., Novi, Mich, were mounted at the pump exit. The operating water pressure was between 15 to 19 psi. The flow rate of water passing through the filter was measured by a rotameter, FM1048B made by Manostat Corporation, New York, which had been calibrated by the manufacturer.

Measurement of Pressure Gradient

Pressure gradients were measured by a 50-inch inclined (14. 27° from the horizontal) differential manometer which was filled with a fluid with a specific gravity 0. 83. Pressure taps (Figure 10) were connected to a 3/64 inch diameter static pressure tubes. All pressure taps, pitot tubes, and preston tubes were connected to a purging system which could supply about 20 psi dry air. A simplified schematic diagram of measurement of pressure gradient is shown in Figure (11).

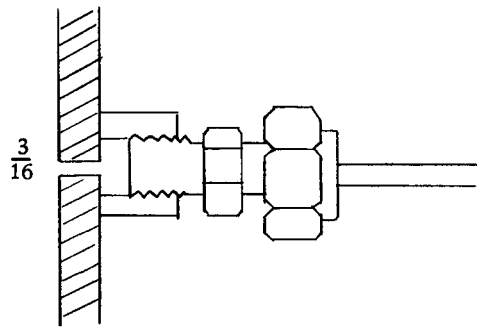

Figure (10) Pressure Top

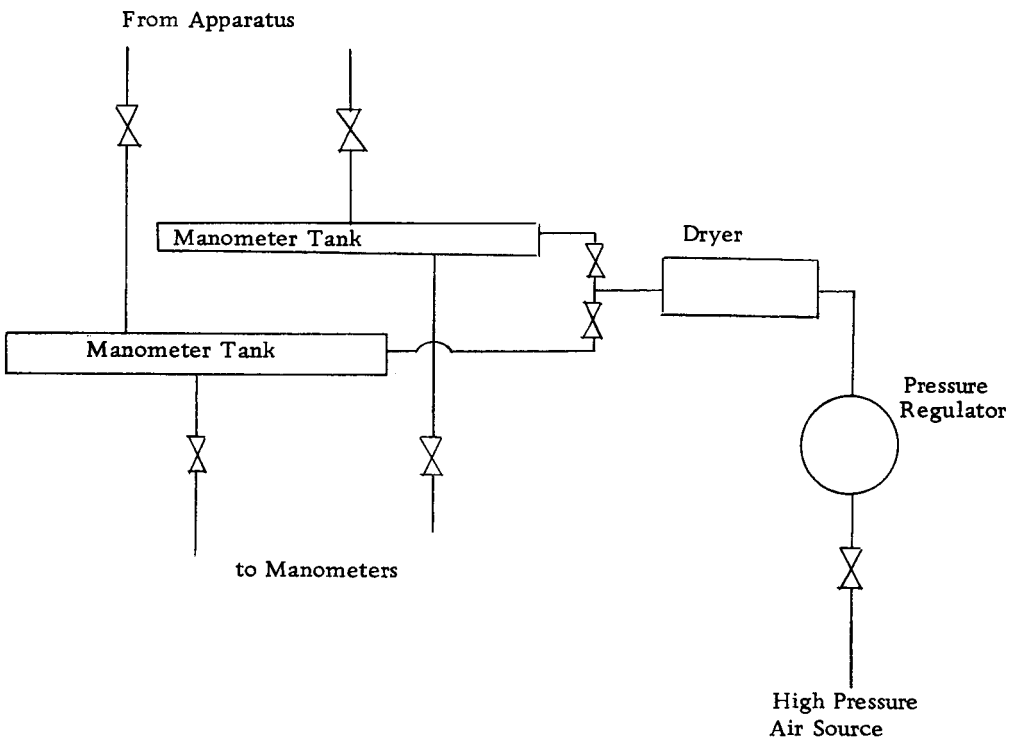

Figure (11) Purging system.

DISCUSSION OF RESULTS

Part One

Pressure Losses

Pressure losses for single phase air flow in the annulus were first determined. The test section was divided into two regions as shown in Figure (4) and pressure gradients were measured in each. This experiment showed that the pressure gradient in the top region was greater than in the bottom by six to seven percent. This indicated that the column was somewhat rougher in the top than in the bottom region. This may have been due to the different number of flange connections, roughness of flange connections, centering screws in each region, and the difficulty in making the two tubes concentric.

The friction factors* determined using the bottom pressure gradient measurement, are about 3.5 to 10.5 percent higher than the generally accepted values for smooth pipe flow for Reynolds numbers between 60,000 and 150,000. Those for the top region are about 12 to 14 percent higher than pipe-flow values. Brighton and Jones (3) report friction factors one to 10 percent higher than

---

*See Equation (13) in Theory Section 1.

pipe-flow values for Reynolds numbers between 60, 000 and 150, 000. From a comparison between the present data and that of Brighton and Jones it was concluded that the column was operating satisfactorily.

Axial-pressure-gradients and friction factors* for both single phase and for climbing film flow are shown in Figures (12), (13), (14), and (15) plotted as a function of air flow rate with water flow rate as a parameter. The results indicate that both top and bottom regions behave similarly. Approximately a 14. 5 to 19 percent increase in the single-phase flow pressure gradient occurred for water flow rate of 0. 47 lbm/min on the wall of inner core. Approximately a 22. 5 to 31 percent higher pressure-gradients were observed for 0. 79 lbm/min water flow rate in the climbing film.

From Figures (12) and (13) Blasius type friction factor equation in the annulus is $f = A(R_e)^{-0.19}$ where A is constant, depending upon the wall condition. The exponents on Reynolds number reported for smooth annulus in Knudsen and Katz (26, p. 198) are from -0. 20 to -0. 25. The agreement between previous work and present study is good. The tendency of decreasing slope as the water film appears can be seen from Figures (12) and (13).

---

*In calculation of the friction factors, the space occupied by water film was neglected since measurements showed that the film thickness was about 0. 01 inch or less.

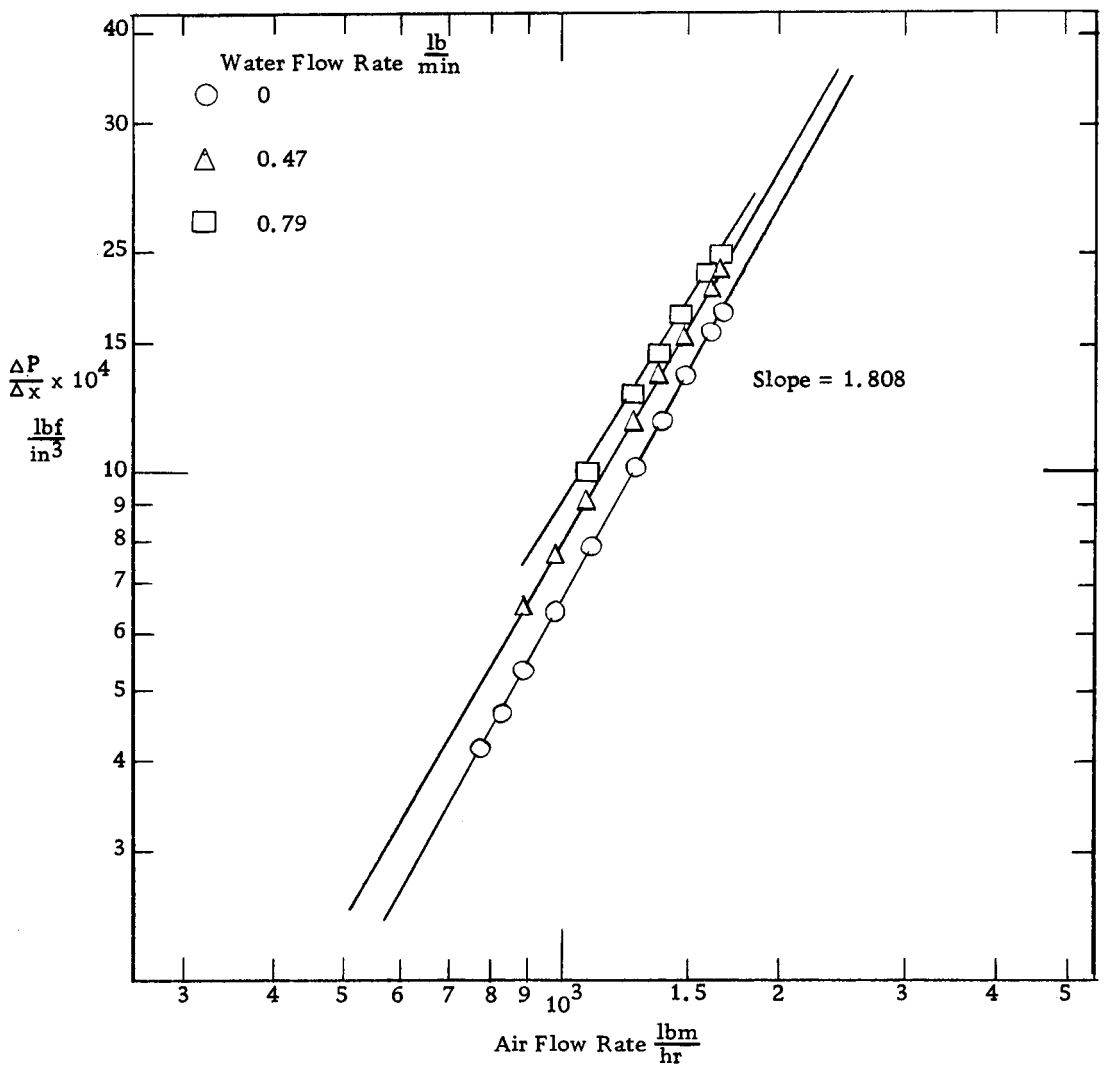

Figure (12) Pressure Losses at the bottom location.

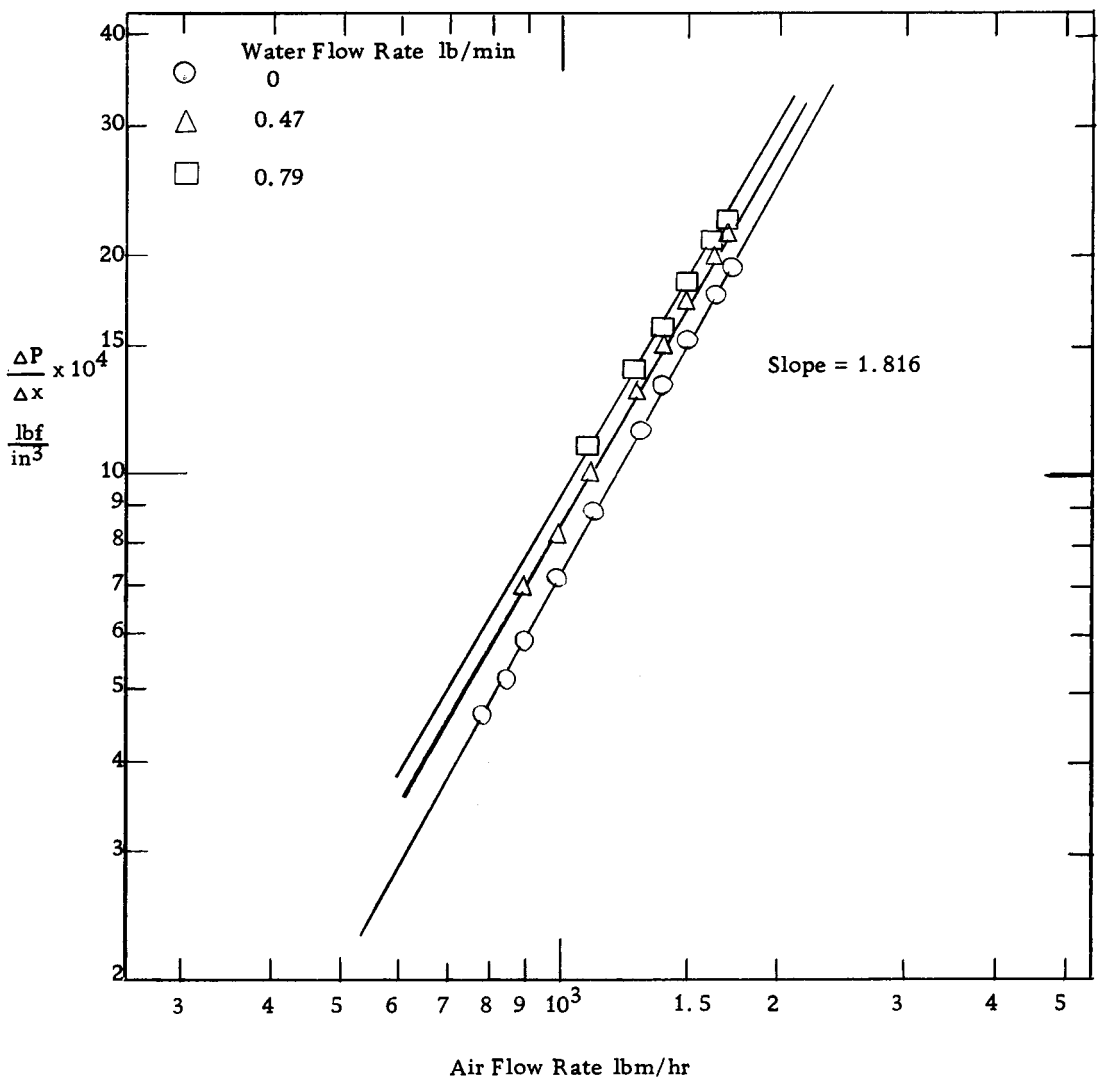

Figure (13) Pressure Losses at the top location.

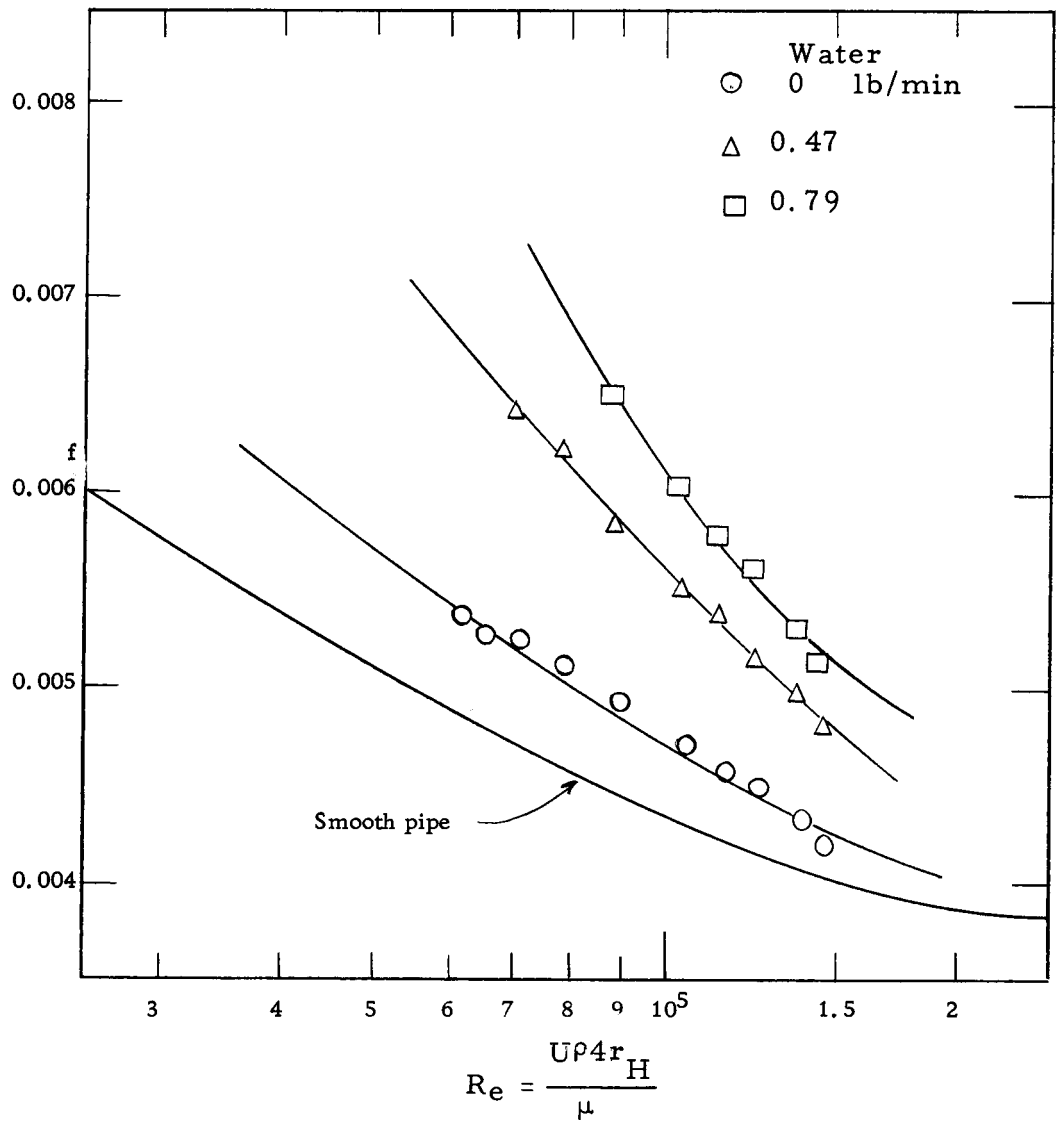

Figure (14) Friction Factors vs. Air Reynolds Numbers at the bottom location.

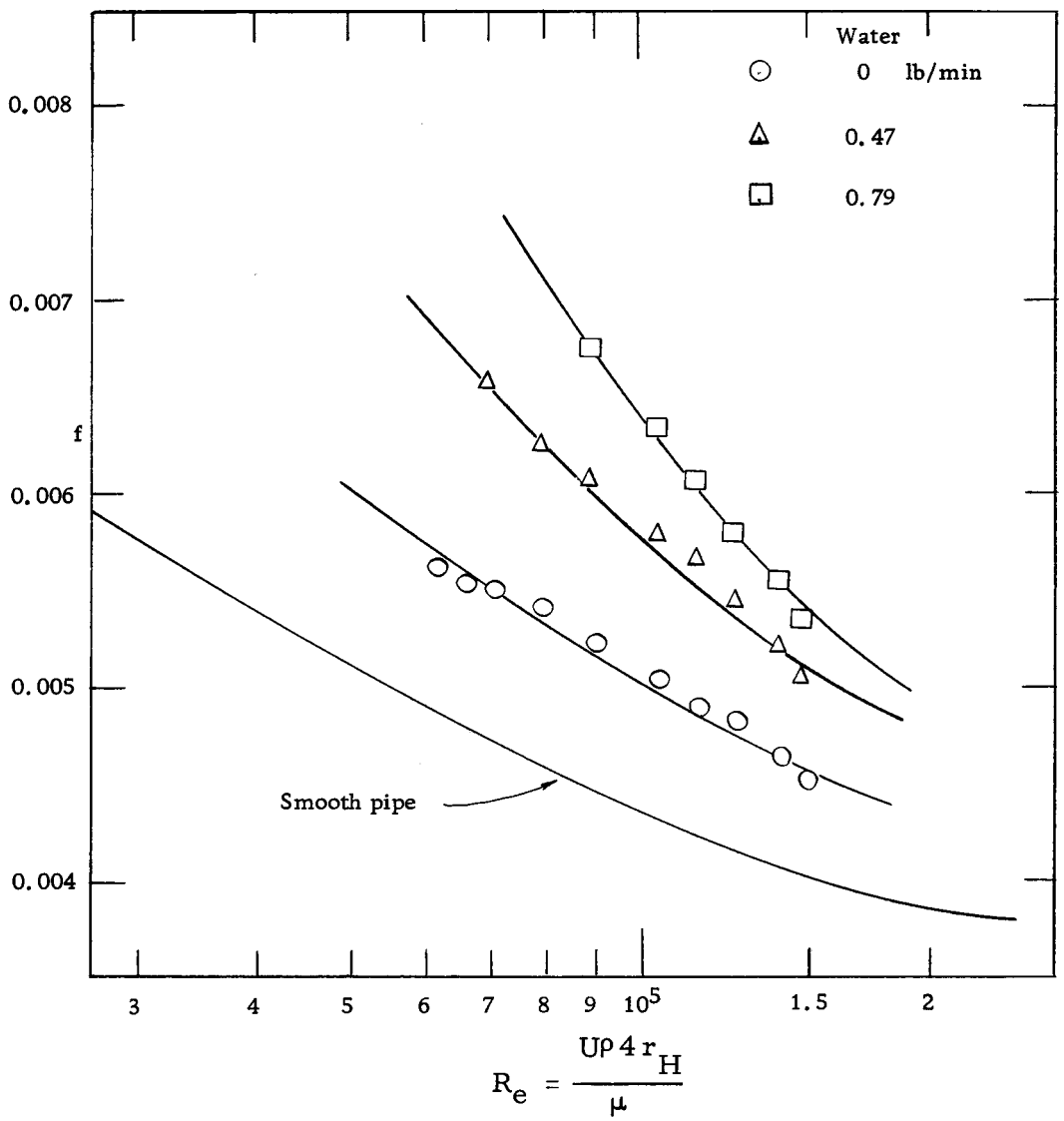

Figure (15) Friction Factors vs. Air Reynolds Numbers at the top location.

A more detailed discussion of pressure losses is presented subsequently in a combination with mean-velocity profile measurements, the water film thickness, wave length, and amplitude.

Mean-velocity Profiles

In order to test the precision of the flow measuring system and to determine the characteristics of the annular test section, the mean velocity profiles for single phase air flow were measured at two locations at various mean air velocities between 85 ft/sec and 150 ft/sec and integrations of the mean velocity were compared with the calibration of orifice by using a critical flow prover. The comparison is excellent as shown in Figure (37). The velocity profiles are shown as U/U_m versus $Y_1/r_2 - r_1$ in Figures (16) and (17). The bottom location is denoted as "a" and the top as "b". The mean-velocity profiles plotted in this manner, both at "a" and at "b", did not change for the range of air flow rates used. The profiles at these two points did not, however, agree with each other in the outer portion of the annulus. The outer portion of velocity profiles of "a" were flatter than those of "b". As mentioned in previous section, the velocity profiles with the diameter ratios 0.125 and 0.375 have been reported by Brighton and Jones. On Figure (18) were plotted the reported velocity profiles with the diameter ratios 0.125 and 0.375 and the present velocity profile, both at "a" and at "b", with a diameter

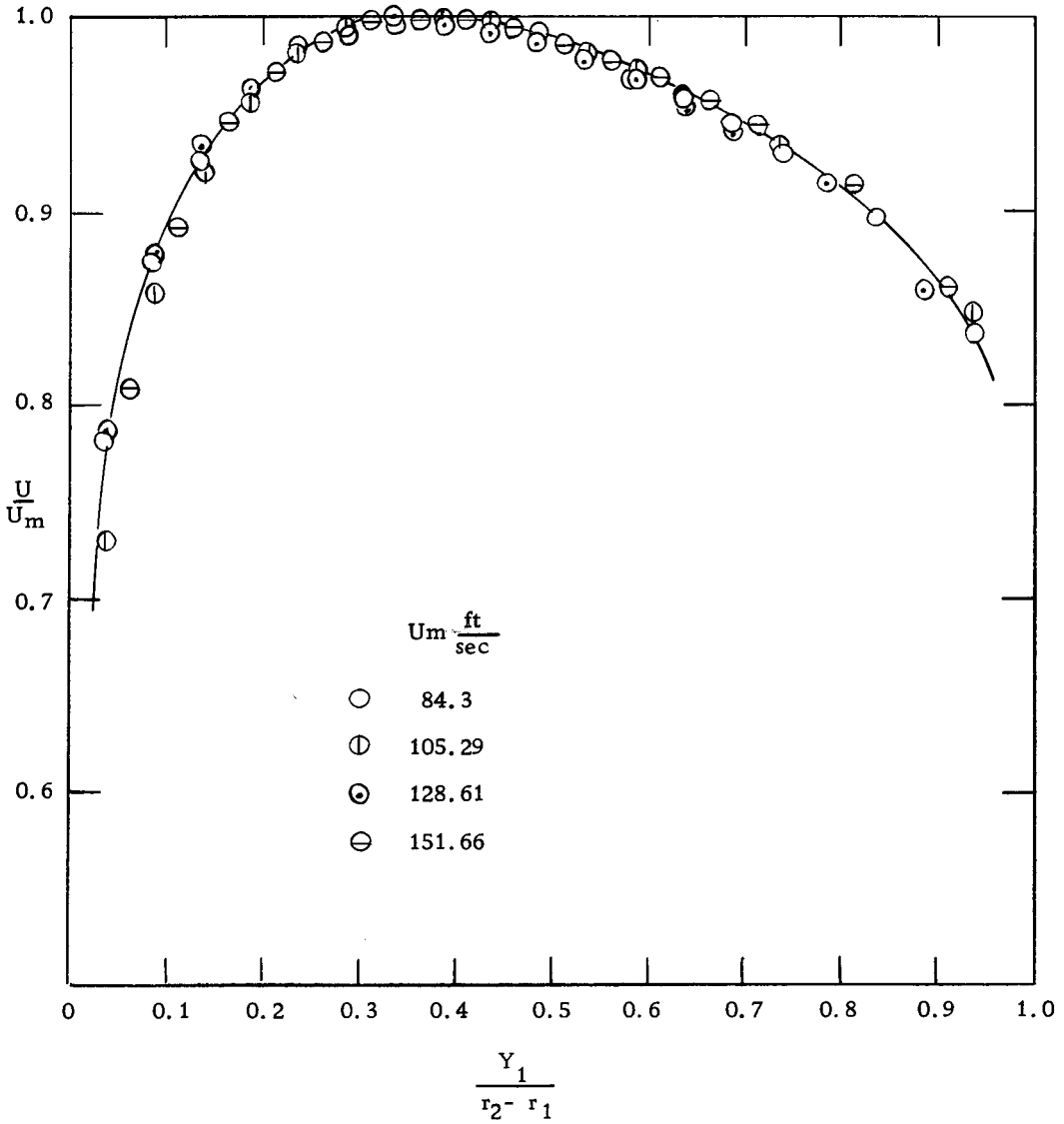

Water 0 lbm/min

Figure (16) Velocity Profile (Bottom)

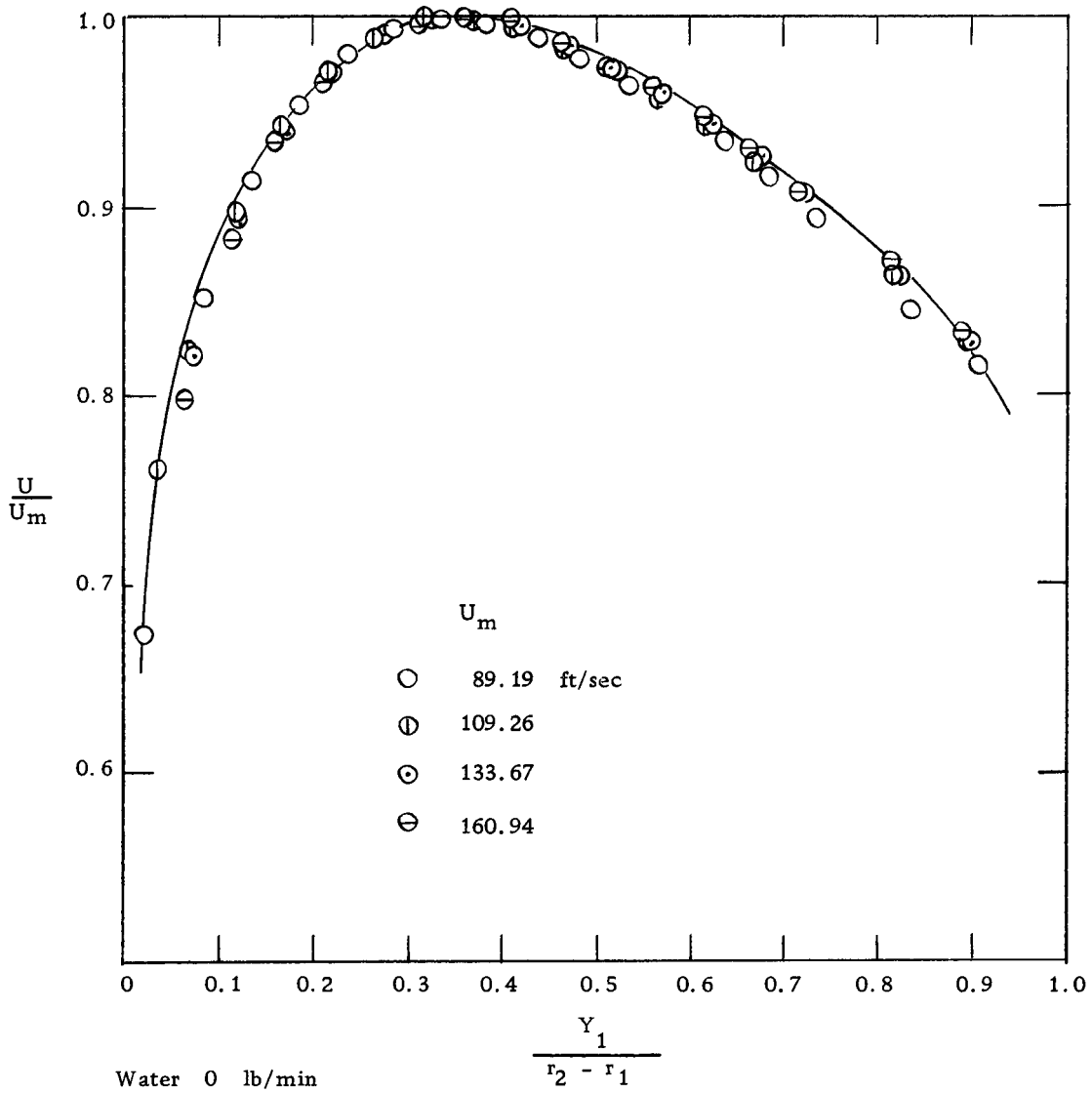

Figure (17) Velocity Profile (Top).

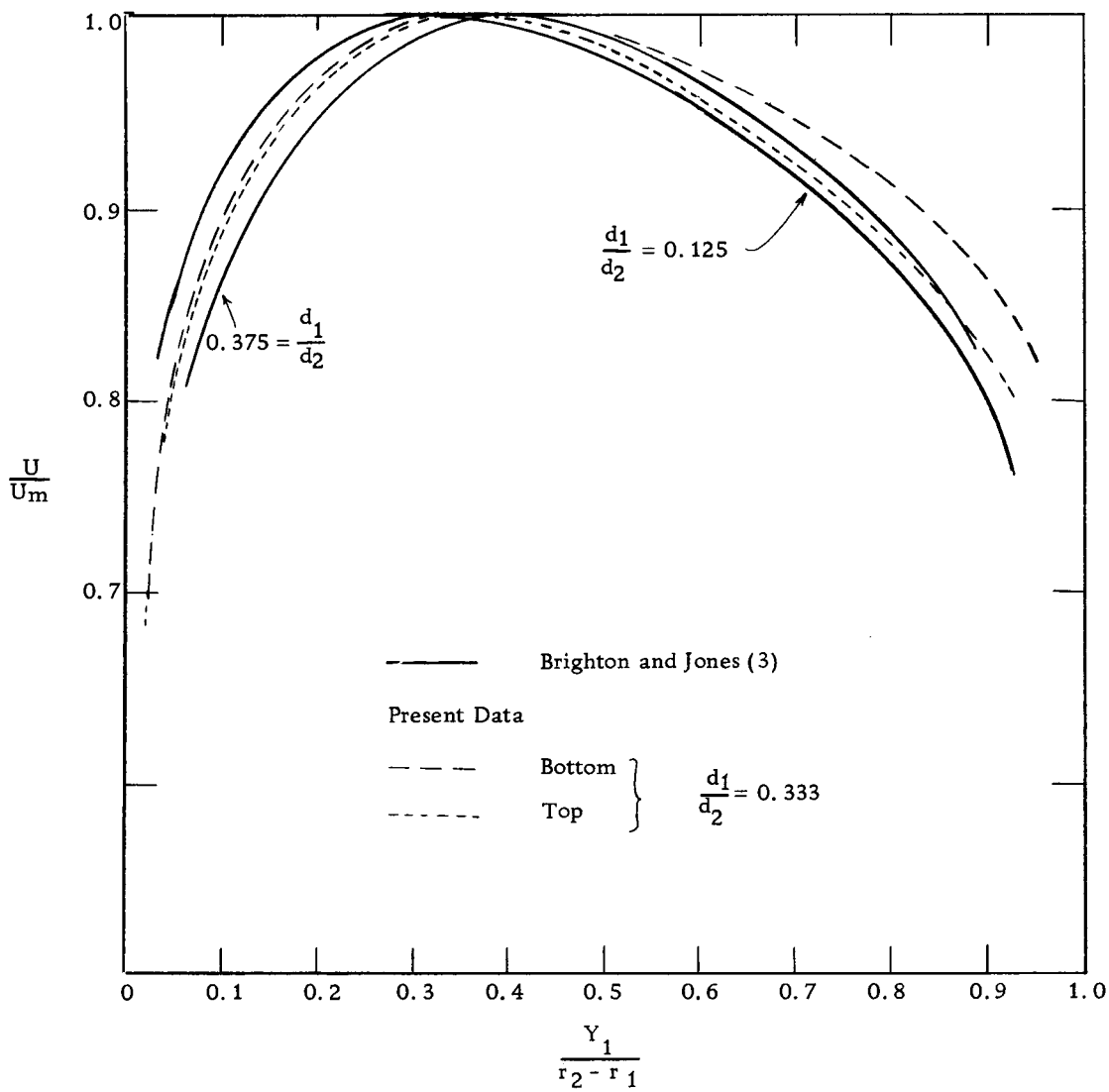

Figure (18) Comparison of Velocity profile.

ratio 0.333. From Figure (18) it was noted that the velocity profile at "b" is between the velocity profiles with a diameter ratio 0.125 and 0.375, whereas the velocity at "a" is outside of the velocity profile with a diameter ratio 0.375 in the outer portion of the annulus. It is, thus, concluded that entrance effects and roughness disturbances exist at the lower observation point. The lower pitot tube was located about five inches above a flange connection which may have been somewhat rough.

From the qualitative agreement of the observed mean-velocity profiles at the top station with the fully developed mean-velocity profiles reported by Brighton and Jones it was concluded that the measuring systems were operating satisfactorily.

For further calculations utilizing mean-velocity profiles only the measurements at the top station are used. The changes in mean-velocity profile due to the climbing liquid film at the bottom are reported, however.

The results of the measurements of the mean air velocity in the presence of the climbing film are plotted as U/U_m vs. Y_1/r_2-r_1 in Figures (19), (20), (21) and (22).

Qualitatively the mean velocity profiles of annular air flow with the climbing film present were modified so that the point of maximum velocity was shifted to the outer wall. This occurred to the same extent at both the top and bottom stations. There is no

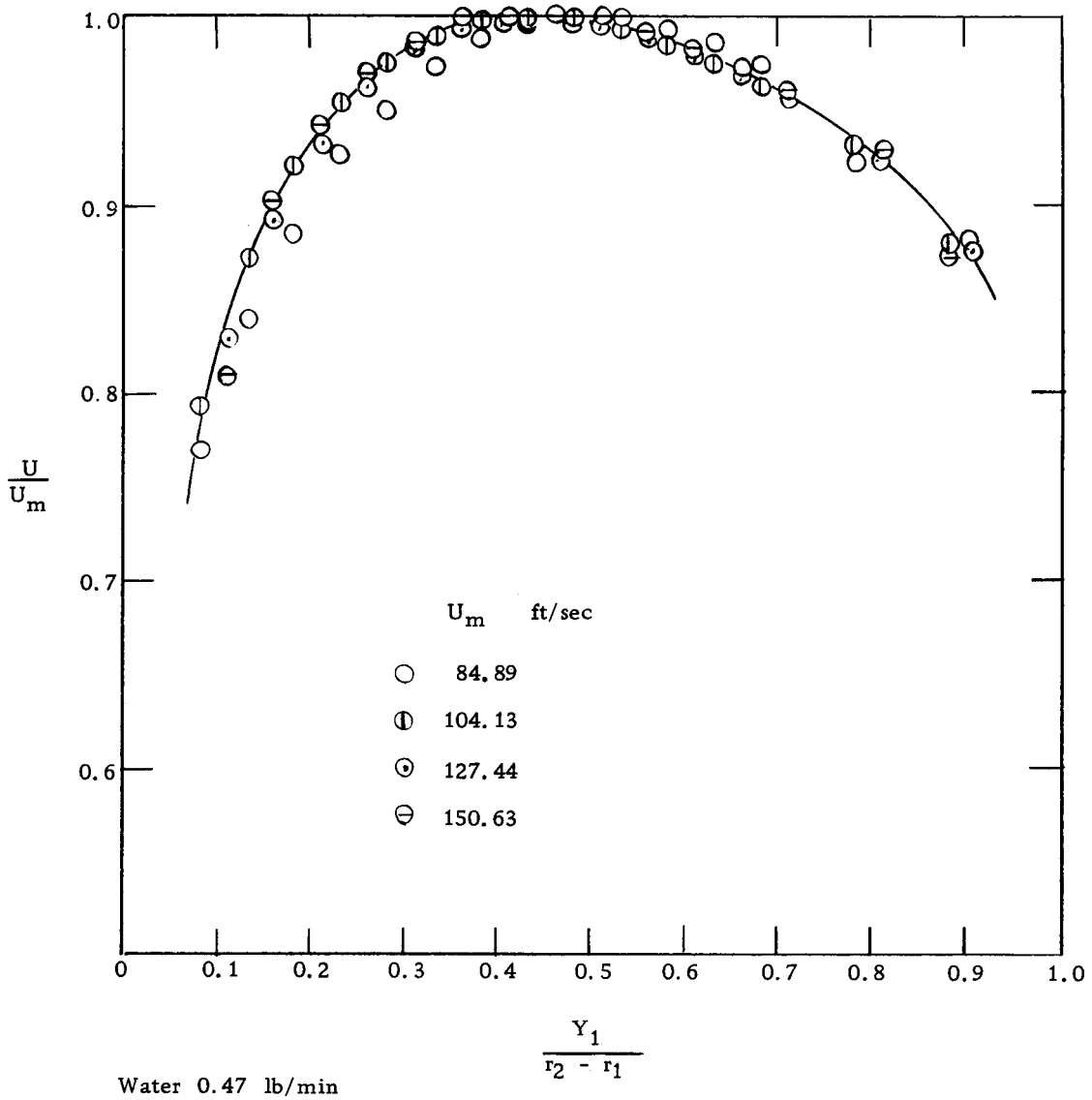

Figure (19) Velocity Profile (Bottom).

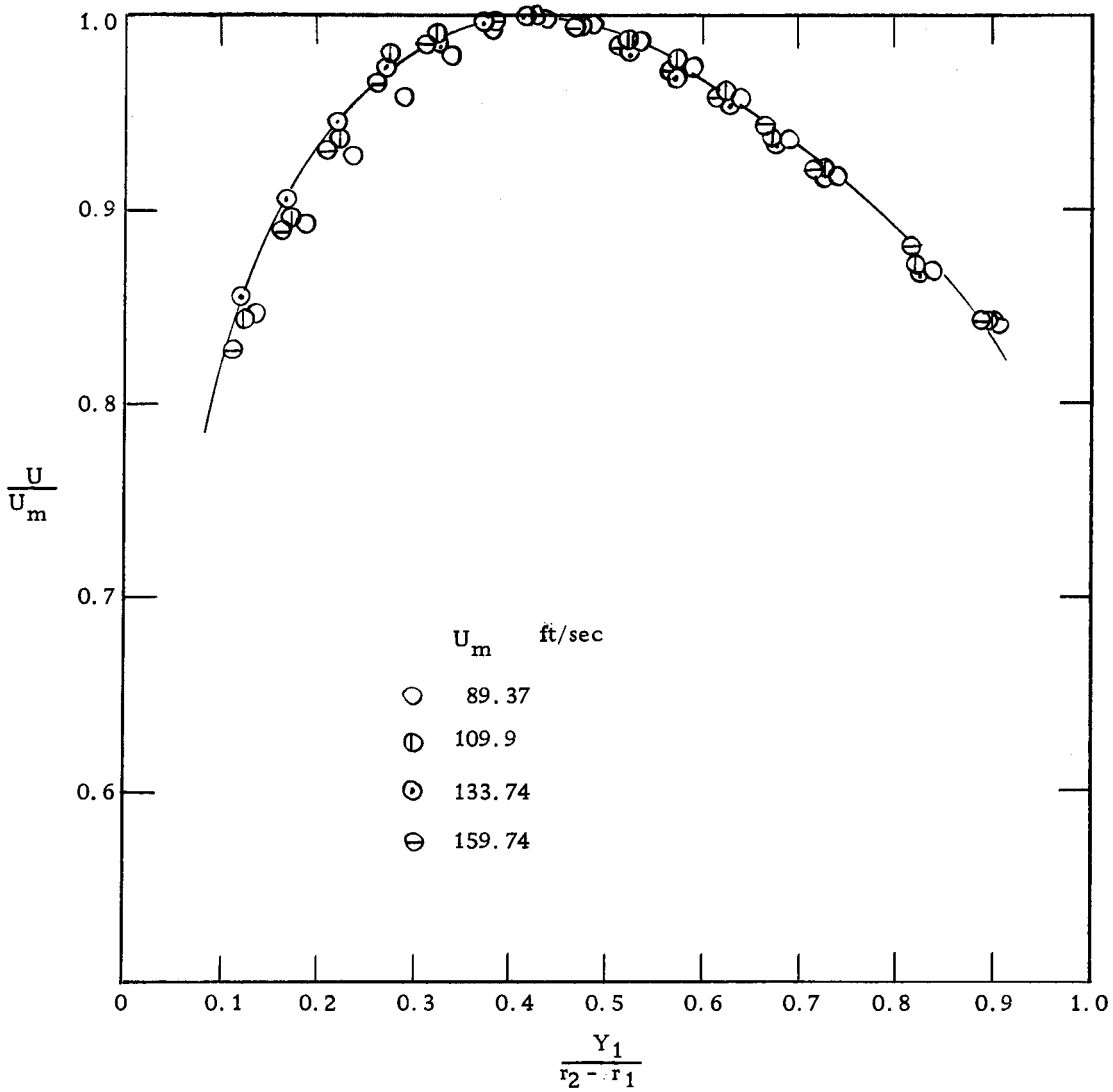

Figure (20) Velocity Profile (Top).

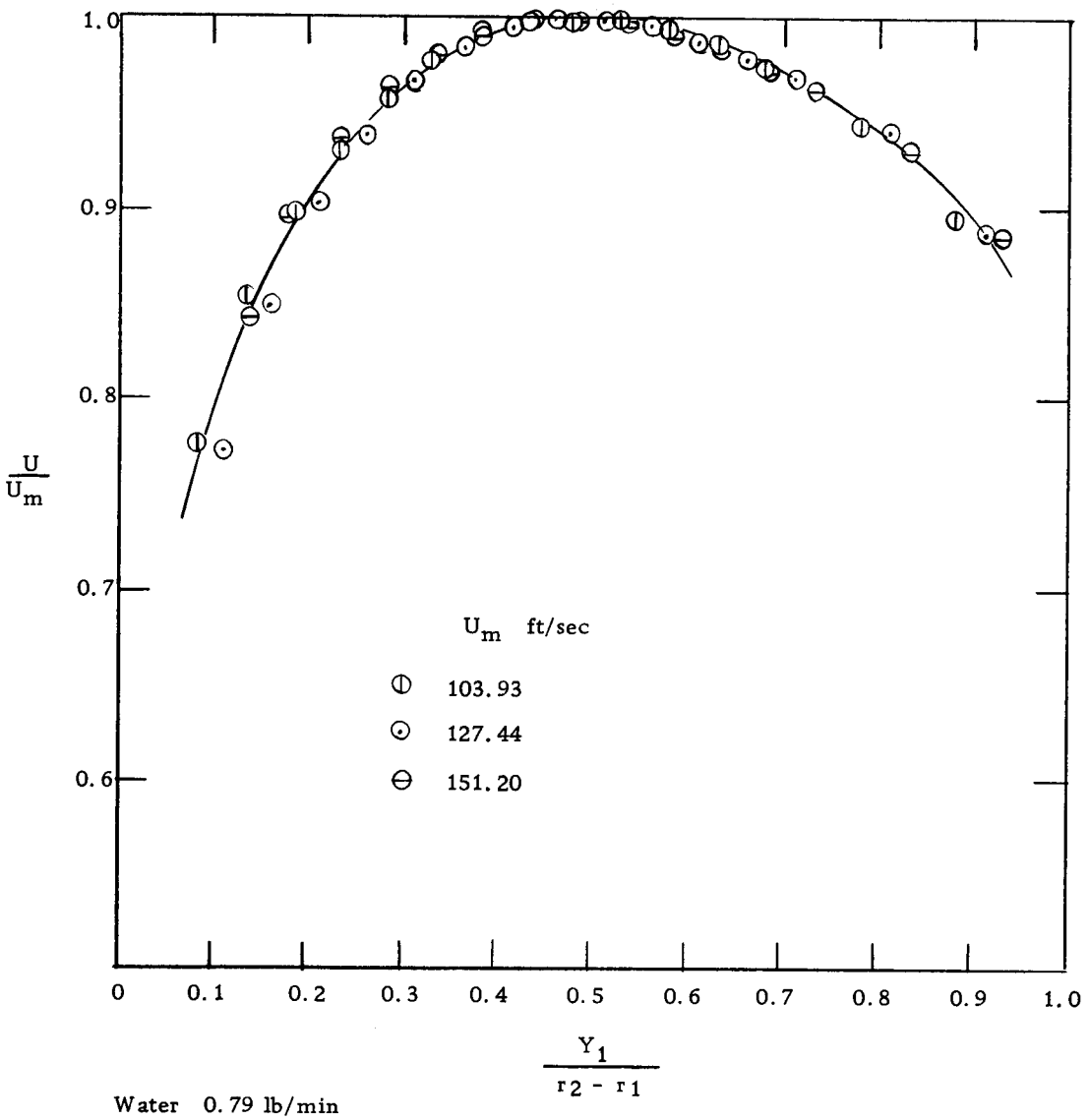

Figure (21) Velocity Profile (Bottom).

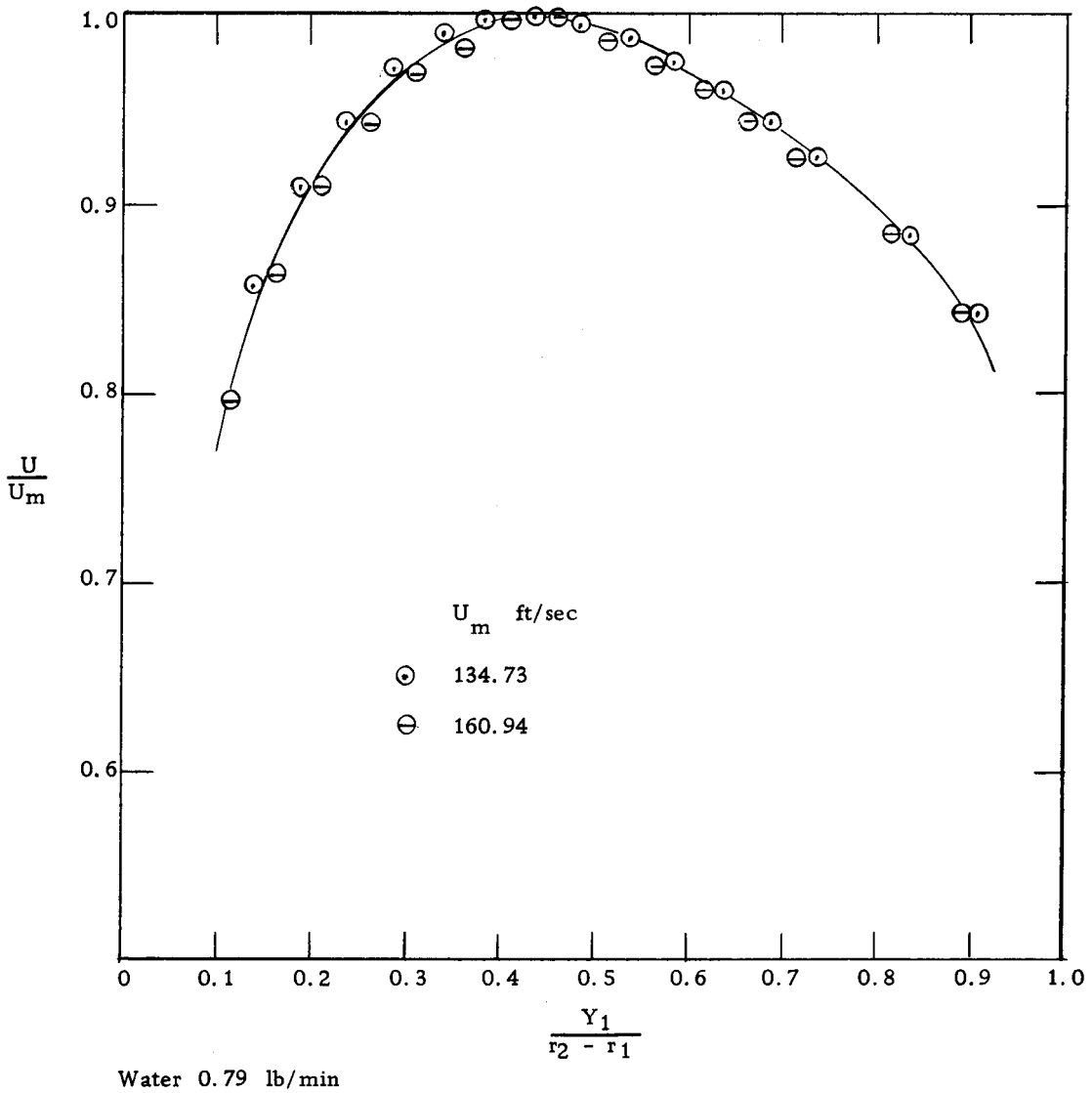

Figure (22) Velocity Profile (Top).

distinct difference in the mean-velocity profiles as the water flow rate is varied between 0.47 lbm/min to 0.79 lbm/min. There is also no difference in the profiles as the air flow rate changed from 190 cfm to 400 cfm (at 1 atm).

For the accurate determination of the point of maximum velocity, the velocity gradients in the region of maximum velocity were calculated by the method of orthogonal polynomials which are discussed by Wylie (48). By the method of least squares a portion of the data can be fitted by a curve of relatively low degree, say a parabola, and then the first derivatives at the central point of the set are taken as the smoothed gradient at that point. The smoothed value of the velocity gradient at the central point of the set, U_{-2}, U_{-1}, U_o, U_1, and U_2, is,

$$\frac{dU}{dy} = \frac{-2U_{-2} - U_{-1} + U_1 + 2U_2}{10\,h} \qquad (1)$$

where h is the equal interval between points. The velocity gradients calculated by this method in the region of maximum velocity are plotted in Appendix (IV). The locations of the maximum velocity (where $\frac{dU}{dy} = 0$) are shown in Table (II).

The mean-velocity gradient distribution in the region of maximum velocity is approximately linear as indicated by Brighton and Jones.

The variation of the point of maximum velocity, Y_m, as water

flow rate is changed from 0 lbm/min to 0.47 lbm/min and to 0.79 lbm/min can be seen from Figure (23) where $\frac{Y_m}{r_2-r_1}$ is plotted versus water flow rate. For the water flow rate 0.47 lbm/min, Y_m is shifted to the outer wall by about 0.055 inch from the position of maximum velocity for the dry wall, and Y_m for 0.79 lbm/min is moved to the outer wall by about 0.08 inch from the position of maximum velocity for the dry wall. The quantitative explanation for change of Y_m in the presence of the water film is not available. However it is discussed later on a qualitative basis. As mentioned in previous section, the present very limited knowledge of turbulent flow makes substantial theoretical progress in this area unlikely without appeal to the experimental study.

The variation of Y_m as air flow rate is changed from 190 cfm to 410 cfm can be seen in Table (II). The locations of the maximum velocity are constant for the range of air flow rates within experimental accuracy, except for the lowest flow rate.

By interpolation of the points of maximum velocities between the diameter ratio 0.125 and 0.375 reported by Brighton and Jones, the point of maximum velocity for the diameter ratio 0.333 was 0.40, whereas present Y_m is 0.36 and Y_m for the laminar flow 0.4539. The disagreement between present and previous Y_m is shown in Figure (24).

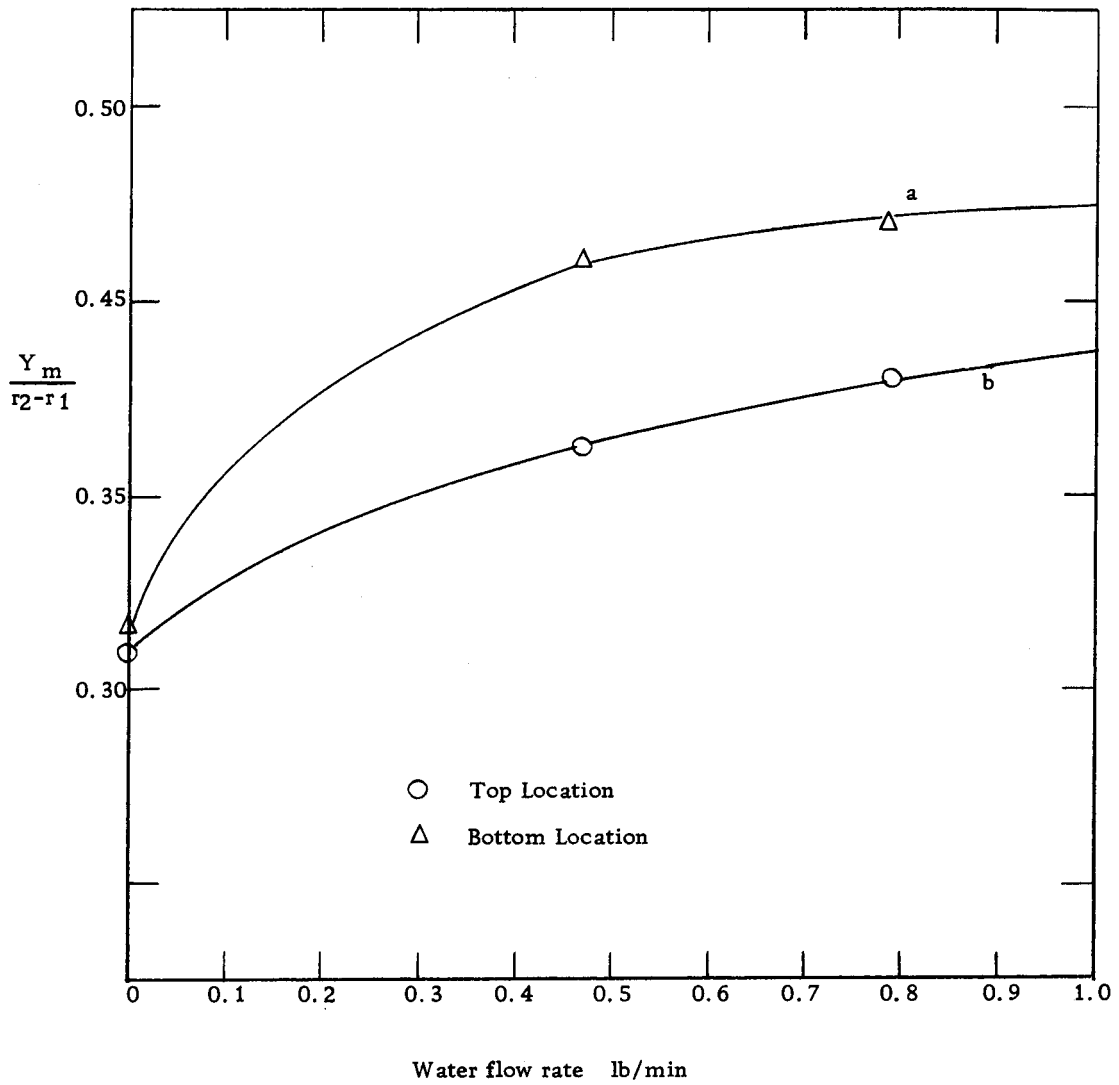

Figure (23) The variation of point of maximum velocity as water flow rate is changed.

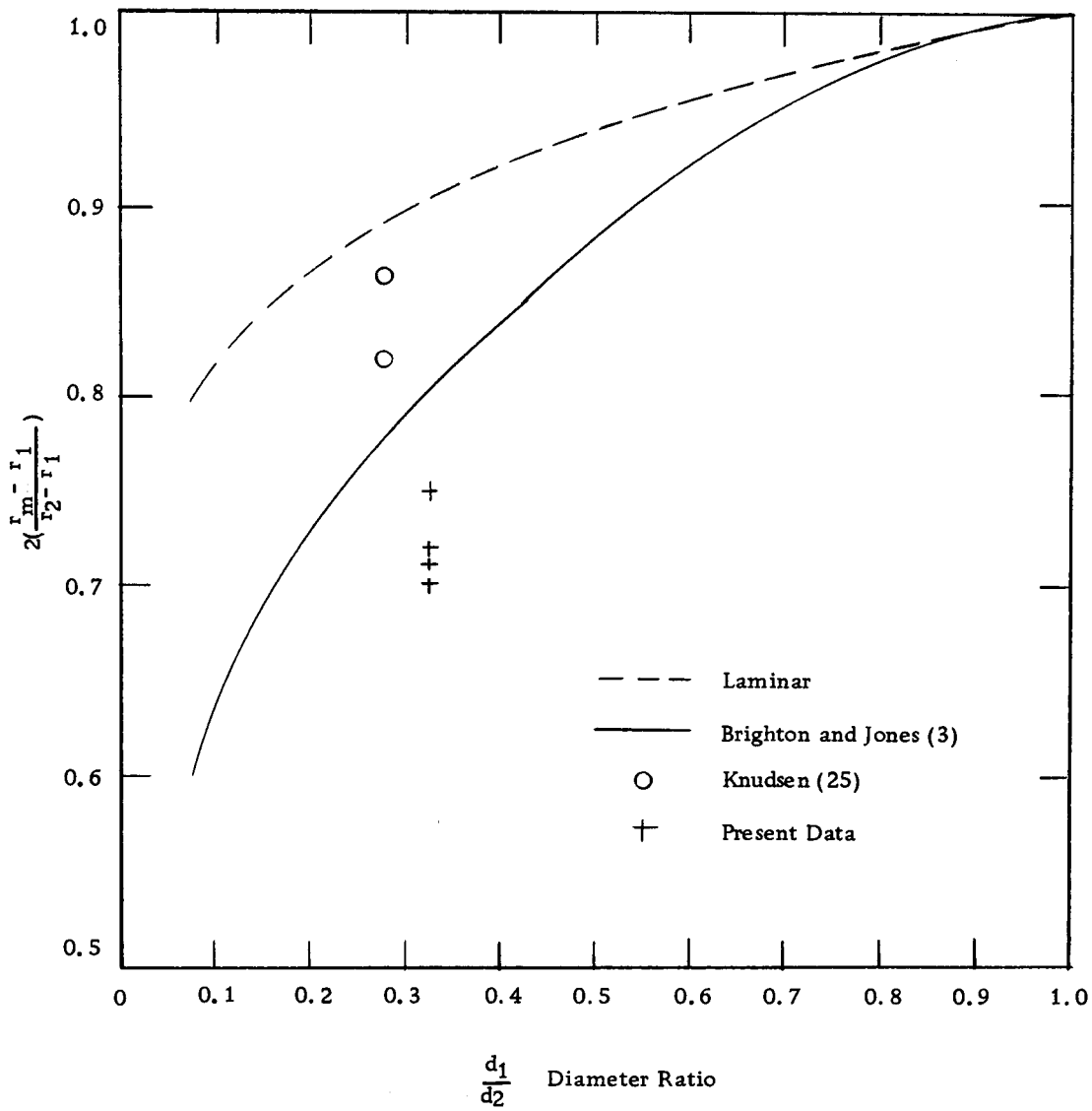

Figure (24) Points of maximum velocity.

Table (II) Points of maximum velocity.

Air Flow Rate cfm*	Water Flow Rate $\frac{lbm}{min}$	Point** of maximum velocity	Location
192	0	0.375	
245	0	0.375	
346	0	0.36	
411	0	0.352	
192	0.47	0.5	"a"
245	0.47	0.458	
346	0.47	0.451	
411	0.47	0.45	
245	0.79	0.487	
346	0.79	0.47	
411	0.79	0.47	
192	0	0.35	
245	0	0.35	
314	0	0.36	
411	0	0.355	
192	0.47	0.44	"b"
245	0.47	0.42	
314	0.47	0.405	
411	0.47	0.405	
314	0.79	0.43	
411	0.79	0.43	

* at 1 atm and 68°F

** The distance from inside wall to the point of maximum velocity in inches

Shear Stress Determinations

Shear Stress on the Dry Outer Wall

The results of direct measurement of shear stress on the outer wall (the dry wall) with the Preston tube at two locations at various air flow rates from 170 cfm to 400 cfm are shown in Tables (III) and (IV) and also plotted in Figures (25) and (26) as shear stress versus air flow rate with water flow rate as parameter.

The shear stresses* calculated from the location of the point of maximum velocity and the pressure gradient are also shown in Tables (III) and (IV). The direct measurements of shear stress are in agreement with those calculated within $\pm$ 4 percent.

The change in the shear stress on the outer wall due to the climbing film is very small. Whereas the 2.0 to 3.5 percent increase in the shear stress at 0.47 lbm/min water flow rate and 3.0 to 4.5 percent increase at 0.79 lbm/min water flow rate were observed at the bottom, about 3.5 percent increase at 0.47 lbm/min water flow rate and 6.0 percent increase at 7.9 lbm/min water flow rate were observed at the top as can be seen from Figures (25) and (26).

---

*Equation used

$$\tau_{w2} = -\frac{(r_2^2 - r_m^2)}{2r_2}\left(\frac{dP}{dx} + \rho_g \cdot \frac{g}{gc}\right)$$

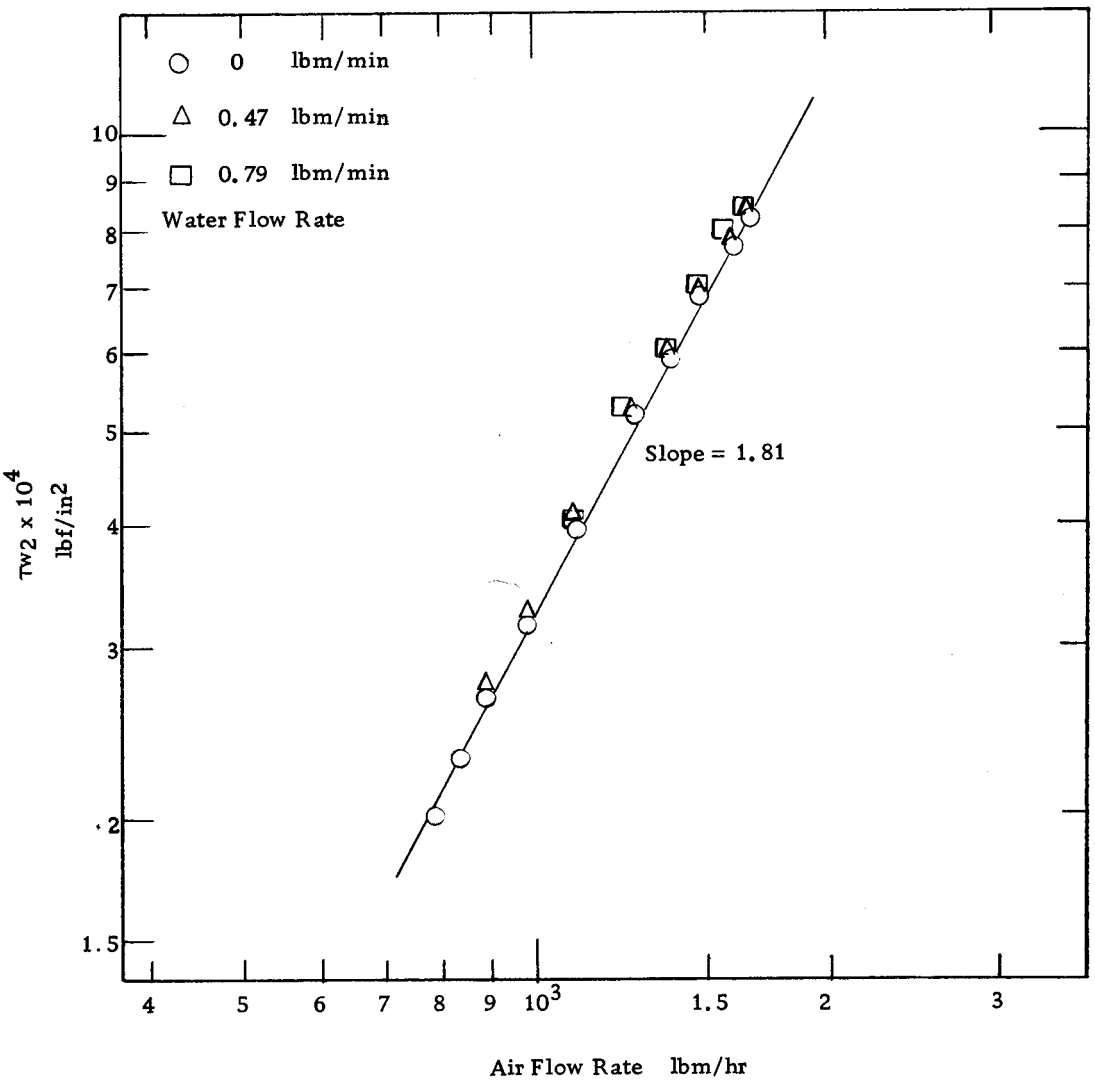

Figure (25) Shear stress on the outer wall (dry) at the bottom location.

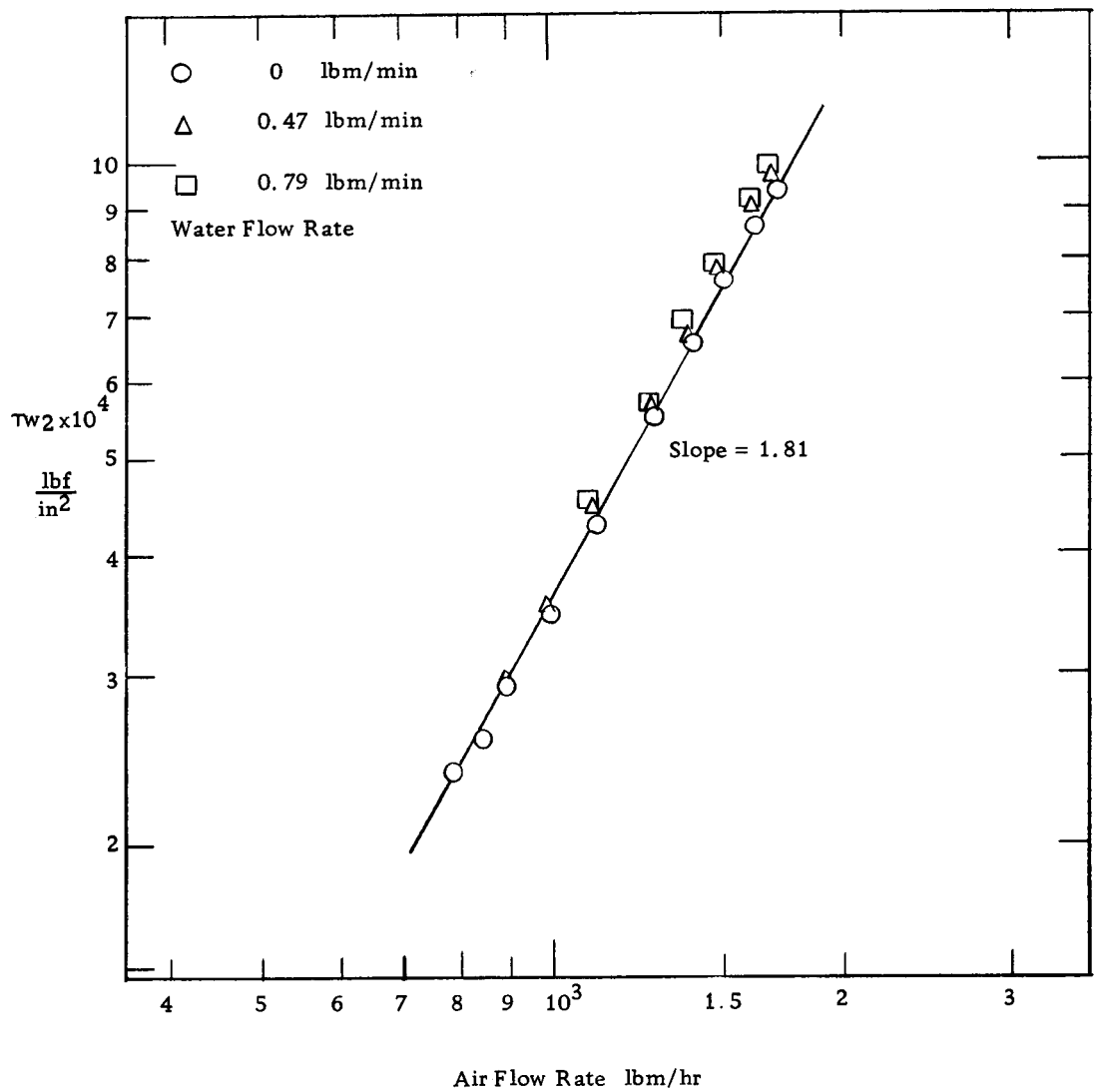

Figure (26) Shear stress on the outer wall (dry) at the top location.

Table (III) Shear Stress on the outer wall (Bottom).

Air cfm*	Water lb/min	Preston** $\Delta_H$inch	Shear Stress lbf/in^2	Calculated Shear Stress lbf/in^2
173	0	0.42	2×10^{-4}	
185	0	0.52	2.3×10^{-4}	
197.5	0	0.62	2.65×10^{-4}	
194	0.47	0.65	2.73×10^{-4}	2.59×10^{-4}
220	0	0.79	3.17×10^{-4}	--
218	0.47	0.81	3.25×10^{-4}	3.13×10^{-4}
249	0	1.06	3.93×10^{-4}	--
246	0.47	1.10	4.07×10^{-4}	4.10×10^{-4}
246	0.79	1.10	4.07×10^{-4}	4.30×10^{-4}
293	0	1.50	5.15×10^{-4}	--
290	0.47	1.54	5.25×10^{-4}	5.25×10^{-4}
290	0.79	1.57	5.3×10^{-4}	5.42×10^{-4}
320	0	1.82	5.9×10^{-4}	--
318	0.47	1.87	6.02×10^{-4}	5.97×10^{-4}
315	0.79	1.92	6.08×10^{-4}	6.15×10^{-4}
351	0	2.19	6.8×10^{-4}	--
349	0.47	2.24	6.93×10^{-4}	6.78×10^{-4}
347	0.79	2.26	6.98×10^{-4}	6.98×10^{-4}
387	0	2.59	7.6×10^{-4}	--
386	0.47	2.63	7.8×10^{-4}	7.72×10^{-4}
382	0.79	2.68	7.95×10^{-4}	7.9×10^{-4}
410	0	2.83	8.2×10^{-4}	--
405	0.47	2.89	8.35×10^{-4}	8.22×10^{-4}
405	0.79	2.94	8.45×10^{-4}	8.5×10^{-4}

* at 1 atm

** S.G. 0.83

Table (IV) Shear stress on the outer wall (Top).

Air cfm*	Water lbm/min	Preston** ΔH inch	Shear Stress lbf/in^2	Calculated Shear Stress lbf/in^2
173	0	.65	2.38×10^{-4}	
185	0	.71	2.575×10^{-4}	
197.5	0	.80	2.9×10^{-4}	--
195	0.47	.82	2.95×10^{-4}	3.05×10^{-4}
220	0	.97	3.47×10^{-4}	--
217	0.47	1.00	3.54×10^{-4}	3.7×10^{-4}
249	0	1.22	4.26×10^{-4}	--
246	0.47	1.25	4.42×10^{-4}	4.67×10^{-4}
246	0.79	1.30	4.54×10^{-4}	
293	0	1.64	5.5×10^{-4}	
290	0.47	1.70	5.63×10^{-4}	
290	0.79	1.74	5.75×10^{-4}	
320	0	1.92	6.52×10^{-4}	
318	0.47	1.99	6.7×10^{-4}	7.0×10^{-4}
315	0.79	2.04	6.9×10^{-4}	7.19×10^{-4}
351	0	2.24	7.55×10^{-4}	
349	0.47	2.33	7.8×10^{-4}	
347	0.79	2.38	7.9×10^{-4}	
387	0	2.64	8.675×10^{-4}	
386	0.47	2.75	9.03×10^{-4}	
382	0.79	2.81	9.2×10^{-4}	
413	0	2.84	9.35×10^{-4}	--
410	0.47	2.99	9.7×10^{-4}	9.87×10^{-4}
406	0.79	3.04	9.9×10^{-4}	10.01×10^{-4}

* at 1 atm

** S. G. 0.83

As expected, the shear stress on the outer wall is also proportional to $(R_e)^{-0.19}$ for Reynolds number between $6x10^4$ and $15x10^4$.

It is concluded that the Preston tube is suitable for measurement of shear stress on the dry wall in climbing film flow.

Shear Stress on the Wetted Wall

The shear stresses on the wetted wall (the inner core) at the top location were measured directly by using the calibrated heating element mentioned in the previous section.

Initially 10.35 watts of power were supplied to the element. This amount of electrical energy badly disturbed the thermal condition of the film. The temperature difference between the film and the element was so high and so changeable that proper measurement of the temperature difference was not possible. The energy input, consequently, was reduced to 3.15 watts (0.5 amperes at 6.3 volts) and more steady conditions were obtained. The temperature difference between the film and the element was measured with a precision potentiometer.

The results of the measurement of the shear stress on the wetted wall are shown in Table (V). The shear stress on the wetted wall were also estimated by using Equations (9), (10), and (11) in Theory section (pages 7 and 8), data of pressure losses and points of maximum velocity of air. The comparison between the

Table (V) Experimental Results of Shear Stress on Inner Core.

Air Flow Rate in cfm at 1 atm	Water Flow Rate in lb/min	Measured at ΔT in m. v.			Shear Stress in lbf/in^2	Calculated Shear Stress
246	0	--	--	--	--	4.158×10^{-4}*
	0.47	0.51	0.51	0.48	1.9×10^{-8}	3.87×10^{-4}
	0.79	0.5	0.47	0.47	2×10^{-8}	--
315	0	--	--	--	--	6.1425×10^{-4}*
	0.47	0.45	0.47	0.46	2.5×10^{-8}	6.79×10^{-4}
	0.79	0.43	0.455	0.43	3×10^{-8}	7.61×10^{-4}
405	0	--	--	--	--	8.41×10^{-4}*
	0.47	0.435	0.42	0.425	3.3×10^{-8}	10.34×10^{-4}
	0.79	0.42	0.402	0.41	3.7×10^{-8}	11.975×10^{-4}

*Shear stress at inner wall when air alone flows.

experimental and the calculated values shows that further heat or mass transfer study near the wall of inner core is necessary to determine the validity of heating element method for measuring shear stress in the climbing film flow. The heating element was calibrated for single phase flow of water and this calibration may not be applicable when only a thin liquid film passes the element. Other methods of measuring heat and mass transfer must be investigated. For the present, the calculated shear stresses are assumed to be most reliable.

Measurement of the Film Characteristics

Film Thickness

The film thicknesses are shown in Table (VI) and Figure (28) together with the amplitude and the wave length. These were determined by the photographic technique mentioned previously.

As shown in Equation (9) and (10) in Theory Section, it is important that the film thickness be established accurately since the values of the inner wall and the interfacial shear stress depend on the square of this quantity.

The photographs to measure mean-film thickness are shown in Figure (27) as examples. The photographs were taken by using the Strobotac at 600 to 1000 flashes per minute. The photographs

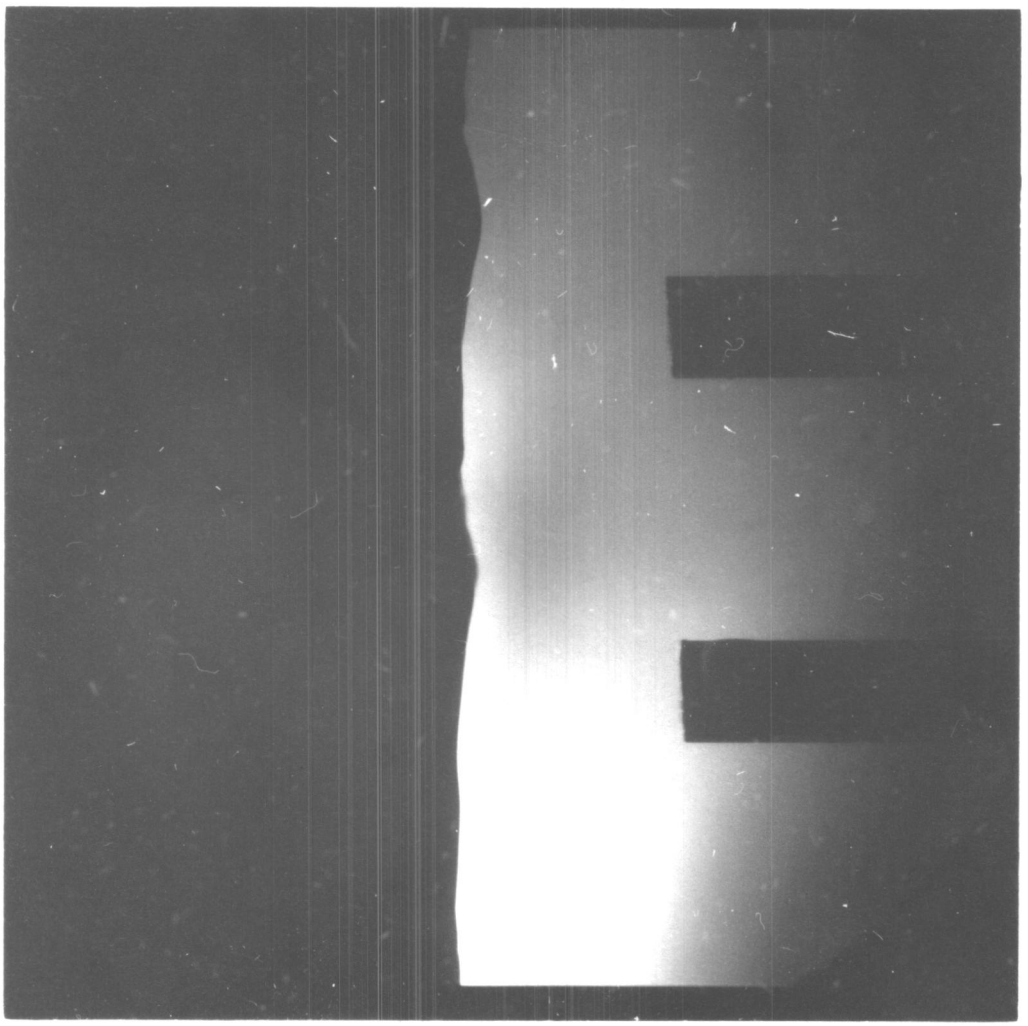

Air Flow Rate 288 cfm
Water Flow Rate 0.47 lbm/min

Figure (27a) Climbing-film flow.

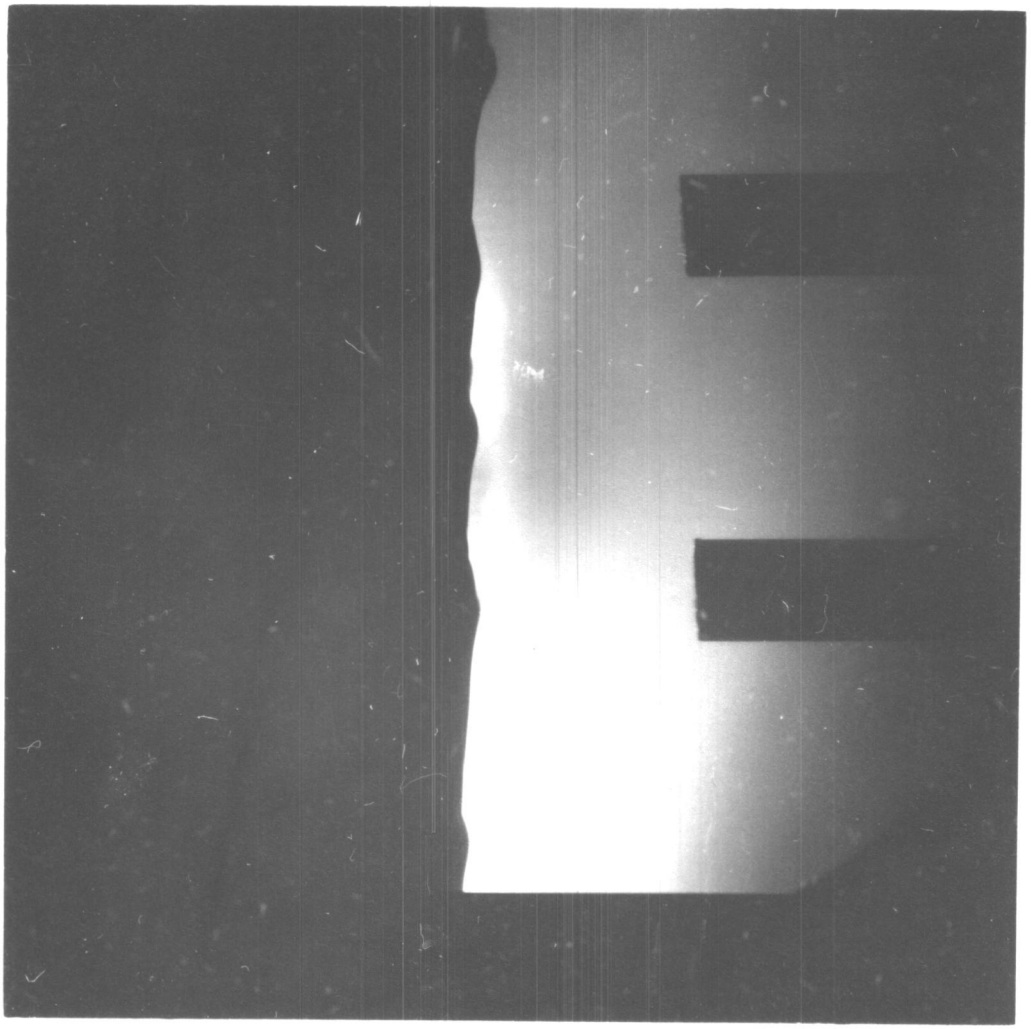

Air Flow Rate 385 cfm
Water Flow Rate 0.47 lbm/min

Figure (27b) Climbing-film flow.

Table (VI) Characteristics of Climbing-film.

cfm at 1 atm Flow Rate of Air	lb/min Flow Rate of Water	inch Film Thickness	inch Amplitude	inch Wave Length
198	0.47	0.0127	0.012	0.20
245	0.47	0.0049	0.0049	0.15
245	0.79	0.008	0.008	0.13
288	0.47	0.0041	0.004	0.13
288	0.79	0.0059	0.0059	0.10
318	0.47	0.0040	0.004	0.09
318	0.79	0.0043	0.004	0.08
350	0.47	0.0037	0.0035	0.08
350	0.79	0.0043	0.004	0.06
385	0.47	0.0029	0.0029	0.06
385	0.79	0.0031	0.0030	0.06+
402	0.47	0.0026	0.0026	0.055
402	0.79	0.0024	0.0024	0.065

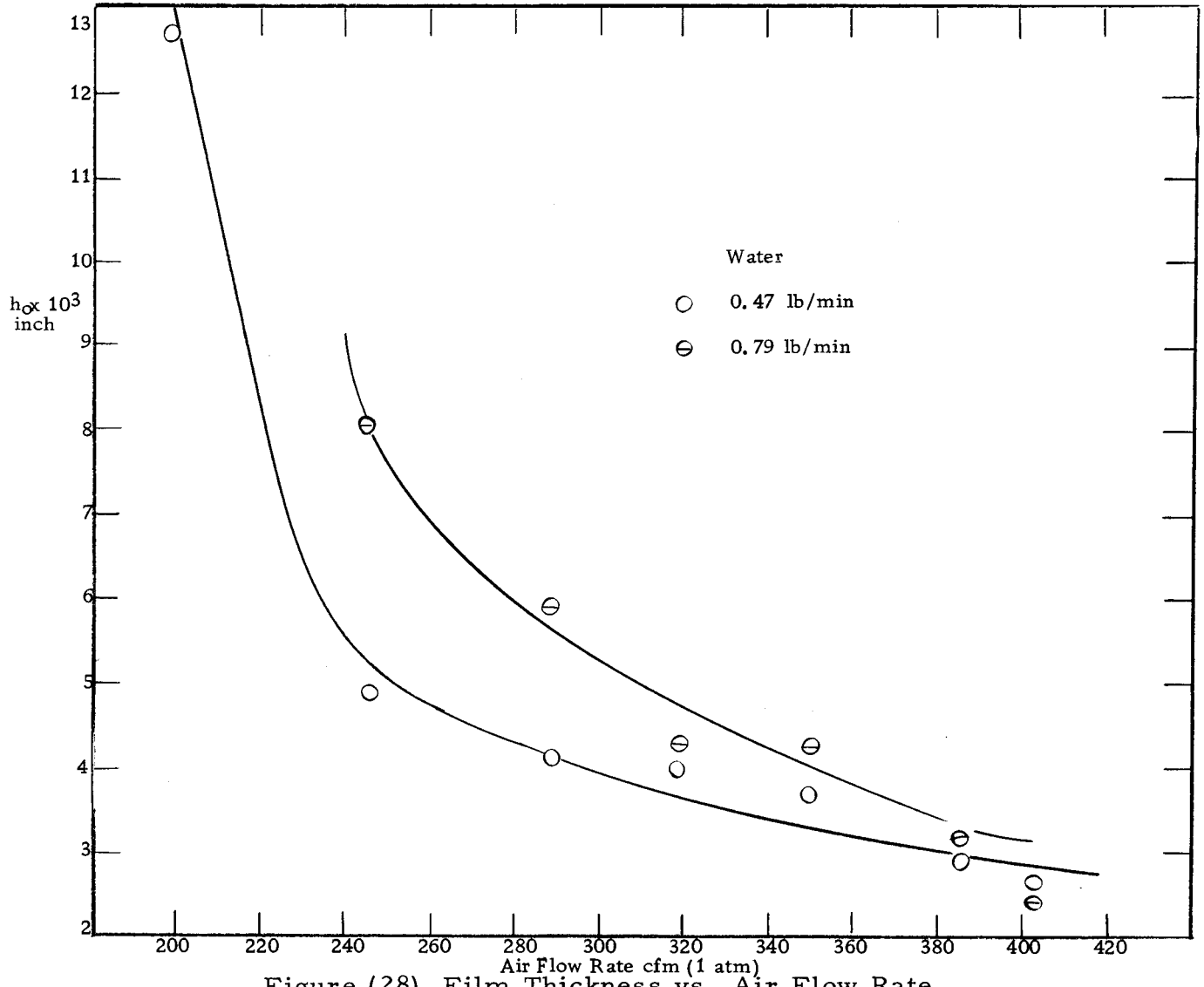

Figure (28) Film Thickness vs. Air Flow Rate.

covered about a 0.5-inch length of the climbing film. The values reported in this section are film thickness averaged over the 0.5-inch long portions. These values were obtained by dividing the film cross sectional area on the photographs measured with a plannimeter by the length of the climbing film shown. A few pictures were taken at the same flow conditions and the average thicknesses were determined for each picture. Then the final arithmetic mean average was determined.

In order to determine the error involved in this method, photographs were also taken with no water flow. On these photographs the precise distances between the inner core to the two reference markers (hypodermic needles) were measured. They agreed with each other within 0.002 inch. If one assumes that no error is involved in measuring the cross-sectional area of film shown on the photographs by a plannimeter (actually $\pm$ 3 percent accuracy), the accuracy in this method to measure the mean-film thickness is $\pm$0.002 inch. It appeared that the main difficulty in this method was elimination of the vibration of the inner core. The photographic method to determine the mean film thickness seems satisfactory for most air flow rates. At the highest air flow rate, the error in measurements of mean film thickness, however, was about 80 percent. It appears that some other method such as fluorescence or conductance should be used for further study of film thickness at

high air flow rates.

Wave Length and Amplitude of Surface Waves

The wave lengths and amplitudes of surface waves are shown in Table (VI).

The shapes of waves shown on the photographs were too irregular to determine precisely the amplitude and the length of waves. The wave lengths were determined by dividing the number of peaks by the length of liquid film shown. The results of measurements of wave length shown are, due to difficulty in counting the peaks, only of qualitative significance. As expected, the wave lengths decrease as air flow rates increase. This means that the climbing film receives more energy from the air stream as air flow rate increases, since shorter wave lengths occur as the energy content of the wave increases. The wave length was not changed as the water flow rate was increased. In order to arrive at definite conclusions concerning the effect of water flow rates on the wave length more data are necessary at higher water flow rates.

The amplitudes of the waves were of approximately the same magnitude as the film thickness as shown on the photographs. Due to irregularity of the wave, it is also very difficult to determine the mean average amplitudes.

From this qualitative data on the climbing film, however, one

may arrive at a conclusion concerning the type of wave motion occuring in the climbing film under the flow conditions employed.

The ratio of the wave length to the amplitude varied from 20 to 30 at the various air and water flow rates as can be seen in Table (VI). Previously, in the Theory section, it was mentioned that if the ratio, $\frac{\lambda}{a}$, was much greater than 1, the wave motion was laminar (Benjamin, 2). From the results of climbing film characteristics the present film must be a laminar wave motion.

The following section will combine all information presented thus far and discuss the particular phenomenon of momentum transfer in climbing-film flow in an annular duct.

Part Two

Pressure Losses (The Lockhart and Martinelli Correlation)

Pressure loss data for climbing-film flow in an annulus were correlated as a function of Φ and X which were defined for two-phase flow in tubes by Lockhart and Martinelli as follows:

$$\Phi^2 = \left(\frac{dP}{dx}\right)_{TP} / \left(\frac{dP}{dx}\right)_g \tag{1}$$

$$X^2 = \left(\frac{dP}{dx}\right)_L / \left(\frac{dP}{dx}\right)_g \tag{2}$$

where $\left(\frac{dP}{dx}\right)_{TP}$ is the pressure gradient of climbing-film flow, $\left(\frac{dP}{dx}\right)_L$ and $\left(\frac{dP}{dx}\right)_g$ are pressure gradients in the annulus when liquid and gas, respectively, flow alone in the channel. Because the liquid Reynolds number (flowing alone in the annulus) was less than 2000 ($R_{e_L} < 10$), $\left(\frac{dP}{dx}\right)_L$ was calculated from equation

$$\left(-\frac{dP}{dx}\right)_L = \frac{32\,\mu\,U}{g_c(d_2^{\,2} + d_1^{\,2} - 2d_m^{\,2})} \tag{3}$$

The results of Φ and X calculated by using the experimental pressure gradients for the climbing film in an annulus are shown in Figure (29). The solid curve is Lockhart and Martinelli's correlation in tubes as expressed in analytical form by Hewitt, King, and Lovegrove (20). The agreement between two climbing-film

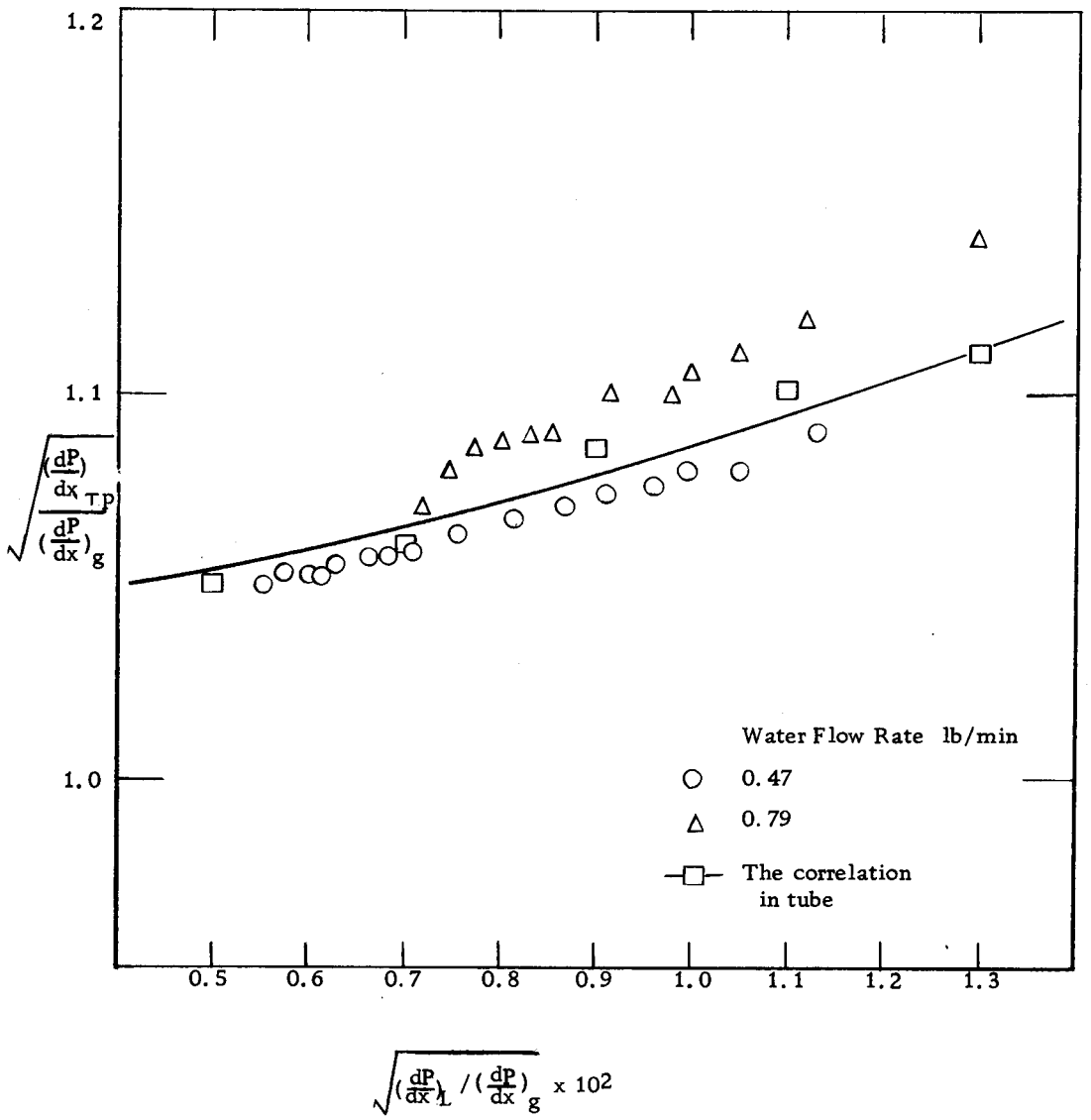

Figure (29) The Lockhart and Martinelli Correlation in an Annular Channel.

flows is good. Thus the correlation for two-phase flow in tubes is recommended for estimation of pressure losses in climbing film flow in an annular duct for the flow region studied. However, it is necessary to study the high water flow rate region to reach a more general conclusion concerning the correlation.

Mean Air Velocity

The mean dimensionless velocities, u_1^+, of air in annular flow with and without the water film are plotted versus the dimensionless distance y_1^+, for the inner profile in Figure (30). Similarly u_2^+ is plotted versus y_2^+ for the outer profile in Figure (32). For evaluation of u_1^+ and u_2^+, the pressure gradient and the point of maximum velocity were used to obtain shear stress on the walls. The film thickness was neglected when the shear stress on the inner core with the film was calculated. These profiles were then compared with the law of wall.

The values of u_1^+ are close to the distribution of Nikuradse's general velocity profile on smooth tube. However in the presence of the water film, the values of u_1^+ are shifted downward although the data are parallel to the data from annular flow without the film. For water flow rate 0.47 lbm/min, the data is best represented by

$$u_1^+ = 1.2 + 2.5 \ln y_1^+ \qquad (4)$$

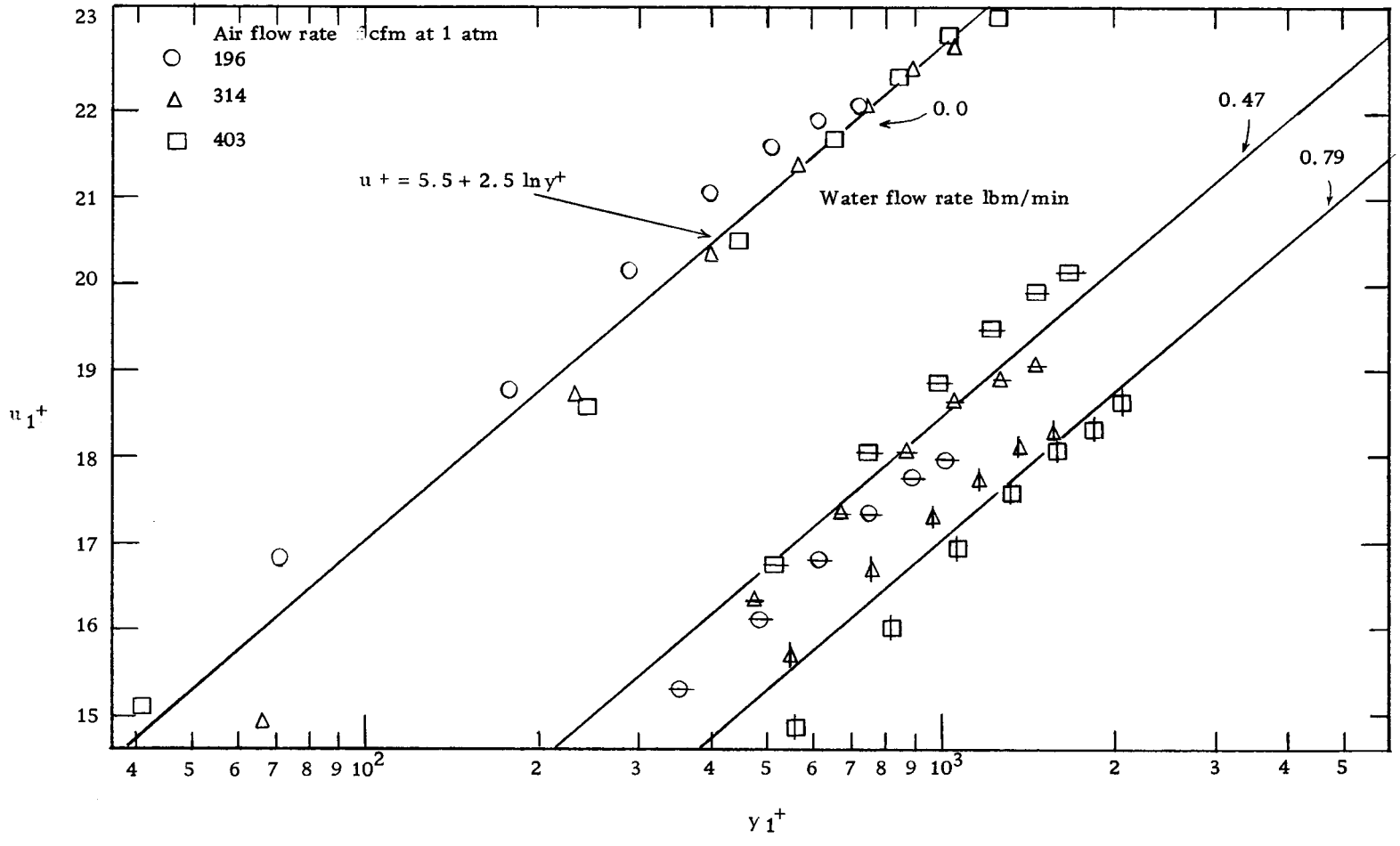

Figure (30) Velocity distribution for the inner portion of the annulus.

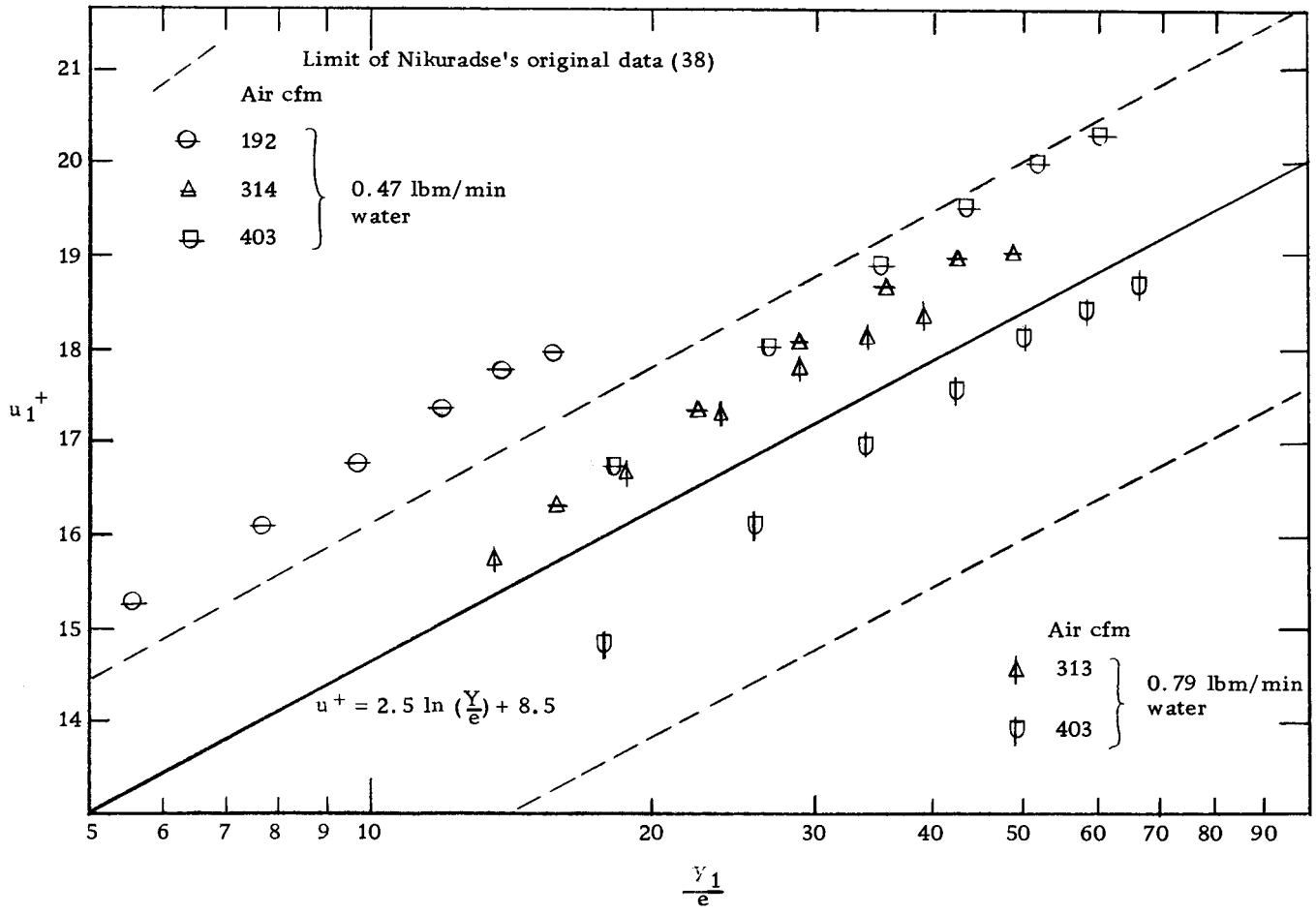

Figure (31) Comparison with Nikuradse's velocity distribution data in rough tubes.

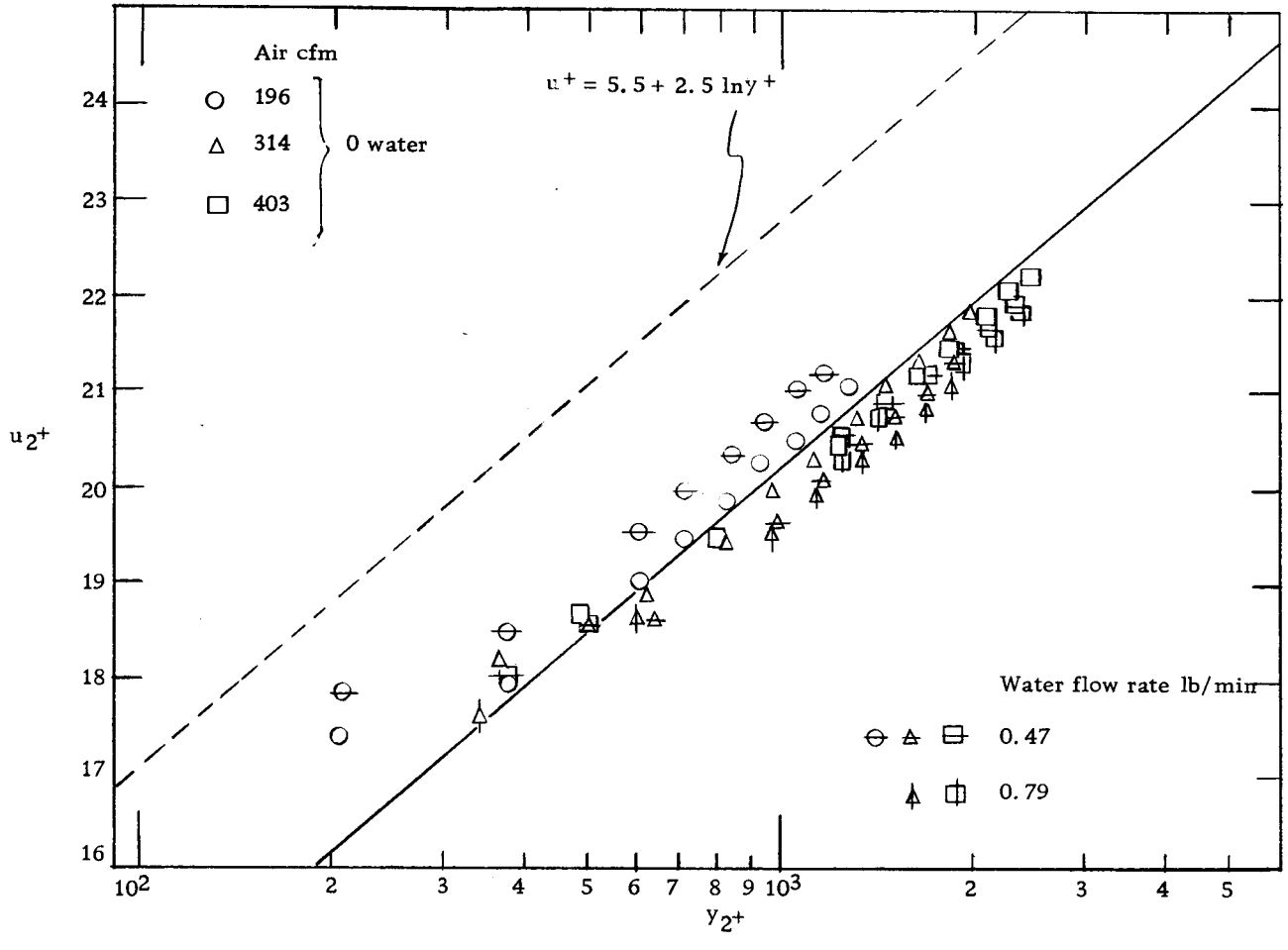

Figure (32) Velocity distribution for the outer portion of the annulus.

For water flow rate 0.79 lb/min,

$$u_1^+ = -0.3 + 2.5 \ln y_1^+ \qquad (5)$$

From the above equations it was concluded that the structure of the turbulence of air annular flow with the climbing-film present is same as that for single phase annular flow and the values of the constant (intercept in the plots) may be related to the effect of the capillary wave of the climbing film on the air velocity.

For further study of the effect of the capillary wave on the air annular flow, the mean velocity measurements in the inner portion of the annulus were compared with the velocity distribution for turbulent flow in rough tubes in Figure (31) where u_1^+ was plotted versus y_1/e. y_1/e is the dimensionless distance from the inner wall where e is the height of roughness. In case of the climbing film flow the height of roughness is almost same as two times of the mean film thickness. The solid line is the recommended equation for the velocity distribution in the turbulent core of rough tubes and is the resultant equation of Nikuradse's experimental velocity data in rough tubes (38). From the comparison of the present values and Nikuradse's original data, it is seen that the velocity profile in the region of inner air annular flow with the presence of climbing-film agrees quite well with that in rough tubes. Thus it may be concluded that the capillary waves do not affect the turbulent structure of annular air flow, other than in creating the rough wall condition.

For the outer profile, the values of u_2^+ do not agree with the distributions of Nikuradse for the tubes. Whereas slopes are very close, the constant term in present velocity profile is lower than Nikuradse's by about 2.5. The present constant, 3.0, is same as that reported by Knudsen and Katz (26) for the outer-portion of the annular velocity profile. The present data may be best represented by

$$u_2^+ = 3.0 + 2.5 \ln y_2^+. \tag{6}$$

As the water flow rate increases the outer velocity profiles do not change.

As result, it is clear that the capillary waves of the climbing film affect only the location of maximum air velocity and the air velocity profile in the inner portion of the annulus.

Mean Film Thickness

The mean film thickness data in the climbing film flow in an annulus were correlated by using Lockhart and Martinelli's correlation parameters, R_L and X, where R_L is the fraction of liquid hold-up, $\frac{r_i^2 - r_1^2}{r_2^2 - r_1^2}$. A correlation between R_L and X for climbing film flow in an annulus is shown as dashed line in Figure (33). Data for climbing film two-phase flow in $1\frac{1}{4}$ inch tube reported by Hewitt, King and Lovegrove (20, 21) are also plotted in Figure (33). The slightly curved solid line is the suggested extrapolation by these

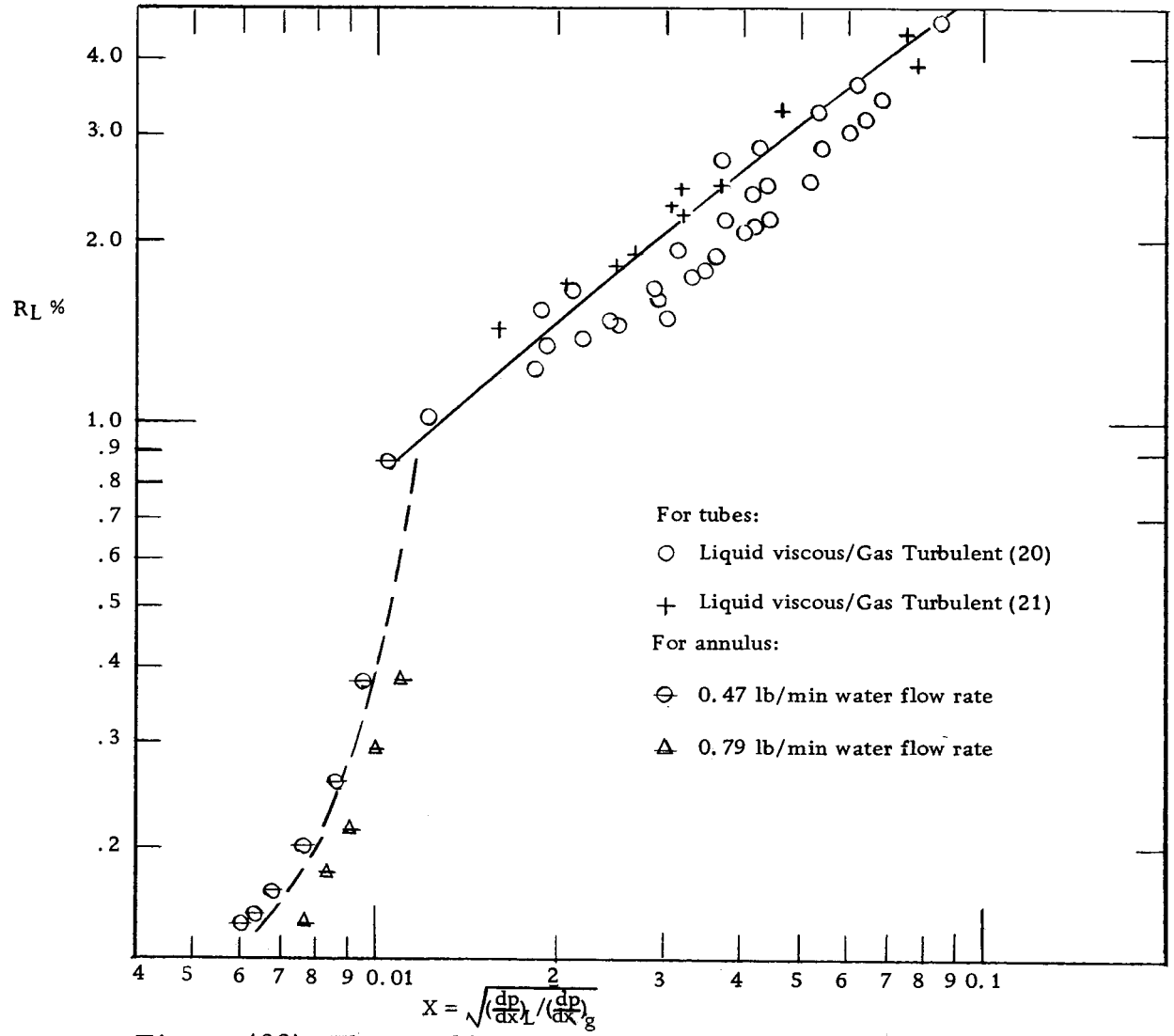

Figure (33) The Lockhart-Martinelli's film thickness correlation.

workers of the original Lockhart and Martinelli line in the small X region for tubes. The correlation curve for the present climbing film is quite different from the extrapolated line for tubes.

The two curves in Figure (33) intersect each other at $X \approx 0.01$. If these curves represent a general correlation for climbing film flow in both tubes and annuli, it would appear that the region in the vicinity of $X = 0.01$ is a transition region. In the present work, the region studied was one of very small entrainment and the film flow was characterized by capillary waves. The data of Hewitt and co-workers (20, 21) was in a region of high entrainment. The present apparatus is limited to the flow rates investigated and further study must be made in order to determine if, in fact, the intersection between the two curves represents a true transition point. Attempts to increase the water flow rate in the present apparatus resulted in a very unstable film which was greatly affected by the centering pins. A new design of centering pins is proposed so that they will not disturb the film.

Distribution of Shear Stress

The shear stresses at the outer wall, the surface of the film, and the inner wall were calculated by using Equations (9), (10), and (11) in Theory section and the experimental pressure gradient, mean film thickness, and location of maximum air velocity. The results

are tabulated in Table (VII). As mentioned previously, only the shear stress on the outer wall was confirmed by experimental data (Preston tube).

Table (VII) Shear stress calculated from the air mean velocity, pressure loss, and film thickness.

cfm at 1 atm Air Flow Rate	lb/min Water Flow Rate	Shear Stress lbf/in^2		
		τ_2 Outer Wall	τ_i Interface	τ_1 Inner Wall
196	0.00	2.95×10^{-4}	--	2.74×10^{-4}
	0.47	2.96×10^{-4}	3.94×10^{-4}	-0.412×10^{-4}
245	0.00	4.48×10^{-4}	--	4.16×10^{-4}
	0.47	4.63×10^{-4}	5.79×10^{-4}	3.87×10^{-4}
314	0.00	6.58×10^{-4}	--	6.09×10^{-4}
	0.47	6.92×10^{-4}	8.14×10^{-4}	6.79×10^{-4}
	0.79	7.16×10^{-4}	9.37×10^{-4}	7.61×10^{-4}
403	0.00	9.32×10^{-4}	--	8.65×10^{-4}
	0.47	9.68×10^{-4}	11.42×10^{-4}	10.34×10^{-4}
	0.79	9.93×10^{-4}	13.08×10^{-4}	11.975×10^{-4}

The shear stress at interface is 20 to 35 percent higher than the shear stress on the outer wall and 10 to 50 percent higher than that on the inner wall. It may be noted from Table (VII) that the shear stress on the inner core changes its sign from negative to

positive as the air flow rate increases. At low air flow rates, a certain portion of the climbing-film near the inner core may fall, since not enough momentum is transferred in from air. However the net liquid flow rate is upward. As the air flow rate increases, more momentum, entirely shear stress, is transferred to the film so that the all liquid in the film flows upwards.

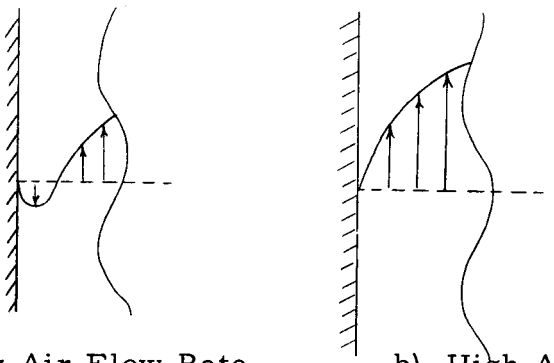

a) Low Air Flow Rate b) High Air Flow Rate

Possible Velocity Profiles of Liquid Film

With informations of shear stresses and pressure gradients, the main mechanism of climbing film flow may be qualitatively explained by a simple force balance.

By neglecting the curvature of the climbing film, the force balance of the film is

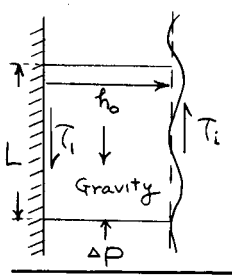

$$\tau_l 2\pi r_1 L + \rho_L 2\pi r_1 L h_o \cdot \frac{g}{g_c}$$

$$= \tau_i 2\pi r_1 L + \Delta P 2\pi r_1 h_o \qquad (7)^*$$

*The interfacial area is assumed as same as the area at inner wall.

By rearrangement the following simple force balance is obtained,

$$\tau_l + \rho_L h_o \frac{g}{gc} = \tau_i + \frac{\Delta P}{L} h_o \qquad (8)$$

Sample Calculation

Given: Air Flow Rate : 314 cfm

Water Flow Rate : 0.47 lb/min

h_o : 3.8×10^{-3} inch

τ_i : 8.14×10^{-4} lbf/in^2

τ_l : 6.79×10^{-4} lbf/in^2

$\frac{\Delta P}{L}$: 14.5×10^{-4} lbf/in^3

ρ_L : 3.61×10^{-2} lbm/in^3

Given data are substituted into equation (8),

Left = $6.79 \times 10^{-4} + (3.61 \times 10^{-2})(3.8 \times 10^{-3}) = 8.16 \times 10^{-4}$

Right = $8.14 \times 10^{-4} + (14.5 \times 10^{-4})(3.8 \times 10^{-3}) = 8.19 \times 10^{-4}$

and agreement is obtained.

This force balance in Equation (8) assumes that the main factor affecting the surface of the water film is the interfacial shear stress at the air-water interface rather than the random fluctuations of air turbulent stream, the latter has received considerable attention as one of the mechanisms of wave generation on the ocean.

For further study of mechanism of climbing film flow, more exact air velocity profiles and the Reynolds stress near the air-water

interface must be determined.

Structure of the Climbing Film

The determination of the transition point from laminar flow to turbulent flow is one of the difficulties involved in the study of climbing film flow. A search of the literature has not revealed information about transition criteria in climbing film flow.

A tentative method is proposed for the present type of film-flow to determine its structure (laminar, turbulent, etc.). The following assumptions were made:

1) The shear distribution is linear in the film, since the film is thin.

2) The flow characteristics in the climbing film are the same as those for flow in tubes. This allows one to use Newton's law of viscosity and the eddy viscosity equations in the climbing-film flow.

With a known shear stress, as shown in Table (VII), at the interface and at the inner core, the velocity and, therefore, the flow rate of water can be determined by integration. In order to do so, Newton's law of viscosity and the semi-empirical Deissler (25) eddy viscosity equation were used.

i) Newton's law of viscosity

The resultant velocity and the flow rates are

$$u = \left(\tau_1 y + \frac{(\tau_i - \tau_1)}{h_o}\frac{y^2}{2}\right)\frac{g_c}{\mu} \tag{9}$$

$$Q = \left(\frac{\tau_1}{2} + \frac{\tau_i - \tau_1}{6}\right)\frac{h_o^2}{\mu} g_c \cdot 2\pi r_1 \tag{10}$$

ii) Deissler's empirical formula

The velocity and the flow rates can not be obtained analytically from the equation and boundary condition,

$$\tau_o + (\tau_i - \tau_o)\frac{y}{h_o} = \left[\frac{\mu}{g_c} + \rho n^2 \bar{u}\, y\left(1 - \exp\frac{-n^2 \bar{u}\, y\, g_c}{\nu}\right)\right]\frac{d\bar{u}}{dy} \tag{11}$$

$$\bar{u} = 0 \quad \text{at} \quad y = 0$$

where n is 0.124 which was evaluated for tubes by Dissler. The modified Adams numerical method together with the modified Euler method (22) was used to obtain velocity distribution and the parabolic rule (Simpson's rule) was used to calculate the liquid flow rate. All calculations were made with aid of an IBM 1410 Computer (Appendix V).

The results are shown in Table (VIII). The values which were obtained using Newton's law of viscosity were closer to the experimental values than those from Deissler's equation. In addition to the above result, the results of the film characteristics support the fact that the climbing film formed on the inner core may be laminar. However neither Newton's law of viscosity nor semiempirical Deissler's eddy viscosity equation is proper to describe the flow of thin climbing film.

Table (VIII) The liquid flow rates.

Inch Film Thickness	Shear Stress lbf/in^2		lb/min Calculated Newton Law	lb/min Calculated Deissler	lb/min Experiment
	Interface	Inner Wall			
0.0053	5.79×10^{-4}	3.87×10^{-4}	0.30	0.255	0.47
0.0038	8.14×10^{-4}	6.79×10^{-4}	0.245	0.189	0.47
0.0030	11.40×10^{-4}	10.34×10^{-4}	0.226	0.165	0.47
0.0049	9.37×10^{-4}	7.61×10^{-4}	0.460	0.380	0.79
0.0031	13.08×10^{-4}	11.98×10^{-4}	0.278	0.250	0.79

Comparison of Mean Film Thickness and Wave Length With the Modified Solution of the Momentum Equation

The results of the modified solution of the climbing-film momentum equation developed in the Theory section were checked with data consisting of the mean film thickness and the wave length of the capillary waves of climbing-film in order to determine the validity of model and method of solution used.

From Equation (32) in Theory section, the following relation between the water flow rate and the mean film thickness was obtained.

$$\frac{3\nu Q}{2\pi r_1 g_c} = \left[\frac{r_2^2 - r_m^2}{2r_2}\left(-\frac{dP}{dx}\right)\frac{r_m^2 - (0.5+h_o)^2}{r_2^2 - r_m^2}\frac{r_2}{0.5+h_o}\right]\frac{3h_o^2}{2\rho}$$

$$-\left(\frac{1}{\rho_L}\frac{dP}{dx} + \frac{g}{g_c}\right)h_o^3 \qquad (12)$$

where the momentum transfer from the air is assumed as same as the shear stress at the air-water interface. All physical properties,

μ and ρ_L, refer to the liquid water. By utilizing the position of maximum air velocity, the mean film thickness, and the pressure gradient, the water flow rates were predicted from the above Equation (12). The comparison between the value predicted and data of experiment are shown in Table (IX).

The predicted values are less than the experimental values by 20 to 60 percent. However the predicted water flow rates by using Equation (12) are closer to the experimental values than the predicted by using Equation (10) or (11). The water flow rate is proportional to the third power of the mean film thickness and thus an error of about 10 percent or 0.0003 inches in measuring the mean film thickness results in a 30 percent error in the calculated flow rate. From this fact, the agreement between the experimental values and the predicted appears to be good, but not entirely satisfactory. It is assumed that the theoretical development gives only approximate results as a prediction of flow rates concerned.

From Equation (38) in Theory section, the values of wave length were predicted.

The wave length λ,

$$\lambda = \frac{2\pi}{k}$$

$$= \frac{2\pi}{\sqrt{\left(\frac{\rho_L}{\sigma\pi r_1}\frac{Q}{h_o^2} - \frac{g_c\rho_L}{2\sigma\mu}F\right)\left(\frac{21}{20\pi r_1}\frac{Q}{h_o} - \frac{g_c}{\mu}\frac{3}{10}Fh_o\right)}}$$

where σ is the surface tension of water, $72.75 \frac{\text{Dynes}}{\text{cm}}$. Table (X)

Table (IX)

Comparison of water flow rates with theoretical values

cfm at 1 atm Air Flow Rate	inch r_m	lbf/in^3 $\frac{dP}{dx}$	inch h_o	lb/min Predicted Q	lb/min Experimental Q
192	0.94	6.5×10^{-4}	0.012	0.356	0.47
314	0.905	14.5×10^{-4}	0.0038	0.244	0.47
403	0.905	20.3×10^{-4}	0.003	0.243	0.47
314	0.93	15.5×10^{-4}	0.0049	0.46	0.79
404	0.93	21.5×10^{-4}	0.0031	0.32	0.79

Table (X)

Comparison of wave length with theoretical values

in^3/sec Water Flow Rate	cfm at 1 atm Air Flow Rate	inch r_m	lbf/in^3 $\frac{dP}{dx}$	inch h_o	inch Predicted λ	inch Experiment λ
0.2167	192	0.94	6.5×10^{-4}	0.012	--	0.2
0.2167	314	0.905	14.5×10^{-4}	0.0038	0.0262	0.09
0.2167	403	0.905	20.3×10^{-4}	0.003	0.0182	0.055
0.3646	314	0.93	15.5×10^{-4}	0.0049	0.0237	0.08
0.3646	403	0.93	21.5×10^{-4}	0.0031	0.0108	0.065

shows that the predicted values are about 60 to 80 percent lower than the experimental values. As mentioned before, the experimental wave length determined by a photographic method has only a qualitative significance, because of the irregularity of wave shapes.

Finally, the velocity profile of the liquid film, the mean film thickness, and the wave length of the climbing film in an annulus can be predicted, as first approximation, by the model and the solution presented in the Theory section.

CONCLUSIONS

The results of this study may be summarized by the following:

1) The friction factors for air flow in annuli with smooth walls are slightly higher (3.5 to 14 percent) than those for pipe flow when compared on the basis of the equivalent hydraulic diameter of the outer portion of the velocity profile. The calculation of the equivalent diameter for the above comparison is based upon the position of maximum velocity being the same as that for laminar flow.

2) The pressure loss data for climbing film flow in an annulus can be correlated by the Lockhart and Martinelli parameters. The correlation for two-phase flow in a tube is very close to that for the climbing film in an annulus. About a 14 to 19 percent increase in the single-phase flow pressure gradient occurred for water flow rate of 0.47 lbm/min. Approximately a 22 to 31 percent higher pressure gradients were observed for 0.79 lbm/min.

3) For an annular duct with a diameter ratio, $\frac{d_1}{d_2} = 0.333$, the location of maximum air velocity is nearer to the inner tube than for laminar flow ($r_m = 0.86$ inch, r_m for laminar $= 0.9539$ inch). The points of maximum velocity obtained in the present work show a discrepancy from those obtained by previous workers (3, 26) as indicated in Figure (24). However the flatness of the

turbulent velocity profile makes it difficult to determine the point of maximum velocity, particularly in a small channel such as was used in the investigation. A certain amount of disturbance caused by flange connections and centering pins may also have had some effect. However, the velocity profiles for the inner portion of the annulus are in excellent agreement with the law of wall,

$$u_1^+ = 3.0 + 2.5 \ln y_1^+$$

whereas those for the outer portion agree with each other except for the constant term. The velocity profile for the outer portion is

$$u_2^+ = 3.0 + 2.5 \ln y_2^+$$

which is the same as that reported by Knudsen and Katz (35).

4) The capillary waves of the climbing film affect only the location of maximum air velocity and the air velocity profile in the inner portion of the annulus. The location of maximum velocity is shifted towards the outer wall as water film is introduced. The air velocity profiles in the inner portion of the annulus with the film present, plotted as u^+ versus y^+, are shifted downward, relative to that for annular flow without the film, although they have the same slope.

5) The capillary waves of the climbing film have essentially no effect on the turbulent structure of air annular flow, other than in creating a rough wall condition.

6) The main mechanism of the climbing phenomena is the interfacial shear stress rather than the random fluctuations of the turbulent air stream in the region of flow rates used.

7) The highest shear stress is observed at the air-water interface.

8) The film thickness data can be correlated by the Lockhart and Martinelli parameters. However the correlation for two-phase flow in a tube does not agree with that for the climbing film in an annulus. The two curves in Figure (33) intersect each other at $x \approx 0.01$. If these curves represent a general correlation for climbing film flow in both tubes and annuli, it would appear that the region in the vicinity of $x = 0.01$ is a transition region. Data at high water flow rates are needed to reach a general conclusion concerning the correlation.

10) As first approximation, Kapitza's theory of wave formation in the vertical plane with downward flow, based on laminar conditions, was extended to the climbing film in an annular duct to obtain an expression for the mean film thickness, the velocity profile of liquid film, and the wave length. The agreement between the theory and the experiment is reasonably good.

RECOMMENDATIONS FOR FURTHER WORK

1. Further data such as pressure gradients, velocity profiles, and film thicknesses for higher water flow rates and with different fluids, for example, high viscous fluids, are necessary to determine the validity of extending the conclusions made in present study over a wider region. In order to increase water flow rate, a modification of the centering pins and of the method of fluid injection may be required.
2. The hydrodynamics of annular flow depend upon the diameter ratio, $\frac{d_1}{d_2}$. Thus the stability of climbing film flow may be dependent of the diameter ratio. This dependency should, therefore, be determined.
3. For the determination of the validity of heating element as a method of measuring the shear stress on the inner core, a study of heat or mass transport at the solid-fluid interface must be done.
4. For further study of transport phenomena at the air-water interface, the mean mass transfer coefficient may be determined by measuring the humidity of the air at several locations along the column and then by using a suitable model, say the penetration theory, the momentum transfer at the air-water interface can be estimated from this. The results obtained can be then compared with the values reported in the present study.

5. Theoretical study of the stability of climbing film flow may be possible with the aid of the approximate series solution reported by Benjamin (2) for free interfaces.

BIBLIOGRAPHY

1. Anderson, G. H. and B. G. Mantzouranis. Two-phase (gas-liquid) flow phenomena-1. Chemical Engineering Science 12: 109-126. 1960.

2. Benjamin, T. B. Wave formation in laminar flow down an inclined plane. Journal of Fluid Mechanics 2:554. 1957.

3. Brighton, J. A. and J. B. Jones. Fully developed turbulent flow in annuli. Transactions of the American Institute of Mechanical Engineers, Journal of Basic Engineering 86:835-844. 1964.

4. Calvert, Seymour and Brymer Williams. Upward cocurrent annular flow of air and water in smooth tubes. Journal of the American Institute of Chemical Engineers 1:78-86. 1955.

5. Collier, J. G. and G. F. Hewitt. Data on the vertical flow of air-water mixtures in the annular and dispersed flow regions. Part II: Film thickness and entrainment data and analysis of pressure drop measurements. Transactions of Institution of Chemical Engineers London 39:127-136. 1961.

6. _____ Film thickness measurement. Harwell, Berkshire, England, 1964. 18p. (United Kingdom Atomic Energy Authority. AERE-R4684)

7. Davis, E. S. Heat transfer and pressure drop in annuli. Transactions of the American Society of Mechanical Engineers 65:755-760. 1943.

8. Dukler, A. E. Fluid mechanics and heat transfer in vertical falling film system. In: Heat transfer-Sorrs. New York, 1960. p. 1-10. (American Institute of Chemical Engineers. Chemical Engineering Progress Symposium Series no. 30)

9. Dukler, A. E. and O. P. Bergelin. Characteristics of flow in falling liquid films. Chemical Engineering Progress 48:557-563. 1952.

10. Dukler, A. E., M. Wicks, III, and R. G. Cleveland. Frictional pressure drop in two-phase flow: A. A comparison of existing correlations for pressure loss and holdup. Journal of the American Institute of Chemical Engineers 10:38-43. 1964.

11. Emmert, E. E. and R. L. Pigford. A study of gas absorption in liquid films. Chemical Engineering Progress 50:87-93. 1954.

12. Fredrickson, A. G. and R. E. Bird. Friction factors for axial non-Newtonian annular flow. Industrial and Engineering Chemistry 50:1599-1600. 1958.

13. Gill, L. E. and G. F. Hewitt. Further data on the annular flow of air-water mixtures in a 1 1/4 inch bore perspex tube. Harwell, Berkshire, England, 1963. p. (United Kingdom Atomic Energy Authority. AERE-R-3935)

14. Gill, L. E., G. F. Hewitt and P. M. C. Lacey. Sampling probe studies of the gas core in annular two-phase flow, Part II. Studies of the effect of phase flow rates on phase and velocity distribution. Harwell, Berkshire, England, 1963. 17p. (United Kingdom Atomic Energy Authority. AERE-R-3955)

15. Grimley, S. S. Liquid flow conditions in packed towers. Transactions of the Institution of Chemical Engineers, London 23:228-235. 1945.

16. Hanratty, T. J. and J. M. Engen. Interaction between a turbulent air stream and a moving water surface. Journal of the American Institute of Chemical Engineers 3:299-304. 1957.

17. Hanratty, T. J. and A. Hershman. Initiation of roll waves. Journal of the American Institute of Chemical Engineers 7:488-497. 1961.

18. Hewitt, G. F. Analysis of annular two-phase flow: application of the Dukler analysis to vertical flow in a tube. Harwell, Berkshire, England, 1961. 39p. (United Kingdom Atomic Energy Authority. AERE-R-3680.

19. _____ Interpretation of pressure drop data from an annular channel. Harwell, Berkshire, England, 1964. 16p. (United Kingdom Atomic Energy Authority. AERE-R-4340)

20. Hewitt, G. F., R. D. King and P. C. Lovegrove. Techniques for liquid film and pressure drop studies in annular two-phase flow. Harwell, Berkshire, England, 1962. 39p. (United Kingdom Atomic Energy Authority. AERE-R-3921)

21. _____ Holdup and pressure drop measurements in the two-phase annular flow of air water mixtures. Harwell, Berkshire, England, (United Kingdom Atomic Energy Authority. AERE-R-3764)

22. Hildebrand, F. B. Introduction to numerical analysis. New York, McGraw-Hill, 1956. 511p.

23. Jefferys, H. On the formation of water waves by wind. Proceedings of the Royal Society of London, Series A 107:189-205. 1925.

24. Kapitza, P. L. Wave flow of thin layers of a viscous liquid. Journal of Experimental and Theoretical Physics (Russian) 18: 3-18. 1948.

25. Knudsen, J. G. and D. L. Katz. Velocity profiles in annuli. In: Proceedings of the Midwestern Conference on Fluid Dynamics, 1st Conference, University of Illinois, p. 175-303. May 1950.

26. _____ Fluid dynamics and heat transfer. New York, McGraw-Hill, 1958. 576p.

27. Lacery, P. M. C., G. F. Hewitt and J. G. Collier. Climbing film flow. Symposium on Two-phase Flow, Institution of Mechanical Engineers, London, 1962. 22p. (Paper no. 1)

28. Laird, A. D. K. Stability of gas flow in a tube as related to vertical annular gas-liquid flow. Transaction of the American Society of Mechanical Engineers 76:1005-1010. 1954.

29. Levich, V. G. Physicochemical hydrodynamics. Englewood Cliffs, N. J., Prentice-Hall, 1962. 700p. (Translated from the Russian)

30. Liepmann, H. W. and G. T. Skinner. Shearing stress measurements by use of a heated element. Washington, 1954, 27p. (U. S. National Advisory Committee for Aeronautics. Technical Note 3268)

31. Lin, C. C. The theory of hydrodynamic stability. Cambridge, England, University Press, 1955. 155p.

32. Lockhart, R. W. and R. C. Martinelli. Proposed correlation of data for isothermal two-phase, two-component flow in pipes. Chemical Engineering Progress 45:39-48. 1949.

33. Ludwieg, H. Instrument for measuring the wall shearing stress of turbulent boundary layers. Washington, 1955. 22p. (U. S. National Advisory Committee for Aeronautics. Technical Memorandum 1284)

34. Ludwieg, H. and W. Tillmann. Investigations of the wall-shearing stress in turbulent boundary layers. Washington, 1950. 25p. (U. S. National Advisory Committee for Aeronautics. Technical Memorandum 1285)

35. Meter, Donald A. and R. Byron Bird. Turbulent Newtonian flow in annuli. Journal of the American Institute of Chemical Engineers 7:41-45. 1961.

36. Miles, J. W. On the generation of surface waves by shear flows. Journal of Fluid Mechanics 3:185-204. 1957.

37. Nikuradse, J. Gesetzmaessigkeiten des turbulenten Stroemung in glatten Rohren. Forschungsheft 3:356. 1932.

38. _____ Stroemungsgesetze in rauhen Rohren. Forschungsheft 361. 1933.

39. Phillips, O. M. On the generation of waves by turbulent wind. Journal of Fluid Mechanics 2:417-445. 1957.

40. Portalski, Stanislaw. Eddy formation in film flow down a vertical plate. Industrial and Engineering Chemistry Fundamentals 3:49-53. 1964.

41. Prengle, R. S. and R. R. Rothfus. Transition phenomena in pipes and annular cross section. Industrial Engineering Chemistry 47:379-386. 1955.

42. Preston, J. H. The determination of turbulent skin friction by means of pitot tubes. Journal of the Royal Aeronautical Society 58:109-121. 1954.

43. Rothfus, R. R. Velocity distribution and fluid friction in concentric annuli. Ph. D. Thesis. Pittsburg, Carnegie Institute of Technology. 1948.

44. Rothfus, R. R., C. C. Monrad and V. E. Sencal. Velocity distribution and fluid friction in smooth concentric annuli. Industrial and Engineering Chemistry 42:2511-2520. 1950.

45. Stirba, C. and D. M. Hurt. Turbulence in falling liquid films. Journal of the American Institute of Chemical Engineers 1:178-184. 1955.

46. Tailby, S. R. and S. Portalski. The hydro-dynamics of liquid film flowing on a vertical surface. Transactions of the Institution of Chemical Engineers, London 38:324-330. 1960.

47. Walker, J. E., G. A. Whan and R. R. Rothfus. Fluid friction in noncircular ducts. Journal of the American Institute of Chemical Engineers 3:484-489. 1957.

48. Wylie, C. R. Advanced engineering mathematics. 2d ed. New York, McGraw-Hill, 1960. 696p.

APPENDICES

APPENDIX I

Preston Tube

Preston Tube

The calibration of the preston tubes at both bottom and top were carried out in the annular column used. The pressure gradients in the axial direction and the pressure differences between kinetic and static tap near the wall were measured by 50 inch inclined manometer.

In calculation of shear stress utilizing the pressure gradients the following equation was used,

$$\tau_2 = \frac{r_2^2 - r_m^2}{2r_2} \left(-\frac{dP_f}{dx}\right)$$

where r_m, the position of maximum mean velocity, was obtained from the data of the mean velocity profile, i. e., 0. 865 inch at the bottom and 0. 86 inch at the top.

The calibration curves are plotted τ_2 in lbf/in^2 versus ΔH in inches in Figure (34) where ΔH is the height of 0. 83 specific gravity manometer fluid corresponding to the pressure difference between kinetic and static. The slopes of calibration curves are . 755 at the bottom and . 875 at the top. Comparing with Preston's equation, it is noted that the slope at top agrees excellently whereas at the bottom deviates much. Disagreement at the bottom is due to the upstream condition as mentioned in discussion section. However, the bottom preston tube is still good to measure shear stress, since relationship between τ_2 and ΔH is also function of up stream condition.

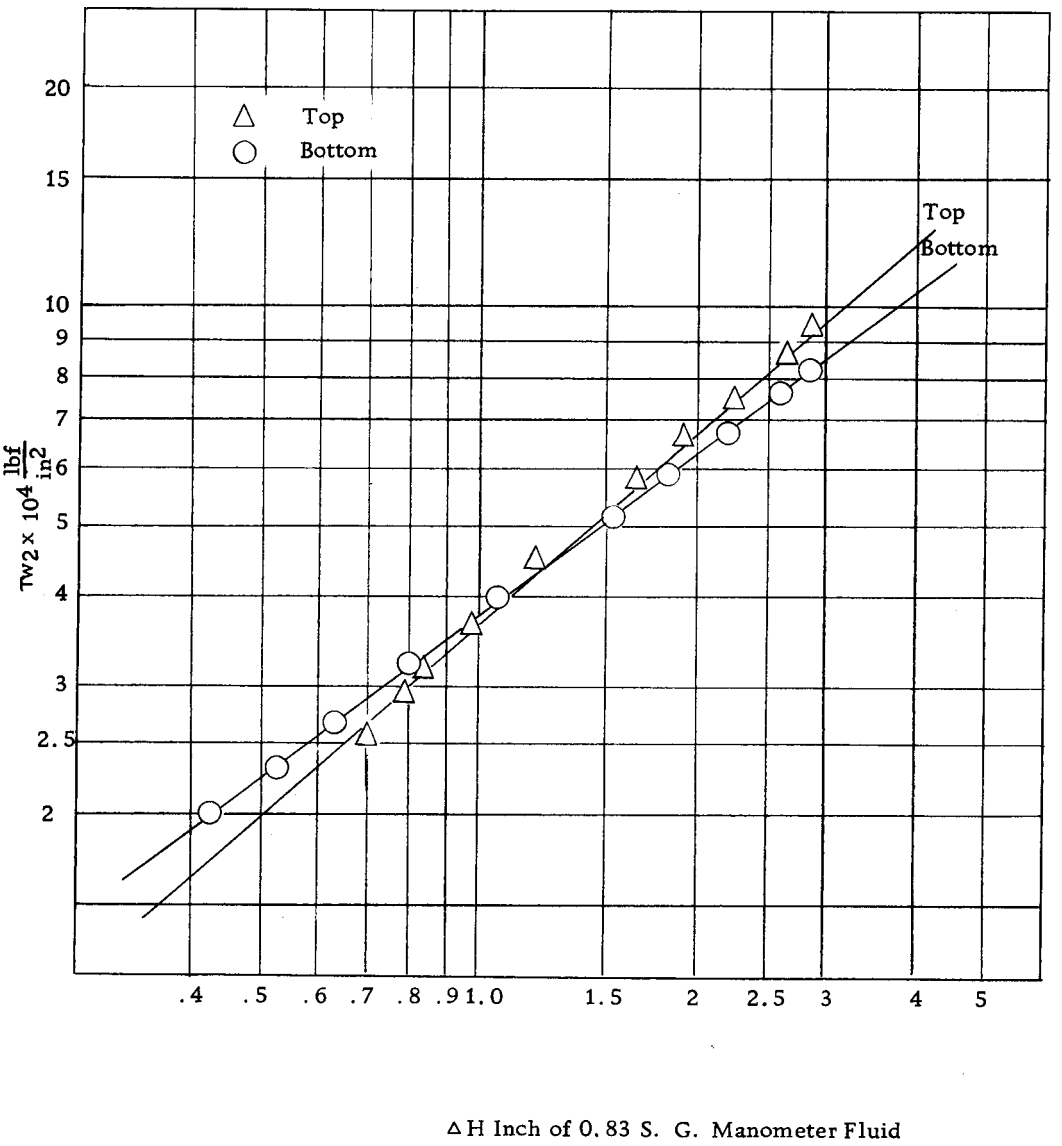

Figure (34) Calibration for Preston tube.

APPENDIX II

A Heating Element

A Heating Element

To date many devices for measuring shear stress have been developed for flow on a flat plate. The heating element method is one of these and is seen as the best method for use on the wetted wall in climbing film flow.

Accordingly, this method was extended to the flow on the outside of a longitudinal cylinder.

Ludwieg (33) and Liepmann and Skinner (30) have developed the heating element method on the flat plate flow. Two assumptions were made to relate the heat transfer to the momentum transfer for this case.

1) The ratio of thermal boundary layer thickness to the laminar sublayer thickness is less than 1 along a heating element.

2) The velocity profile in the sublayer is $u = cy$ where c is $\frac{\tau_w}{\mu}$.

From these assumptions, the subsequent relationship was obtained for flat plate,

$$Nu_x = \frac{hx}{k_o} = \frac{x}{0.893}\left(\frac{c}{9\alpha x}\right)^{1/3} \tag{1}$$

which is known as the Leveque's solution (26, p. 366). By rearranging Equation (1), one may get easily

$$\frac{q_x}{k_o \Delta T} = \frac{1}{9^{1/3} \cdot 0.893} Pr^{1/3} Re_x^{2/3} \left(\frac{\tau_w}{\rho U^2}\right)^{1/3} \tag{2}$$

If the film thickness is thin and a laminar sublayer exists on the surface of the cylinder, the problem of longitudinal cylinder will have the similarity with the flat plate in the geometry and in the transport phenomena. This means that the same relationship such as Equation (2) will hold for the longitudinal cylinder,

$$\frac{qx}{k_o \Delta T} \propto Pr^{1/3} Re_x^{2/3} \left(\frac{\tau_w}{\rho U^2}\right)^{1/3} \qquad (3)$$

The proportional constant can be evaluated by a simple experiment which is called calibration.

Calibration

The calibration channel consisted of concentric plexiglas and aluminum pipes. The outer plexiglas pipe had two-inch inside diameter and the inner aluminum pipe was one inch outside diameter. They were about 10 ft long. The element designed was inserted in the inner pipe at about eight feet above the entrance. The static pressure taps were connected to one inch inclined manometer which was filled with S. G. 1.595 fluid to measure the pressure gradients.

Water was used during the calibration. About 10 watts electrical energy was supplied by a 12 volt battery. The temperature differences between the element and the water were measured by a precision potentiometer.

The results are plotted in Figure (35) as $\frac{1}{\Delta T}$ versus τ_w shear stress where ΔT is in millivolt (copper-constantan).

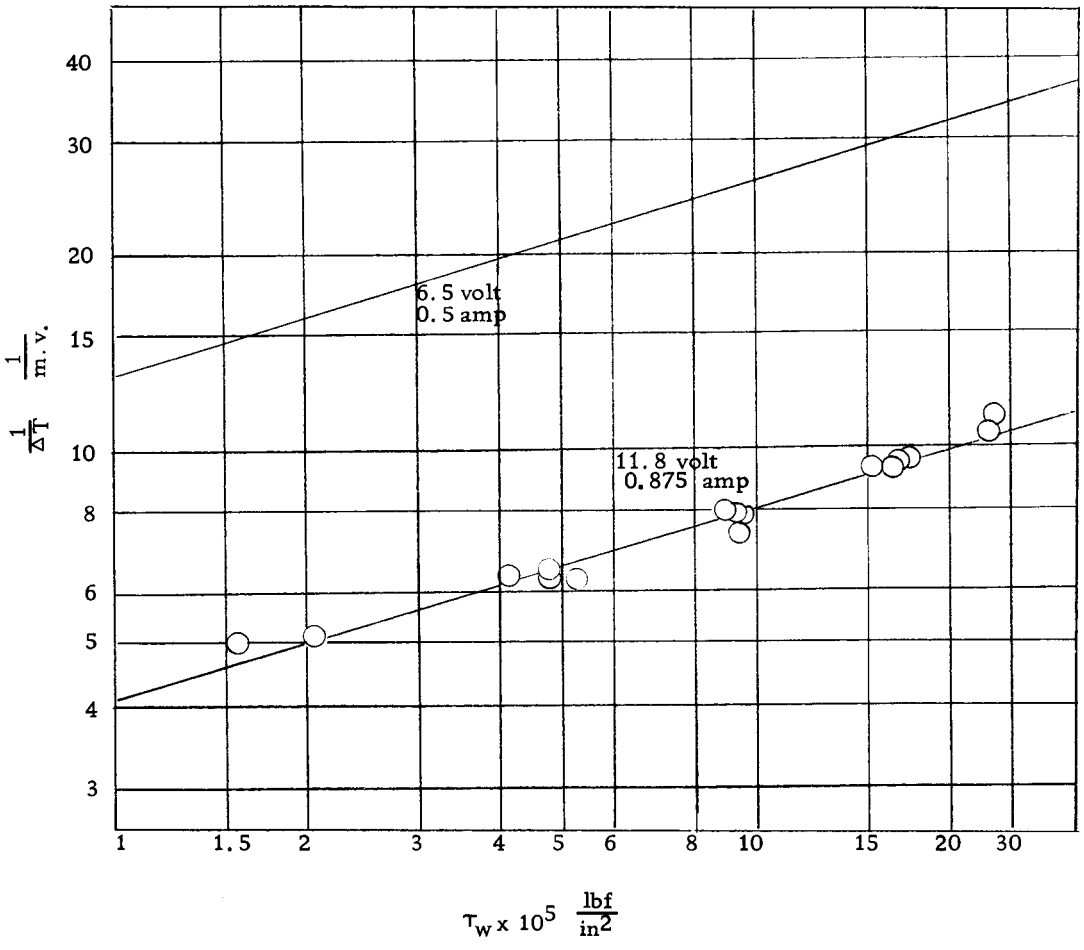

Figure (35) Calibration for heating element.

APPENDIX III

Calibration of Orifice

Calibration of Flow Orifice

A two inch sharp-edged orifice was made out of brass. The orifice was calibrated with a critical flow probe (Meteric Orifice Flow Prover Type CR, size 2) made by the American Meter Company and from the measurements of the mean-velocity profile.

The critical flow prover consisted of a pair of flanges which could be fitted with various sizes of streamlined nozzles. A thermometer and a pressure gage were installed upstream from the nozzle. Each nozzle had been calibrated by the manufacturer, and the standard air time had been stamped on each nozzle. The standard air time is the time in seconds for the nozzle to pass one cubic foot of gas at the acoustic velocity. If the gas attains the acoustic velocity at nozzle, the pressure ratio $\frac{P_2}{P_1}$ should be less than the pressure ratio $(\frac{P_2}{P_1})_c$ where 1 denotes the upstream and 2 at nozzle, and

$$(\frac{P_2}{P_1})_c = (\frac{2}{k+1})^{\frac{k}{k-1}}, \quad k = \frac{C_p}{C_v}$$

Since the mass velocity through a streamlined nozzle depends only on the upstream conditions, the temperature and pressure ahead of the nozzle and the critical flow time were the only data necessary to calculate the flow rate.

The critical flow prover assembly was installed as shown in

schematic drawing in Figure (36). The high pressure air was produced by an air compressor. A pressure control valve was installed to stabilize the pressure at the upstream side of the nozzle. After flowing through the critical flow prover, the air passed through the orifice being calibrated and was discharged to the atmosphere. The pressure drop across this orifice was determined while several different streamlined nozzles and different up-stream pressures were used.

The flow rate through the orifice was calculated by using the following equation

$$Q = \frac{60}{fF}\left(\frac{P+P_b}{14.7}\right)\left(\frac{528}{460+t_a}\right)$$

where Q = Air Flow Rate in cfm at 68 F at 1 atm

f = Correction Factor for Temperature and ratio of specific heat

F = Critical flow time

P = Pressure ahead of nozzle psig

P_b = Barometric Pressure psia

t_a = Temperature of air, ^oF

By the measurements of the mean-velocity profile and integrating using a numerical method, the orifice was calibrated in the high air flow rate regions where the capacity of the compressor used for air source in critical flow prover was not enough.

The results of calibration are plotted in Figure (37) as cfm

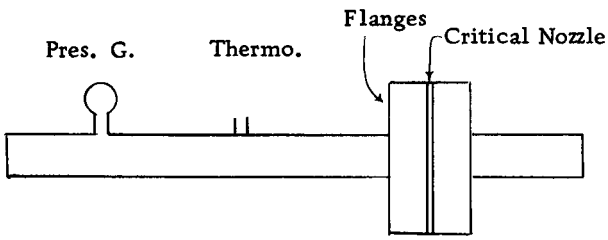

Critical Flow Prover

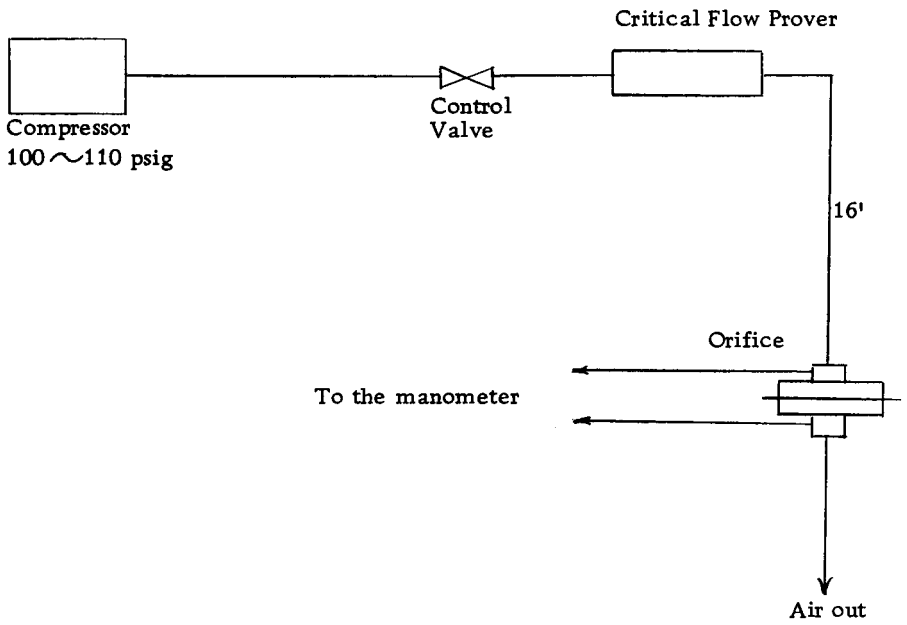

Figure (36) Flow Diagram.

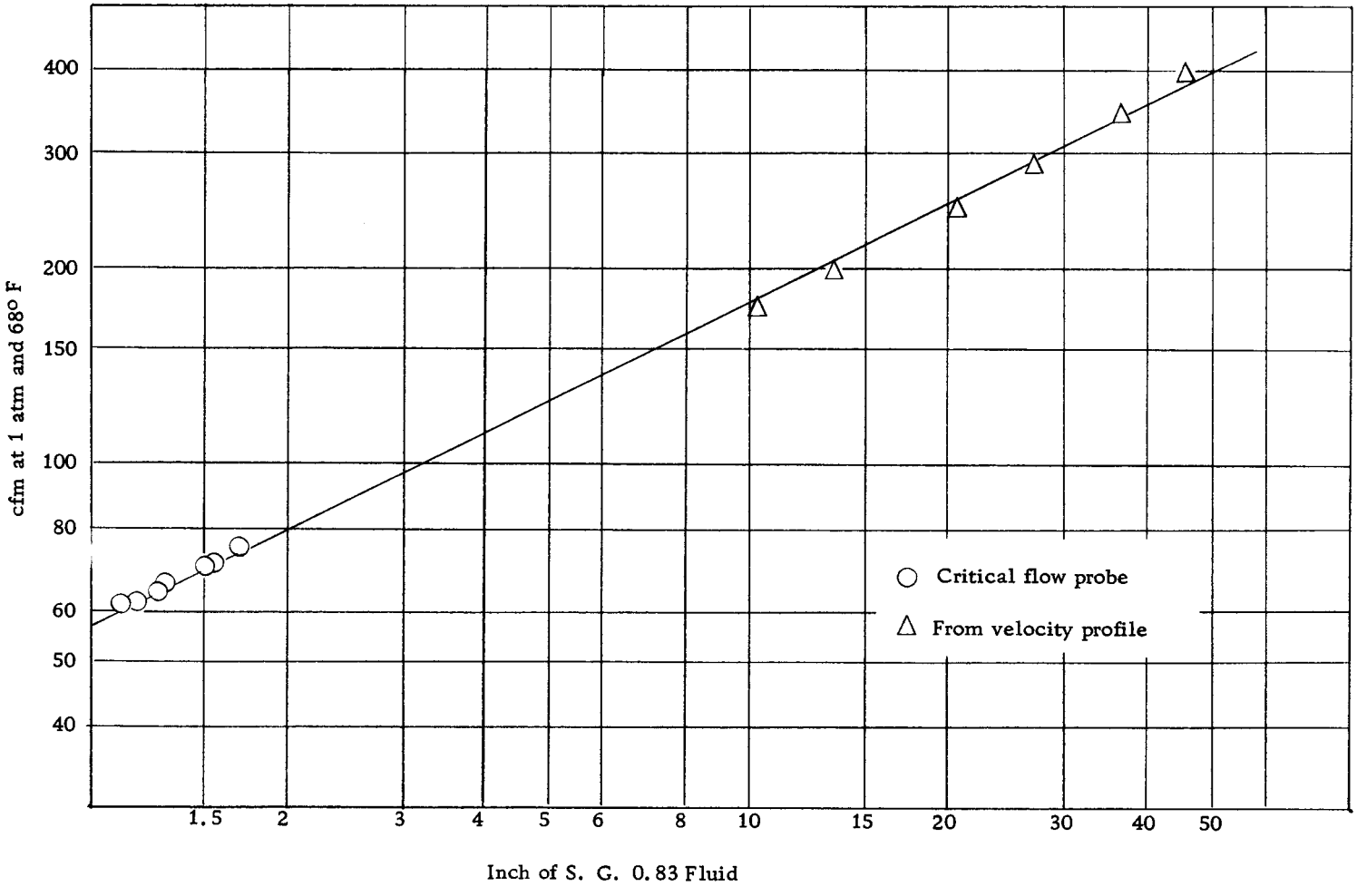

Figure (37) Calibration for Orifice.

of air at $68^{\circ}F$ and at 1 atm versus the hight of S. G. 0. 83 Manometer fluid. The calibrations with a critical flow prover agreed well with those from the measurements of mean velocity.

APPENDIX IV

Mean Velocity Gradients in the region of maximum velocity

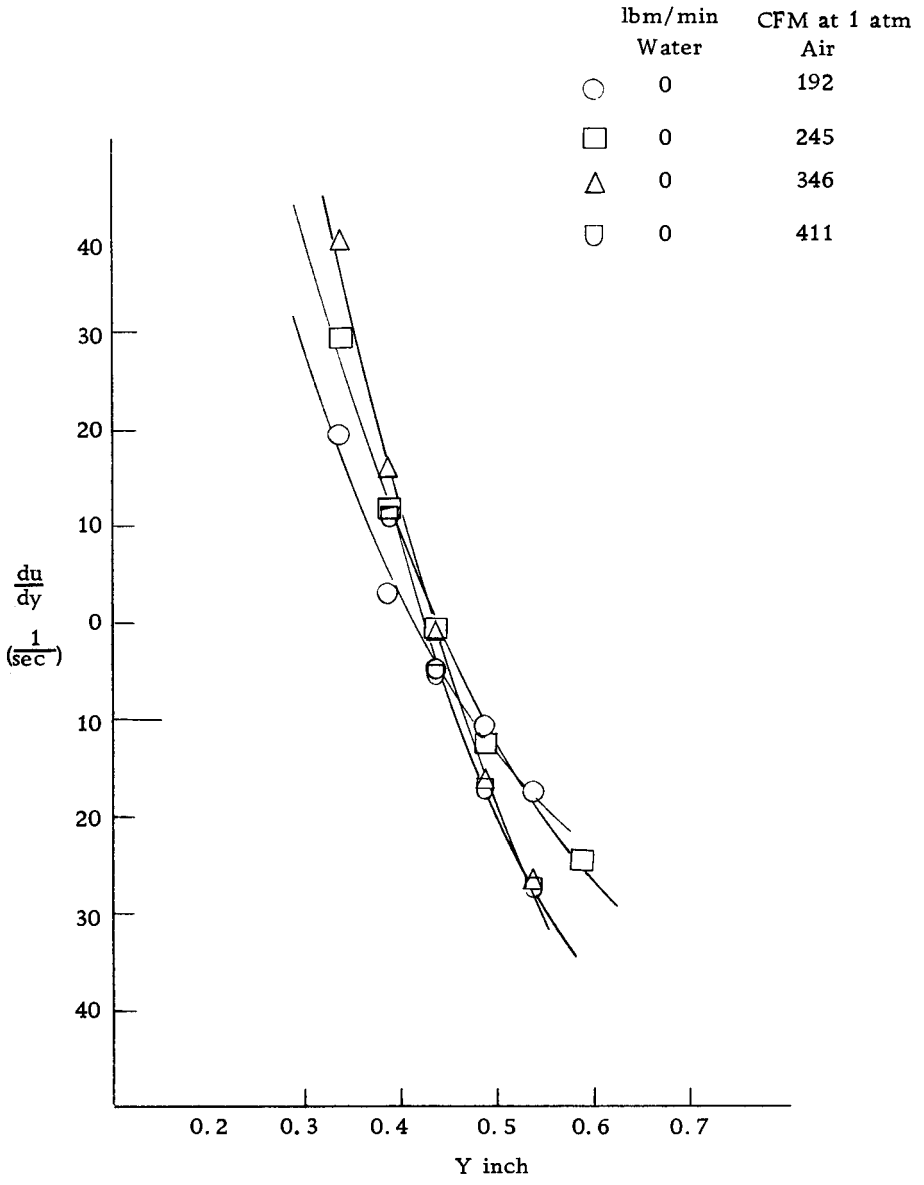

Figure (38) Velocity gradients in near region of maximum velocity (Bottom).

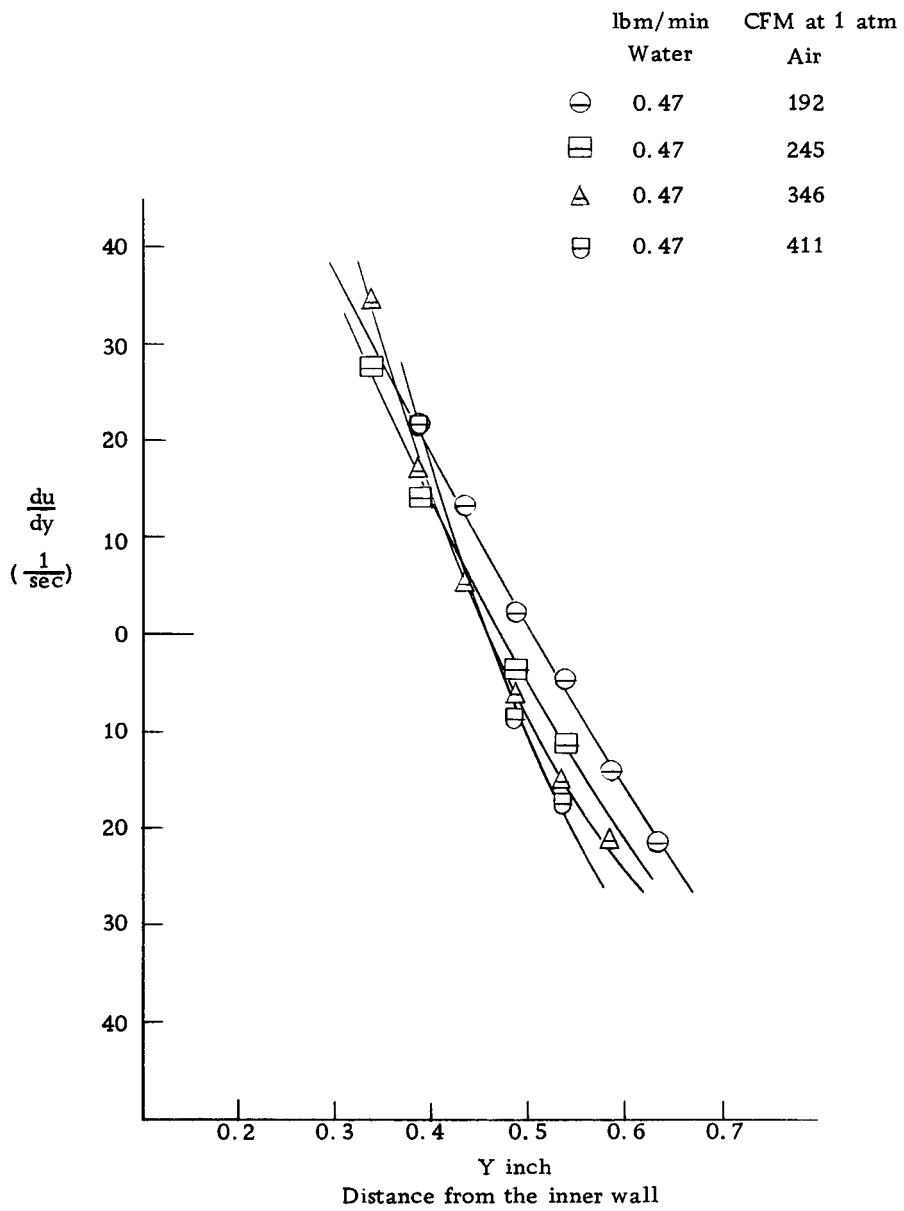

Figure (39) Velocity gradients in near region of maximum velocity (Bottom).

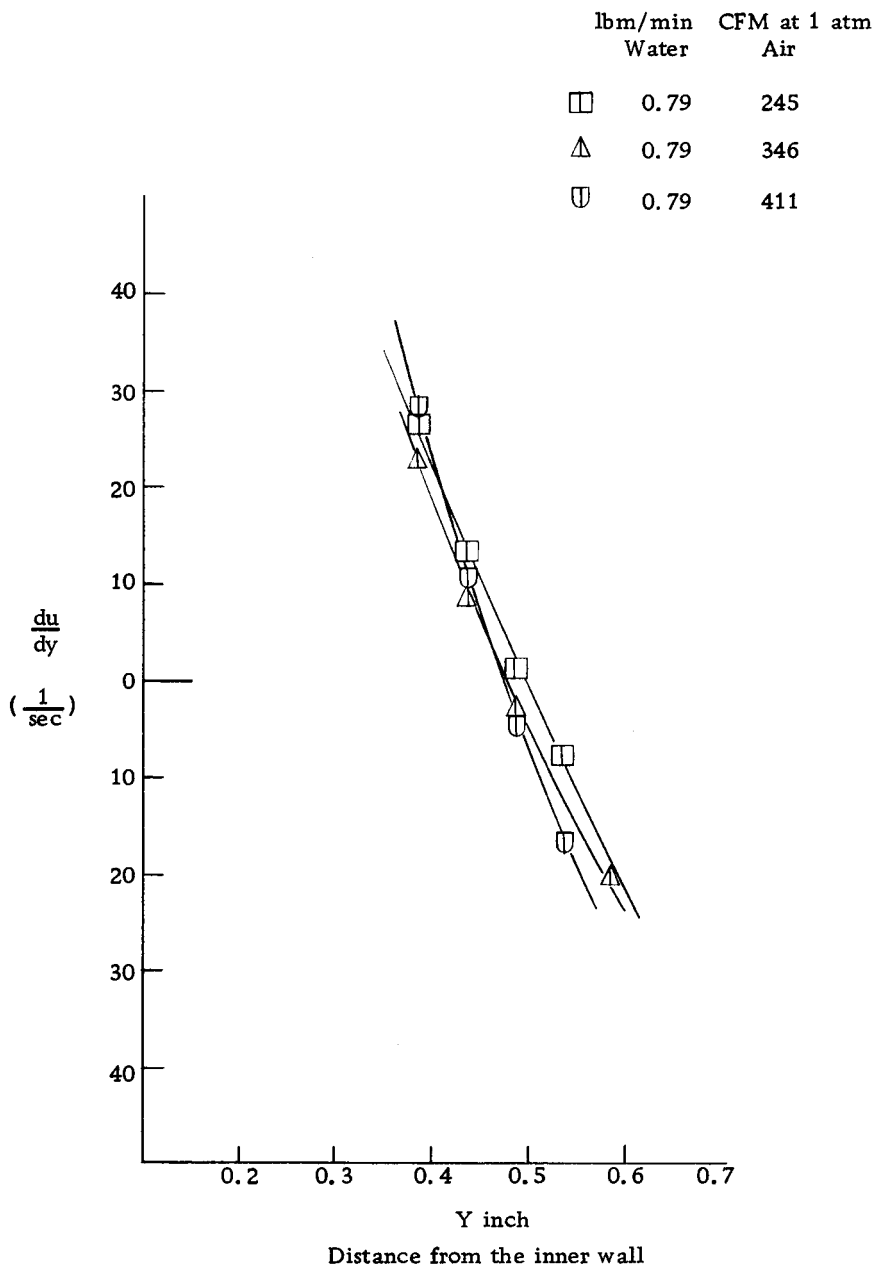

Figure (40) Velocity gradients in near region of maximum velocity (Bottom).

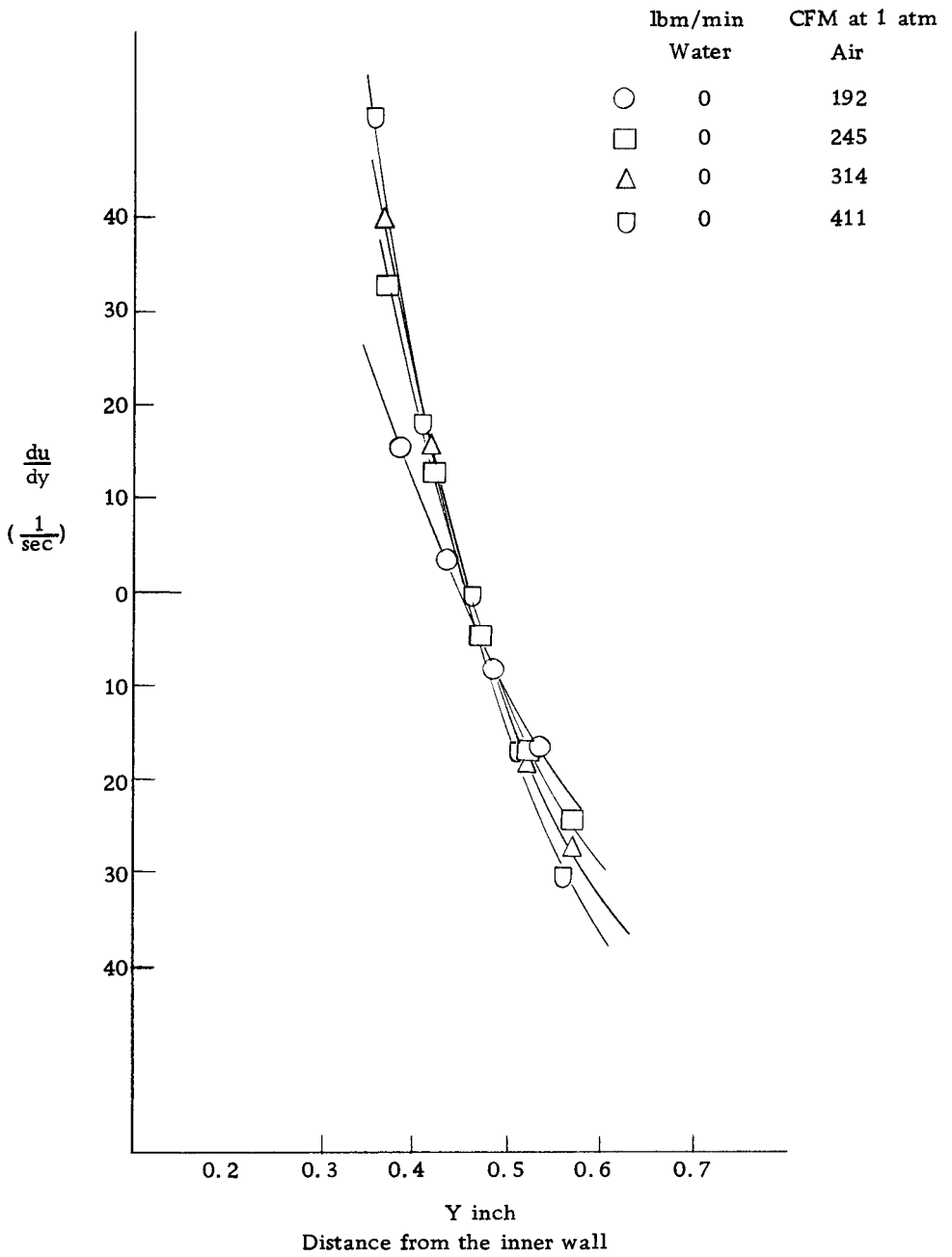

Figure (41) Velocity gradients in near region of maximum velocity (Top).

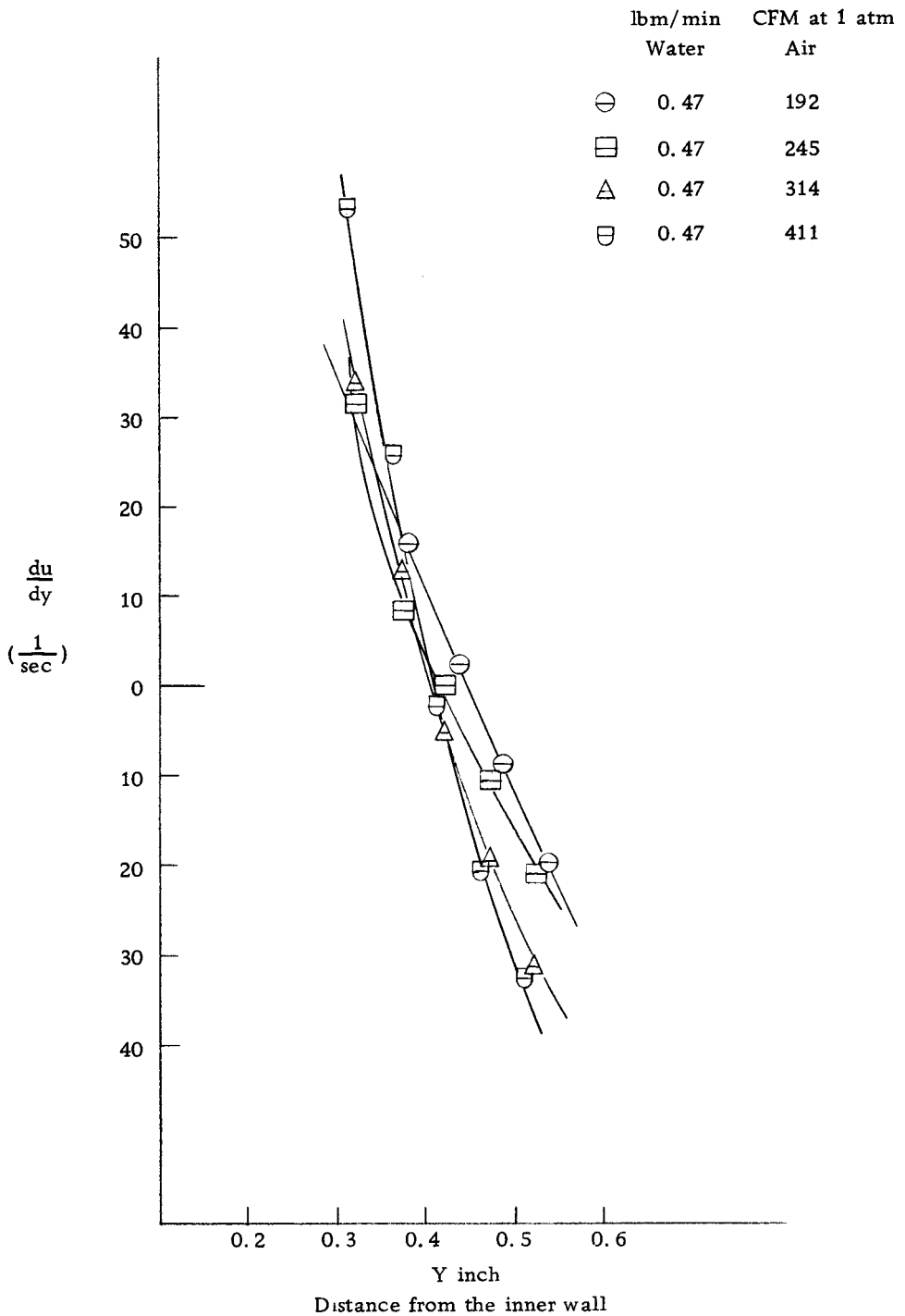

Figure (42) Velocity gradients in near region of maximum velocity (Top).

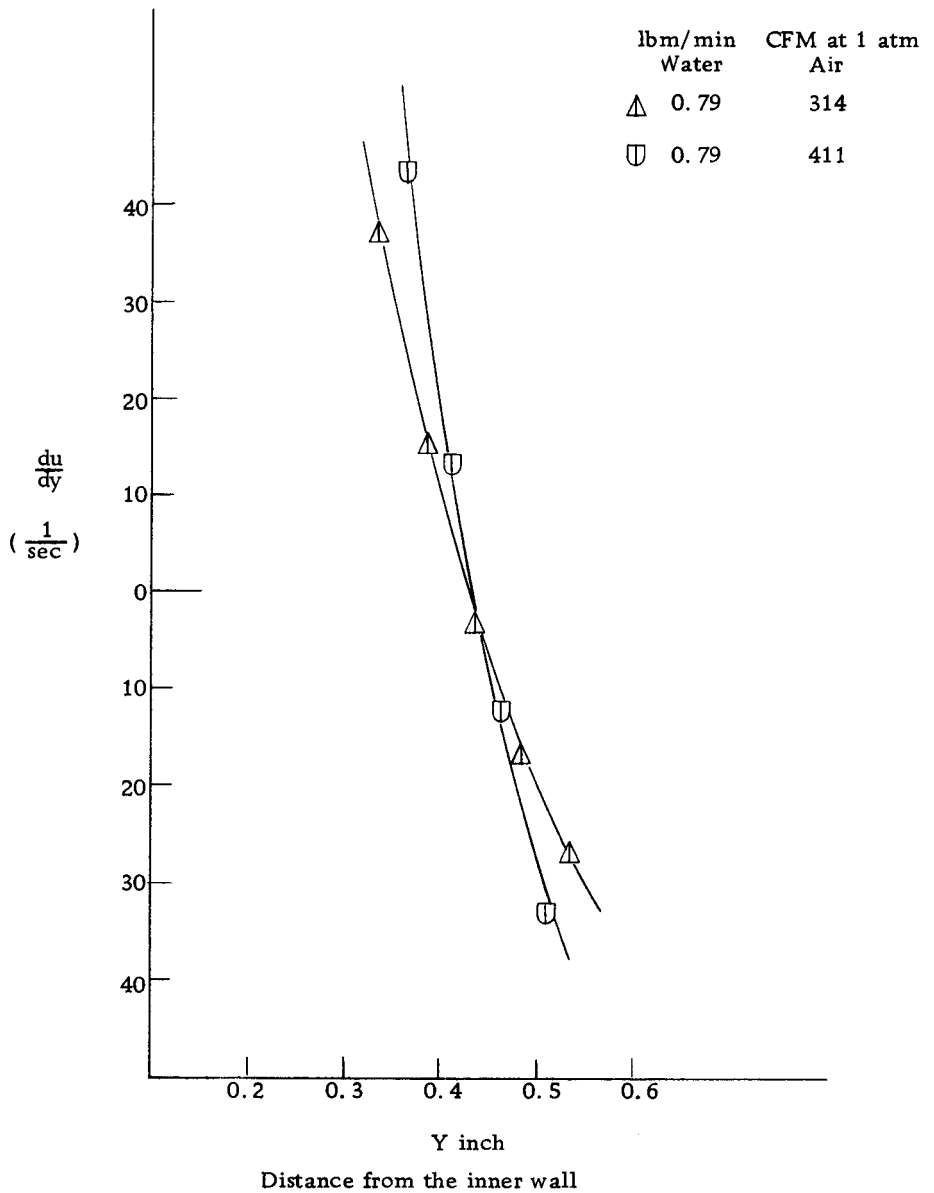

Figure (43) Velocity gradients in near region of maximum velocity (Top).

APPENDIX V

Computer Program

```
C       CALCULATION OF CLIMBING FILM FLOW DEISSLER
        DIMENSIONTO(100), TI(100), Y(150), T3(150), U(150), UA(150), UAA(150), H(100), T3A(150)
00022   FORMAT(F4. 4, 2X, F6. 6, 2X, F6. 6)
00025   FORMAT(17H VELOCITY PROFILE)
00033   FORMAT(4H Y= F6. 4, 2X, 5H T3= F14. 6, 2X, 4H U= F14. 6)
00034   FORMAT(4H Y= F6. 4, 2X, 5H T3= F14. 6, 2X, 4H U= F10. 6, 2X, 4H= F4. 2, 2X, 5H TO= F9. 7, 2X, 5H TI= F9. 7)
00035   FORMAT(4H Y= F6. 4, 2X, 5H T3= F14. 6, 2X, 4H U= F10. 6, 2X, 4H= F4. 2, 2X, 5H TO= F9. 7, 2X, 5H TI= F9. 7)
00023   FORMAT(17H LIQUID FLOW RATE)
00036   FORMAT(4H Q= F14. 7, 2X, 7H H(J)= F9. 7, 2X, 8H TO(J)= F9. 7, 2X, 8H TI(J) = F9. 7//)
        DO1J=1, 5
        READ(1, 22)H(J), TI(J), TO(J)
        WRITE(3, 25)
        V=5. 6E-5/386. 4
        Y2=0. 0002
        Y3=0. 0
        U3=0. 0
        X=5. 55E-4/386. 4
        T33=TO(J)/V
        UU=Y2*T33
        WRITE(3, 33)Y2, T33, UU
        DO4L=1, 4
        A=L
        Y(L)=0. 0002*A
        U(L)=UU+(T33*Y2)
        Y(L)=Y(L)+Y2
        TT1=TO(J)+((TI(J)-TO(J))*Y(L)/H(J))
        TT2=V+(X*U(L)*Y(L)*(1. -EXP(-X*U(L)*Y(L)/V)))
        TT3=TT1/TT2
        T3(L)=TT3
        WRITE(3, 34)Y(L), T3(L), U(L), H(J), TO(J), TI(J)
        UU=U(L)
        T33=T3(L)
00004   CONTINUE
        I=4
```

```
00075  U(I+1)=U(I)+(Y2/24.*((55.*TE(I))-(59.*T3(I-1))+(37.*T3(I-2))-(9.*T3(I-3))))
       Y(I+1)=Y(I)+Y2
       T1=TO(J)+((TI(J)-TO(J))*Y(I+1)/H(J))
00072  T2=V+(X*U(I+1)*Y(I+1)*(1.0-EXP(-X*U(I+1)*Y(I+1)/V)))
       T3(I+1)=T1/T2
       UA(I+1)=U(I)+(Y2/24.*))9.*T3(I+1))+(19.*T3(I))-(5.*T3(I-1))+T3(I-2)))
       T2=V+(X*UA(I+1)*Y(I+1)*(1.-EXP(-X*UA(I+1)*Y(I+1)/V)))
       T3A(I+1)=T1/T2
       UAA(I+1)=U(I)+(Y2/24.*((9.*T3A(I+1))+(19.*T3(I))-(5.*T3(I-1))+T3(I-2)))
       D=UAA(I+1)-UA(I+1)
       D=ABS(D)
       IF(D.LE.0.005)GOTO71
       U(I+1)=UAA(I+1)
       GOTO72
00071  U(I+1)=UAA(I+1)
       T3(I+1)=T3A(I+1)
       WRITE(3,35)Y(I+1),T3(I+1),U(I+1),H(J),TO(J),TI(J)
       DD=Y(I+1)-H(J)
       IF(DD.GE.0.0)GOTO5
       I=I+1
       GOTO75
00005  SUM=U(I)
       I=I-1
       WRITE(3,23)
       DO2K=1,I,2
       Q1=4.*U(K)
       SUM=Q1+SUM
00002  CONTINUE
       I=I-1
       DO3K=2,I,2
       Q2=2.*U(K)
       SUM=SUM+Q2
00003  CONTINUE
       Q=SUM*0.0002/3.0
       Q=Q*3.14
       WRITE(3,36)Q,H(J),TO(J),TI(J)
00001  CONTINUE
       STOP
       END
```

APPENDIX VI

Nomenclature

NOMENCLATURE

The fundamental dimensions are represented by the following letters: F = force, L = length, m = mass, t = time.

Roman Symbols

Symbol	Meaning	Dimensions
c	phase velocity	$\frac{L}{t}$
d	diameter of Preston tube	L
d_1	inner core diameter	L
d_2	outer tube diameter	L
de_1	equivalent diameter defined by $\frac{2(r_m^2 - r_1^2)}{r_1}$	L
de_2	equivalent diameter defined by $\frac{2(r_m^2 - r_1^2)}{r_1}$	L
$\overline{\dot{E}}$	mean rate of energy transfer	$\frac{FL}{t}$
$\overline{E_d}$	rate of averaged energy dissipation per unit area	$\frac{FL}{t}\frac{1}{L^2}$
f_1^1	friction factor defined by Equation (19) in Theory section	
f_2^1	friction factor defined by Equation (13) in Theory section	
$F(x, t)$	momentum transfer at air-water interface	$\frac{F}{L^2}$

Symbol	Meaning	Dimensions
g	acceleration of gravity	$\frac{L}{t^2}$
g_c	force-mass conversion factor	$\frac{m}{F}\frac{L}{t^2}$
h	instantaneous film thickness	L
h_o	mean film thickness	L
k_o	thermal conductivity	$\frac{BTu}{t \cdot L \cdot {}^oF}$
k	wave number	
K	von Karman constant 0.368	
P	static pressure	$\frac{F}{L^2}$
ΔP_f	pressure difference due to friction	$\frac{F}{L^2}$
P_k	kinetic pressure	$\frac{F}{L^2}$
P_σ	surface pressure	$\frac{F}{L^2}$
P_G	gas stream pressure	$\frac{F}{L^2}$
P_r	Prandtl number	
Q	water flow rate	$\frac{L^3}{t}$
q	heat flux	$\frac{BTu}{t \cdot L^2}$
r	radius	L
r_1	inner core radius	L
r_2	outer tube radius	L
r_i	interface radius	L
r_H	equivalent hydraulic diameter defined by Equation (11) in Theory section	L

Symbols	Meaning	Dimensions
r_m	radius of point of maximum velocity	L
R_1	$\frac{r_m^2 - r_i^2}{r_2^2 - r_1^2}$	
R_2	$\frac{r_2^2 - r_m^2}{r_2^2 - r_1^2}$	
R_L	$\frac{r_i^2 - r_1^2}{r_2^2 - r_1^2}$	
R_G	$\frac{r_2^2 - r_i^2}{r_2^2 - r_1^2}$	
R_{e_1}	Reynolds number defined by Equation (15) in Theory section	
R_{e_2}	Reynolds number defined by Equation (16) in Theory section	
T	temperature	^oF
u, v	point velocity	$\frac{L}{t}$
u_m	maximum velocity	$\frac{L}{t}$
u^*	friction velocity $\sqrt{\frac{\tau_w}{\rho}}$	$\frac{L}{t}$
u^+	u/u^*	
u_o	velocity at average stream cross section h_o	$\frac{L}{t}$
$\bar{u}$	velocity defined by Equation (17) in Theory section	$\frac{L}{t}$

Symbol	Meaning	Dimensions
U	mean velocity	$\frac{L}{t}$
U_1	mean velocity in inner region of annulus	$\frac{L}{t}$
U_2	mean velocity in outer region of annulus	$\frac{L}{t}$
X	Lockhart and Martinelli parameter	
x, y	direction coordinate	
Y_m	distance from inner wall to the point of maximum velocity	L
y^+	dimensionless distance $\frac{yu^* \rho}{\mu}$	
y_1	distance from the inner wall	L
y_2	distance from the outer wall	L

Greek Symbols

α	thermal diffusivity	$\frac{L^2}{t}$
μ	coefficient of viscosity	$\frac{m}{Lt}$
ν	kinematic viscosity	$\frac{L^2}{t}$
ρ	density	$\frac{m}{L^3}$
ρ_G	density of air	$\frac{m}{L^3}$
ρ_L	density of water	$\frac{m}{L^3}$
σ	coefficient of surface tension of water	$\frac{F}{L}$

Symbol	Meaning	Dimensions
τ	shear stress	$\frac{F}{L^2}$
τ_1	shear stress on the inner wall	$\frac{F}{L^2}$
τ_2	shear stress on the outer wall	$\frac{F}{L^2}$
τ_i	shear stress at air-water interface	$\frac{F}{L^2}$
τ_w	shear stress on wall	$\frac{F}{L^2}$
ϕ	defined by Equation 23 in Theory section	
Φ	Lockhart and Martinelli parameter	
λ	wave length	L